Regulation of the deubiquitinase CYLD in innate immune signalling



Derek Malcolm Leske

Brasenose College

University of Oxford

A thesis submitted for the degree of

Doctor of Philosophy

Trinity 2018

Acknowledgements

I would very much like to thank Prof. Mads Gyrd-Hansen for taking me as one of his first students following his move to Oxford. I cannot express my gratitude for the wonderful supervision that was the perfect balance between allowing me to explore my own ideas and also guiding me through the difficulties and discoveries. My time under your supervision has been invaluable and has taught me lessons that I will remember for the rest of my life. I would also like to thank Dr. John Christianson for his role as my second supervisor as well as Prof. David Komander and Dr. Paul Elliott for their collaboration and support with this work. I would also like to thank the Ludwig and all its support staff for their support over the last four years.

To Mattia: My Ludwig brother, I was so sure you were going to be an absolute pain before we met (well... you turned up late on your first day!), but I have to say that I have never found someone who I connected with so quickly – it has to be the fact that you share my love for mid-2000s music (a.k.a. the golden age of pop-punk, metalcore, and emo). Your friendship is one of the best things I've gained from my time in Oxford and is something I know I'm going to cherish for the rest of my life.

To all members of the Gyrd-Hansen lab, past and present (Matous, Katrin, Berthe, Mattia, Leila, Corinne, Ruoshi, Gianluca, Lisa, Yusuf, Svanhild, and Biao): I have never been in a more accepting and fun working environment and I'm grateful to be a part of such a great team of amazing scientists and people! The lab was my second home for these four years and I'm particularly grateful to Ruoshi who never fails to make me laugh and also has helped with the troubleshooting of many experiments.

To all my friends here: Thanks for making Oxford feel like home! To Lorenzo, my good man: One of the first people I met in Oxford and arguably one of the nicest guys I know. Thanks for all the Wolfson memories, even if we weren't so enthralled by the place to begin with! To Paige, my fellow crazy dog person: You are such a genuine and caring person and an absolute inspiration to me. I know your time in Oxford was like a roller coaster to say the least, but I'm immensely happy and proud that you absolutely smashed it! I know you're going to go on to do amazing things and I can't wait to see what those will be!

To Robbie, my oldest friend: Being away from Ayrshire presents challenges for seeing each other so often, but I'm glad that when we do meet, it's like picking up right where we left off. Your continued friendship means more to me than you will ever know, and your kindness is something I aspire to. Here's to many more years to come!

To Laura: Thank you for your love and support over these years. Without you, Oxford would have been a very different experience and I'm happy you were here to support me, even at times when lab work had to be my priority. My time here was worth it just to have met you and I look forward to our next adventure together.

To Colin, my younger brother: You are more of a friend than a brother really. Thank you for all the phone calls, games of LoL, and reminding me of my roots. I appreciate everything you do back home and I can't wait to see you live up to your potential. And to Raymond, my older brother, and my nephews Oliver and Danyl, thank you for all the memories growing up and your continued support. I wish you all the happiness in the future and will always be there to offer a helping hand if needed.

Finally, I would like to thank my parents, Martin and Ellis. I am forever grateful that you raised me to be independent, diligent, and ambitious, and I wholly attribute my success thus far to your continued support. Thank you for all the phone calls over the last 12 years where you shared my success but also encouraged me when things weren't going so well. I couldn't have done any of this without you both.

Abstract

Innate immune receptors are vital for protection against invading pathogens and the downstream signalling events of these are controlled by ubiquitination. Classically, ubiquitin was described to serve as a degradative signal. However, of the eight possible types of ubiquitin linkages, most have been assigned non-degradative roles and instead serve scaffolding functions for recruitment and activation of proteins. M1- and K63- chains are two such linkages and have crucial roles in mediating immune signalling events, with the balance between their deposition onto receptor components, and removal, determining the magnitude and duration of the signalling.

Linear ubiquitin chain assembly complex (LUBAC) is the only E3 known to generate M1-chains and is essential for productive signalling. It is regulated by its two associated deubiquitinating enzymes (DUBs), CYLD and OTULIN, which associate with the catalytic subunit, HOIP. However, the mechanism through which CYLD interacts with LUBAC is unclear. As such, this study aimed to characterise how CYLD is specifically recruited to the LUBAC complex and subsequently determine the factors that are mediating its activation.

In this thesis, I describe the identification of SPATA2 as a factor linking CYLD with LUBAC, thereby facilitating regulation of innate immune signalling by CYLD. In the second part of the thesis I investigate the regulation of CYLD's catalytic activity by phosphorylation. My studies reveal a novel phosphorylation site (S568) on CYLD which regulates CYLD activity and its ability to restrict innate immune signalling.

In summary, this study identified a novel binding partner of CYLD and characterised the phosphorylation-mediated activation of its DUB activity. This provides an explanation as to how CYLD is recruited to signalling complexes in a LUBAC-dependent manner, as well as novel mechanistic insight into how innate immune signalling events may be fine-tuned by regulation of CYLD.

Contents

List of Abbreviations **viii**

1 Introduction **1**
1.1 The ubiquitin system . . . 2
1.1.1 Ubiquitin and ubiquitin-like proteins . . . 2
1.1.2 Ubiquitination . . . 3
1.1.3 The structure of ubiquitin modifications . . . 8
1.1.4 Ubiquitin-binding domains . . . 9
1.1.5 Deubiquitinating enzymes . . . 11
1.1.6 Cellular functions of ubiquitin chains . . . 15
1.2 The innate immune system and pattern recognition receptors (PRRs) 17
1.2.1 Pattern recognition receptors (PRRs) . . . 18
1.2.2 NOD1 and NOD2 receptor signalling . . . 22
1.2.3 TNF receptor signalling . . . 26
1.3 The Linear ubiquitin chain assembly complex (LUBAC) . . . 28
1.3.1 The structure and function of HOIP . . . 29
1.3.2 The association of CYLD and OTULIN with LUBAC . . . 31
1.3.3 Cellular functions of LUBAC . . . 31
1.4 The deubiquitinase, CYLD . . . 34
1.4.1 Structure and function of CYLD . . . 34
1.4.2 CYLD in immune signalling . . . 35
1.4.3 Regulation of CYLD function . . . 36
1.5 Spermatogenesis-associated protein 2 . . . 36
1.6 Aims of the study . . . 38

2 Materials **39**
2.1 Materials . . . 39
2.1.1 Chemicals, reagents, and consumables . . . 39
2.1.2 Buffers and solutions . . . 42
2.1.3 Commercial kits . . . 43
2.1.4 Antibodies . . . 43
2.1.5 Plasmids . . . 44
2.1.6 Oligos . . . 45
2.1.7 Cell lines . . . 46

3 Methods **48**
3.1 Cell biology . . . 49
3.1.1 Cell culture . . . 49
3.1.2 Transient transfection of cells . . . 49
3.1.3 Stable transduction by γ- retrovirus . . . 50
3.1.4 Flow cytometry . . . 51
3.1.5 RNA isolation, cDNA synthesis, and qRT-PCR . . . 51
3.2 Protein biochemistry . . . 53
3.2.1 Immunoblotting . . . 53
3.2.2 Immunoprecipitation of tagged proteins . . . 54
3.2.3 Pulldown of the TNFR1 complex . . . 54
3.2.4 Purification of endogenous ubiquitin conjugates . . . 55
3.2.5 Protein dephosphorylation by lambda phosphatase . . . 56
3.2.6 Identifying phosphorylation sites by mass spectrometry . . . 56
3.2.7 Sucrose gradient sedimentation . . . 58
3.3 Molecular biology . . . 59
3.3.1 Generation of knock-out cell lines with CRISPR/Cas9 . . . 59
3.3.2 Plasmid preparation . . . 59
3.3.3 Cloning and mutagenesis . . . 60
3.4 Statistical analyses . . . 63

4 SPATA2 links CYLD and HOIP to regulate immune signalling **64**
4.1 Introduction . . . 65
4.2 SPATA2 interactions with CYLD and HOIP . . . 65
4.2.1 SPATA2 binds CYLD in a B-box-dependent manner . . . 65
4.2.2 SPATA2 interaction with CYLD . . . 66
4.2.3 SPATA2 interaction with HOIP . . . 70
4.2.4 SPATA2 links CYLD to LUBAC . . . 73
4.3 SPATA2 bridges CYLD to receptor complexes . . . 75
4.3.1 SPATA2 is required for CYLD recruitment to the TNFR complex I . . . 75
4.3.2 Loss of SPATA2 leads to a loss of CYLD in high molecular weight complexes . . . 76
4.4 SPATA2 regulates CYLD-mediated NF-κB responses . . . 78
4.4.1 SPATA2 controls the ubiquitin landscape of TNFR1 and NOD2 adaptor proteins . . . 78
4.4.2 Loss of SPATA2 leads to less ubiquitinated substrates within the TNFR complex I but little effect on downstream signalling 81
4.4.3 Loss of SPATA2 leads to enhanced NF-κB activity in the NOD2 signalling pathway . . . 84

4.5 CYLD does not regulate auto-ubiquitination of the LUBAC complex 86
4.6 Discussion 87

5 The activity of CYLD is dependent on phosphorylation 91
5.1 Introduction 92
5.2 CYLD is phosphorylated in response to TNF and L18-MDP stimulation 92
5.2.1 Confirmation that CYLD within the TNFR complex I is phosphorylated. 92
5.2.2 CYLD in phosphorylated in an IKK/TAK1-dependent manner 94
5.3 Identifying novel TNF-induced CYLD phosphorylation sites 96
5.3.1 LC-MS/MS analysis to identify novel TNF-induced phosphorylation sites 96
5.4 S568 and S418 regulate the DUB activity of CYLD 99
5.4.1 $CYLD^{S568A}$ and $CYLD^{S418A/S568A}$ stable lines display enhanced phospho-mediated signalling 100
5.4.2 $CYLD^{S418A/S568A}$ shows enhanced pro-inflammatory transcript production in TNF and NOD2 signalling 101
5.4.3 $CYLD^{S418A/S568A}$ shows enhanced CXCL-8 production with NOD2 signalling 103
5.4.4 $CYLD^{S418A/S568A}$ impairs CYLDs ability to regulate the ubiquitin landscape of the NOD2 receptor complex 103
5.4.5 $CYLD^{S418A/S568A}$ shows deregulation of TNFR complex I ubiquitin landscape 106
5.5 Discussion 108

6 Discussion 111
6.1 CYLD, OTULIN, and A20 in immune signalling 111
6.2 The recruitment of DUBs to LUBAC 113
6.3 Summary and future perspectives 116

7 Appendices 118
7.1 Supplementary figures 118
7.2 Publications 125

References 126

List of Figures 141

List of Tables 147

List of Abbreviations

A . . . . . Alanine

APS . . . . . Ammonium peroxide sulphate

BCL-2 . . . . . B-cell lymphoma 2

BSA . . . . . Bovine serum albumin

C- . . . . . Carboxy -

CARD . . . . . Caspase recruitment domain

Cas . . . . . CRISPR associated

CD . . . . . Cluster of differentiation

cIAP . . . . . Cellular inhibitors of apoptosis

CLR . . . . . C-type lectin receptor

Conc. . . . . . Concentration

CRISPR . . . Clustered regularly interspaced short palindromic repeats

CYLD . . . . . Cylindromatosis

DAMPs . . . . Danger-associated molecular patterns

DD . . . . . Death domain

ddH_2O . . . . . double-distilled H_2O

DED . . . . . Death effector domain

DISC . . . . . Death inducing signalling complex

DMEM . . . . Dulbecco's modified eagle medium

DMSO . . . . . Dimethyl sulphoxide

DNA . . . . . Deoxyribonucleic acid

dNTP . . . . . Deoxyribonucleotide triphosphate

DR . . . . . Death receptor

DTT . . . . . Dithiothreitol

DUB . . . . . Deubiquitinase

E1 . . . . . Enzyme 1 (Ubiquitin-activating)

E2 . . . . . Enzyme 2 (Ubiquitin-conjugating)

E3 . . . . . Enzyme 3 (Ubiquitin-ligase)

e.g. . . . . . Exempli gratia (for example)

ECL . . . . . Enhanced chemiluminescence

EDTA . . . . . Ethylene diamine tetra acetic acid

ERK . . . . . Extracellular-signal regulated kinase

et al . . . . . Et alia

EV . . . . . Empty vector

FACS . . . . . Fluorescence assisted cell sorting

FADD . . . . . Fas-associated protein with death domain

FBS . . . . . Foetal bovine serum

FLIP . . . . . FLICE-inhibitory protein

h . . . . . Human

HECT . . . . . Homologous with E6-associated protein C-terminus

HOIL-1 . . . . Heme-oxidised IRP2 ubiquitin ligase 1

HOIP . . . . . HOIL-1 interacting protein/RNF31

HRP . . . . . Horseradish peroxidase

IAP . . . . . Inhibitor of apoptosis

IBD . . . . . Inflammatory bowel disease

IBR . . . . . In-between RING

IFN . . . . . Interferon

IKK . . . . . IκB kinases

IL . . . . . Interleukin

IP . . . . . Immunoprecipitation

IκBα . . . . . Inhibitor of kappa B alpha

JNK . . . . . c-Jun N-terminal kinase

K . . . . . Lysine

kDa . . . . . Kilodalton

KO . . . . . Knock out

lN_2 . . . . . Liquid nitrogen

L . . . . . Leucine

LB medium . Luria-broth medium

LPS . . . . . Lipopolysaccharide

LUBAC . . . . Linear ubiquitin chain assembly complex

m . . . . . Murine

M . . . . . Methionine

MAPK . . . . Mitogen activated protein kinase

MAPKK . . . Mitogen activated protein kinase kinase

MAPKKK . . Mitogen activated protein kinase kinase kinase

MEF . . . . . Mouse embryonic fibloblast

MLKL . . . . . Mixed lineage kinase domain-like

MS . . . . . Mass spectrometry

N- . . . . . Amino-

Nec1s . . . . . Necrostatin-1 specific

NEDD8 . . . . Neural precursor cell-expressed developmentally down regulated gene 8

NEMO . . . . NFκB essential modulator protein/IKKγ

NLR . . . . . Nod-like receptor

NOD . . . . . Nucleotide-binding oligomerisation domain-like

OTULIN . . . Ovarian tumour deubiquitinase with linear linkage specificity

P . . . . . Proline

P/S . . . . . Penicillin/streptomycin

PAGE . . . . . Polyacrylamide gel electrophoresis

PAMP . . . . . Pathogen-associated molecular pattern

PBS . . . . . Phosphate-buffered saline

PBST . . . . . Phosphate-buffered saline + 0.1% Tween 20

PCR . . . . . Polymerase chain reaction

PIM . . . . . PUB-interacting motif

PRR . . . . . Pattern-recognition receptor

PTM . . . . . Post-translational modification

PUB . . . . . N-terminal PNGase/UBA or UBX containing protein domain

RBR . . . . . RING-in-between-RING

RHIM . . . . . RIP homotypic interaction motif

RING . . . . . Really interesting new gene

RIPK . . . . . Receptor interacting protein kinase

RLR . . . . . RIG-I like receptor

RNA . . . . . Ribonucleic acid

RT . . . . . Room temperature

S . . . . . Serine

SDS . . . . . Sodium dodecyl sulphate

SDS-PAGE . . Sodium dodecyl sulphate polyacrylamide gel electrophoresis

SHARPIN . . SHANK-associated RH domain interactor

SMAC . . . . . Second mitochondria-derived activator of caspases

SOC . . . . . Super optimal broth with catabolic repressor

SPATA2 . . . . Spermatogenesis-associated protein 2

SUMO . . . . Small ubiquitin-like modifier

T . . . . . Threonine

TAB2/3 . . . . TAK1 binding protein 2/3

TAK1 . . . . . TGF activated kinase 1

TBS . . . . . Tris-buffered saline

TBST . . . . . Tris-buffered saline + 0.1% Tween 20

TGF . . . . . Transforming growth factor

TLR . . . . . Toll-like receptor

TNF . . . . . Tumour necrosis factor

TNFR . . . . . Tumour necrosis factor receptor

TNF-RSC . . Tumour necrosis factor receptor signalling complex

TRADD . . . TNFR type 1 - associated death domain protein

TRAIL . . . . TNF-related apoptosis-inducing ligand

UBA . . . . . Ubiquitin associated

UBAN . . . . . Ubiquitin binding in ABIN and NEMO

UBC . . . . . Ubiquitin-conjugating

UBD . . . . . Ubiquitin binding domain

UBE . . . . . Ubiquitin-activating enzyme

Ubl . . . . . Ubiquitin-like protein

UCH . . . . . Ubiquitin C-terminal hydrolase

UIM . . . . . Ubiquitin-interaction motif

USP . . . . . Ubiquitin-specific protease

WT . . . . . Wild type

ZnF . . . . . Zinc finger

Symbols and Units

α . . . . . Alpha

β . . . . . Beta

γ . . . . . Gamma

ϵ . . . . . Epsilon

^{o}**C** . . . . . Degree centigrade

g . . . . . Gram

h . . . . . Hour

L . . . . . Litre

m . . . . . 10^{-3}

M . . . . . Molar

min . . . . . Minutes

O/N . . . . . Overnight

RT . . . . . Room temperature

sec . . . . . Second

μ . . . . . 10^{-6}

1 Introduction

Contents

1.1 The ubiquitin system 2
1.1.1 Ubiquitin and ubiquitin-like proteins 2
1.1.2 Ubiquitination 3
1.1.3 The structure of ubiquitin modifications 8
1.1.4 Ubiquitin-binding domains 9
1.1.5 Deubiquitinating enzymes 11
1.1.6 Cellular functions of ubiquitin chains 15
1.2 The innate immune system and pattern recognition receptors (PRRs) 17
1.2.1 Pattern recognition receptors (PRRs) 18
1.2.2 NOD1 and NOD2 receptor signalling 22
1.2.3 TNF receptor signalling 26
1.3 The Linear ubiquitin chain assembly complex (LUBAC) 28
1.3.1 The structure and function of HOIP 29
1.3.2 The association of CYLD and OTULIN with LUBAC . 31
1.3.3 Cellular functions of LUBAC 31
1.4 The deubiquitinase, CYLD 34
1.4.1 Structure and function of CYLD 34
1.4.2 CYLD in immune signalling 35
1.4.3 Regulation of CYLD function 36
1.5 Spermatogenesis-associated protein 2 36
1.6 Aims of the study 38

1.1 The ubiquitin system

According to the international human genome consortium, it is estimated that the human genome encodes roughly 20,000 proteins and, to date, over 200 distinct modifications of amino acid residues have been described [1]. One of the most widespread and dynamic of these modifications is the covalent attachment of ubiquitin to residues, known as ubiquitination, a process deemed so important that its discovery won the 2004 Nobel prize in Chemistry [2].

1.1.1 Ubiquitin and ubiquitin-like proteins

Ubiquitin

Ubiquitin is a highly conserved 76 amino acid protein present in all eukaryotes but absent from bacteria and archaea, which have separate but functionally similar systems known as pupylation and SAMPylation respectively [3–5]. It acts as a post translational modification (PTM) through its conjugation to lysine (Lys; K) residues of substrate proteins via its C-terminal glycine residue (a process known as ubiquitination). In the 1980's, this conjugation of ubiquitin to target substrates was discovered as a PTM leading to proteasomal degradation of the substrates [6–8]; however, in addition to proteasomal degradation, ubiquitination has now also been characterised to have non-degradative functions such as modulating protein functions and mediating assembly of multi-protein signalling complexes [2, 9].

The translation of ubiquitin is mediated via four genes. UBA52 and RPS27A specifically encode for a single copy of ubiquitin fused to the ribosomal proteins L40 and S27A, respectively; whereas the UBB and UBC genes encode for polyubiquitin precursors (chains of ubiquitin akin to 'beads on a string', which must be processed prior to their cellular use) [10, 11].

Ubiquitin-like proteins

Ubiquitin-like proteins (Ubls) consist of a family of around 17 proteins (including NEDD8 and SUMO), which share structural and evolutionary similarity to ubiquitin. Each member possesses a β-grasp fold consisting of five β-sheets partially wrapped

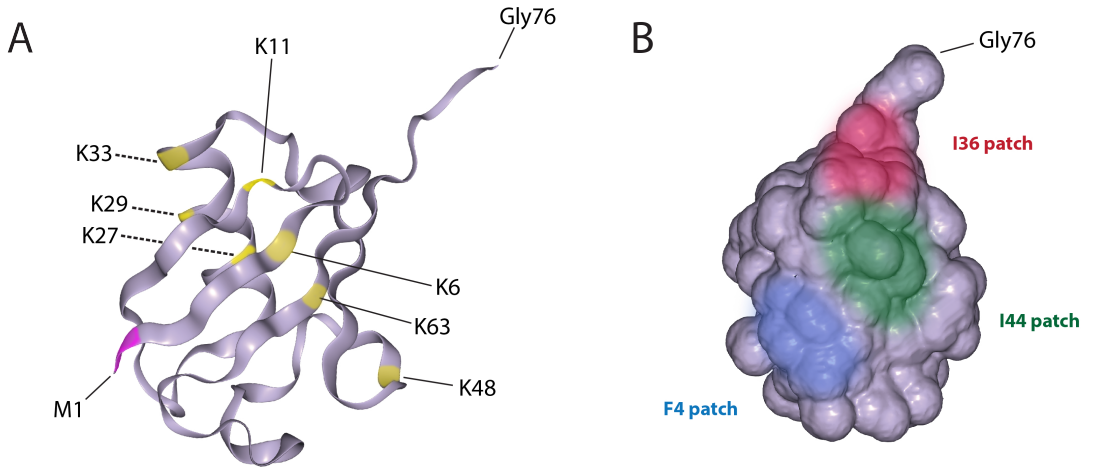


Figure 1.1: Crystal structure of ubiquitin. (A) Ribbon structure of ubiquitin highlighting key lysine residues (yellow) and the N-terminal methionine (pink). Structure from PDB code: 1UBQ [12]. (B) Structure of ubiquitin (rotated relative to ribbon structure) showing each of the hydrophobic patches implicated in typical ubiquitin interactions with ubiquitin-binding domains (UBDs).

around a central α-helix [13, 14]. They are also divided into two sub-groups based on whether they are conjugated to substrates, with type I, but not type II, Ubls being conjugated [15].

Type II Ubls are typically multi-domain proteins which cannot be conjugated to substrates and contain members found in aspects of the ubiquitination cascade including E1 enzymes, E3 enzymes, and deubiquitinating enzymes (DUBs) - discussed later [14]. In contrast, type I Ubls are activated and conjugated to substrates and include NEDD8, SUMO, ATG8, ATG12, FAT10, UFM1, and ISG15 [13, 14].

1.1.2 Ubiquitination

Ubiquitination as a PTM involves the reversible, ATP-dependent attachment of a ubiquitin protein to a residue on a substrate protein through a three-step enzymatic cascade involving a ubiquitin-activating enzyme (E1), a ubiquitin-conjugating enzyme (E2), and a ubiquitin ligase (E3) [10, 11].

An E1 activates ubiquitin through ATP-hydrolysis to generate a high energy E1:ubiquitin thioester between its active site cysteine residue and the C-terminal carboxy group of ubiquitin. The E1 subsequently binds an E2 and transfers the

ubiquitin to the active site cysteine of the E2 to create an E2:ubiquitin thioester. In the final step, ubiquitin is conjugated to a substrate via an E3, which mediates the formation of a covalent isopeptide bond between the carboxy group of the C-terminal of ubiquitin and the ϵ-amino group of a Lys residue in the target substrate protein (figure 1.2) [10, 11]. The conjugation of a single ubiquitin to a substrate is known as monoubiquitination and may occur on a single, or multiple (multi-monoubiquitination), sites (figure 1.4).

Ubiquitin itself has seven lysine residues (K6, K11, K27, K29, K33, K48, K63), and an N-terminal methionine (Met; M), which can act as a target site for conjugation of a second ubiquitin. In this process, the first 'acceptor' ubiquitin pre-conjugated to a substrate protein acts as a substrate for the conjugation of a second 'donor' ubiquitin to one of its Lys residues, or the Met residue, to create a di-ubiquitin chain. Subsequent reactions may then build upon this to create polyubiquitin chains containing many ubiquitin moieties. Conjugation of ubiquitin to a Met residue appears unique to ubiquitin as a substrate (as it is usually conjugated to Lys residues in substrates) and, as opposed to an isopeptide bond for conjugation to Lys, its linkage to Met creates a canonical peptide bond [16]. These polyubiquitin chains are characterised by the Lys (or Met) they are linked by e.g. a polyubiquitin chain where each ubiquitin moiety is linked via their Lys at position 48 is designated a K48-linked chain. This is true for homogeneous polyubiquitin chains where each subsequently attached ubiquitin is conjugated to the Lys or Met at the same position as previous; however, heterotypic mixed linkage chains are also possible whereby the Lys conjugation varies along the chain. Furthermore, chains may branch through conjugation of multiple 'donor' ubiquitins to a single 'acceptor' ubiquitin.

Enzymes mediating the ubiquitin cascade

The human genome encodes two E1s, 37 E2s, and around 600 E3s for the ubiquitination cascade [17–23].

Showing only modest evolution from slime-mould to humans, E1s consist of three domains: Firstly, they contain an adenylation domain consisting of two ThiF-

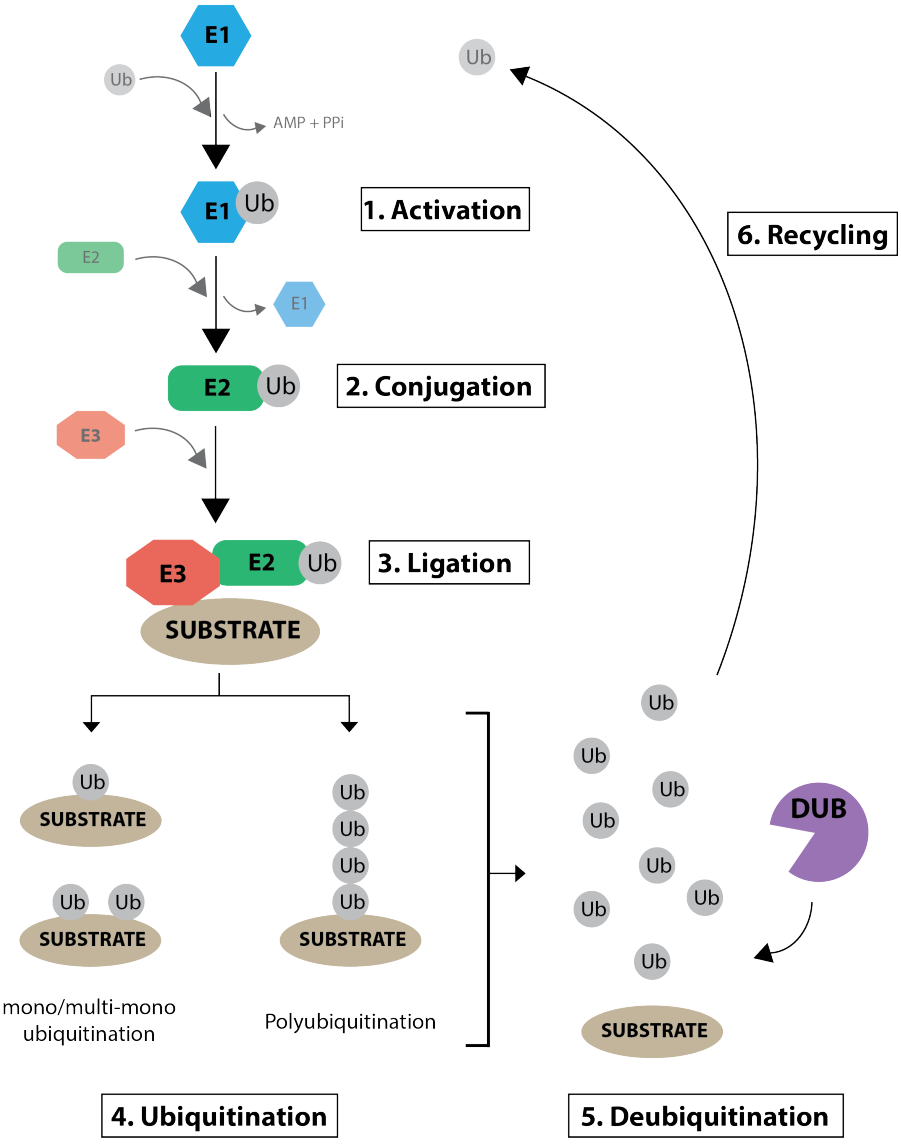


Figure 1.2: The enzymatic cascade of ubiquitination. Diagrammatic representation of the enzymatic cascade for: 1. Activation of the ubiquitin by an E1; 2. The E1 facilitates the transfer of the ubiquitin to the activate site cysteine of an E2; 3. an E3 facilitates the transfer of ubiquitin to a lysine residue on a target protein; 4. ubiquitinated substrates me be modified in various ways include the addition of a single (mono) ubiquitin on one or more (multi-mono) sites. Alternatively, ubiquitin may be conjugated to an existing ubiquitin molecule to facilitate the production of polyubiquitin chains; 5. a group of enzymes collectively known as deubiquitinating enzymes (DUBs) facilitates the removal of these ubiquitins; 6. free ubiquitin is often recycled for conjugation to another substrate in a separate reaction.

homology motifs, which binds ATP and ubiquitin; secondly, a catalytic cysteine domain (CCD), which is the acyl carrier for ubiquitin; and thirdly, a C-terminal β-grasp fold, which binds to specific E2s [18, 24, 25].

E2 enzymes each contain a ubiquitin conjugating (UBC) domain, which harbours a highly conserved active site cysteine residue [26]. Some E2s are restricted to conjugating ubiquitin to a substrate and so can only create monoubiquitin modifications; whereas other E2s facilitate chain elongation through conjugation to ubiquitin as a substrate [26]. E2s also play a major role in determining the type of polyubiquitin linkage produced. For example, the dimeric E2 complex UBE2N-UBE2V2 exclusively forms K63-linked polyubiquitin chains, whilst UBE2C and UBE2S mediate K11-linked polyubiquitin chain formation [26–28]. However, not all E2s are limited to specifying a particular type of polyubiquitin linkage, as shown by the non-specific UBE2D family members [26].

Ubiquitin ligases (E3s) represent the largest group of the enzymes involved in the ubiquitin cascade and can provide specificity due to interacting with both the E2:ubiquitin and the substrate to be ubiquitinated [26, 29]. These interactions are mediated by E3 binding domains specific to E2s and substrates, which recognise specific structural elements or sequences [30–32].

The E3 family consists of three main sub-groups, the Homologous to E6-AP C-terminus (HECT)-, the Really interesting new gene (RING)-, and the RING-inbetween-RING (RBR)-containing E3s.

Around 30 HECT E3s exist in the human genome, which form a covalent E3:ubiquitin thioester intermediate prior to conjugation of the ubiquitin to the substrate. This occurs via transfer of the activated ubiquitin from the E2:ubiquitin to the active site cysteine within the HECT domain of the E3. The conjugation of the ubiquitin to the substrate then occurs directly from the E3 and, as such, this sub-group of E3s may confer chain specificity independent of the E2 (figure 1.3) [33, 34].

RING E3s constitute the largest group of E3s with around 600 members [35]. The RING domain of this subgroup contains a conserved set of cysteine and histidine

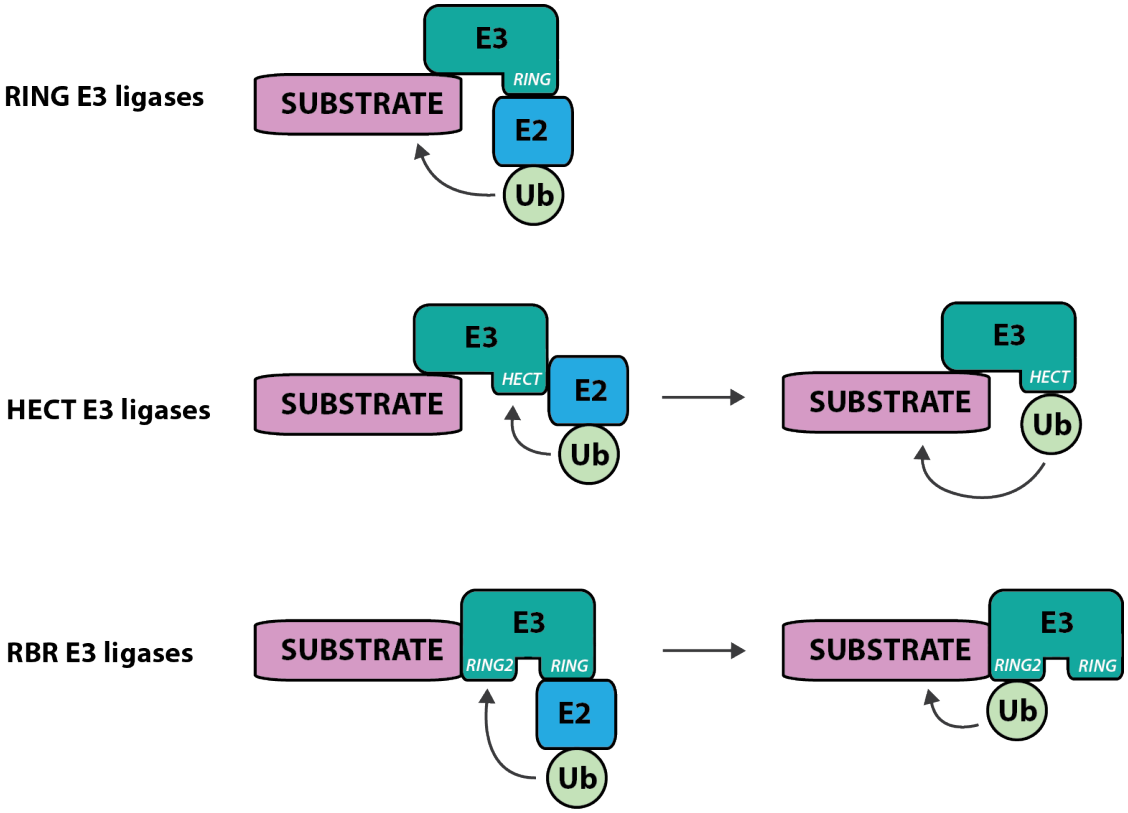


Figure 1.3: Cartoon representation of the E3 ligase classes. Diagrammatic representation of the mode of action of each class of E3.

residues, which coordinates two zinc ions to maintain domain structure. In contrast to the HECT E3s, RING-containing E3s do not have a bona fide catalytic centre and as such do not form an intermediate E3:ubiquitin thioester prior to ubiquitin ligation to substrates. Instead, these enzymes simultaneously bind both the E2:ubiquitin and the target substrate, bringing them in close proximity to allow for the transfer of ubiquitin to the substrate (figure 1.3) [35]. As the polyubiquitin linkage type is generally determined by the factor forming the last thioester intermediate with ubiquitin, RING E3s generally do not confer linkage specificity but rely on the specificity of the E2 enzyme [26, 35].

RBR E3s function through a hybrid RING/HECT mechanism and contain two RING domains and an in-between RING (IBR) domain, which they utilise for their ligase activity. Ubiquitin transfer is initiated by a canonical interaction between their RING1 domain and the E2:Ub to facilitate the formation of an intermediate HECT-type thioester between the ubiquitin and their RING2 domain. Ubiquitin

is then transferred from the RING2 domain to the target substrate, explaining how some RBR E3s (e.g. HOIP) can determine linkage type independent of the E2 (figure 1.3) [2].

1.1.3 The structure of ubiquitin modifications

Proteins can be ubiquitinated on a single Lys residue (monoubiquitination), on two or more lysine residues (multi-monoubiquitination), or conjugated into polyubiquitin chains. Recognition of these modifications by ubiquitin-interacting proteins is via a set of hydrophobic patches located around the isoleucine 44 (I44 patch), isoleucine 36 (I36 patch), or phenylalanine 4 (F4 patch) (figure 1.1B). The structure of ubiquitin(s) attached to a substrate, and the distribution/availability of these patches constitutes the 'signal' of each modification [2].

Monoubiquitination and multi-monoubiquitination modifications constitute a significant portion of total ubiquitin modifications within cells and hold key roles in various cellular processes e.g. in DNA repair and endosomal sorting of membrane receptors [36, 37]. It is believed that recognition of these modifications involves interacting proteins simultaneously recognising the ubiquitin (via the I44 patch) in combination with the substrate [38, 39].

The seven ϵ-amino groups of the Lys residues, and α-amino group of the N-terminal met, of ubiquitin can all serve as substrates for ubiquitination and, as these are spread over the surface of ubiquitin, this imparts unique structural properties for each chain type when conjugated into polyubiquitin modifications.

Structural studies on the conformation of each linkage type shows they adopt extended or closed conformations [2]. K6, K11, and K48 linked chains form more compact structures where adjacent ubiquitin moieties form extensive interactions with each other; however, K63, M1, K29, and K33 chains form extended structures where there is minimal contact between ubiquitin moieties other than the conjugation site (figure 1.4) [40].

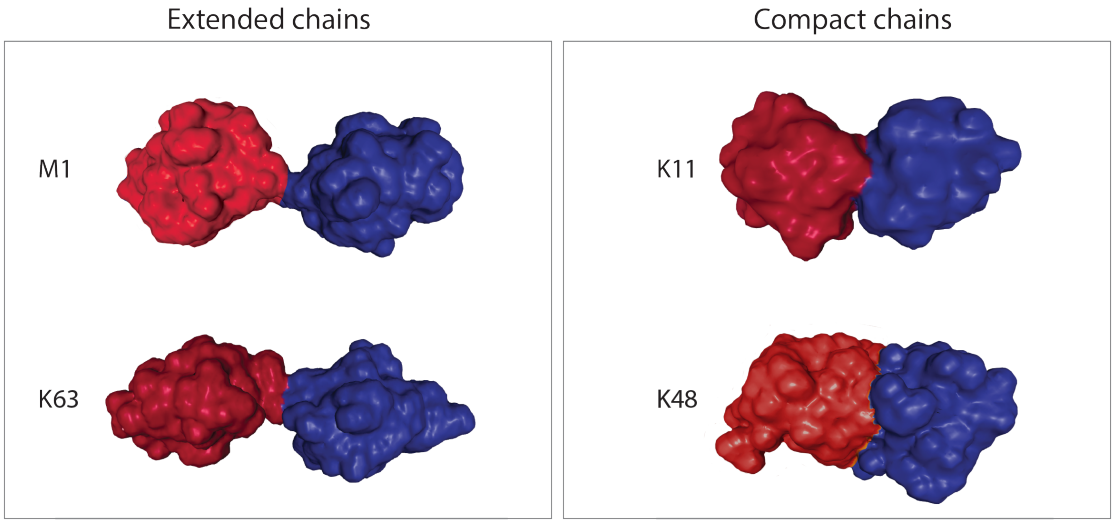


Figure 1.4: Structural representation of closed and extended chains. Shown are examples of the extended (M1 (2W9N) and K63 (2JF5)) and closed (K11 (2MBO) and K48 (5GOI)) structure, which polyubiquitin chains adopt.

1.1.4 Ubiquitin-binding domains

The human genome encodes more than 20 families of proteins harbouring UBDs able to interact with ubiquitin including but not limited to: ubiquitin-associated (UBA) domains, ubiquitin-interacting motifs (UIMs), double-sided ubiquitin-interacting motifs (DUIMs), Npl4 zinc finger (NZF) domains, coupling of Ubiquitin-conjugation to endoplasmic reticulum (ER) degradation (CUE) domains, ubiquitin-conjugating enzyme variants (UEVs), GRAM-like ubiquitin-binding in Eap45 (GLUE), Vps / HRS / STAM (VHS) domains, Golgi-associated gamma-adaptin homologous and TOM1 (GGA) domains, and polyubiquitin-associated zinc finger (PAZ) domains [41, 42].

These are relatively small domains of around 20-150 amino acids that bind non-covalently to ubiquitin and display greater affinity for polyubiquitin chains than monoubiquitin modifications (Km $>$ 100 μM), furthering the hypothesis that monoubiquitin modifications recruit proteins recognising both the ubiquitin and substrate [36, 37, 41–43].

Most UBDs recognise the I44 patch, though some also interact with the other hydrophobic patches and surface features of ubiquitin including an acidic hydrophilic

asparagine 58 (N58) - centred face and the extreme C-terminus of ubiquitin (when not conjugated to a substrate) [44]. Importantly, binding to these patches is not mutually exclusive and can allow for recognition by multiple UBDs (from the same or different ubiquitin-binding proteins) [45]. An example of this is the association of the UBA domain of p62, and the ZnF domain of ZNF216, with the I44 and N58-centred face of ubiquitin as they bind simultaneously and unhindered to a single ubiquitin moiety [45].

The interactions between these sites and the UBDs occurs with low affinity, particularly for monoubiquitin. However, multiple low-affinity interactions involving tandem UBDs are the basis for higher affinity binding (1 - 15 μM) with polyubiquitin chains driven by avidity effects [46]. This reliance on the avidity effects of multiple interactions is important as the cellular pool of ubiquitin is estimated to exist in the low micromolar range [47].

The distance between the I44 patches of ubiquitin in each linkage type can also allow for the specific recognition by ubiquitin-binding proteins e.g. through a spacer of a defined length between their UBDs. This is the case for receptor associated protein 80 (RAP80: a DNA repair protein), a subunit of the BRCA1 E3, which uses two UIMs separated by seven amino acids to specifically recognise K63 chains [48]. TAK1-binding protein 2 (TAB2), however, uses chain flexibility to achieve specificity through binding of its NZF domains to K63-linked chains, bending them to a more 'closed' conformation [49].

The flexibility and structure of particular linkages can also be used to achieve specificity by the binding of a UBD to multiple ubiquitin moieties simultaneously. This is shown with the UBA domain (UBA1) of hHR23A, which inserts between two K48-linked ubiquitin moieties to make contact with the I44 patches of both molecules [50].

Whilst a variety of mechanisms are employed by UBDs to bind specific linkages, it is important to note that they can also be subject to regulation by a variety of PTMs. For example, UBD-containing proteins can be monoubiquitinated in a process known as coupled-monoubiquitination. This occurs independently of E3s

but through the interaction of a UBD with a reactive E2:ubiquitin complex [51]. This is thought to regulate UBDs by inhibiting their ability to bind ubiquitin in *trans* by promoting intramolecular binding of the UBD to the attached ubiquitin [51]. Another PTM shown to mediate UBD interactions is phosphorylation e.g. phosphorylation of the UBD domain of p62 increases its affinity for K63 chains and enhances its ability to shuttle protein aggregates to autophagosomes [52].

1.1.5 Deubiquitinating enzymes

Ubiquitination is a dynamic process regulating a variety of cellular functions and, like other PTMs, it has the potential to be reversed. This is achieved by a group of peptidases called deubiquitinating enzymes (DUBs). The human genome encodes around 100 DUBs, which can be divided into six families based on their sequence and domain conservation: USPs (ubiquitin specific proteases), UCHs (ubiquitin-carboxy-terminal hydrolases), MJDs (Machado-Josephin domain-containing proteases), OTUs (ovarian tumour proteases), MINDYs (motif-interacting with ubiquitin-containing novel DUB family), and JAMMs (JAB1, MPN, MOV34 family). These enzymes are cysteine proteases with the exception of the JAMM family, which are metalloproteases [53, 54]. Furthermore, whilst there are around 100 identified DUBs, around 10 of these are not catalytically active (table 1.1) [54].

DUB family	Total members	Active members
USP	57	51
OTU	16	15
JAMM	12	9
MINDY	4	4
MJD	4	4
UCH	4	4

Table 1.1: The total members of each DUB family with details of the number of catalytically active members. Table adapted from [55].

The function of these families can be divided through their roles in ubiquitin processing such as cleaving ubiquitin directly from substrate proteins, editing ubiquitin chains, and processing ubiquitin precursors [53]. For example, the four

members of the UCH family of DUBs are primarily responsible for the processing of the ubiquitin precursors into single ubiquitin proteins.

DUBs may also be specific for the cleavage of monoubiquitin modifications or preferentially hydrolyse polyubiquitin chains. Furthermore, DUBs which regulate the formation of polyubiquitin chains can also have additional specificity by displaying exo- or endo-deubiquitinating activity, cleaving chains either from the distal end of a chain or internally, respectively [53].

USP DUBs constitute the largest family with around 57 members and are generally unspecific, instead being targeted to substrates via interaction domains or adaptor proteins [53, 56]. However, linkage specific USPs have been described e.g. USP14, which hydrolyses K48 chains; and cylindromatosis (CYLD) which shows specificity for M1 and K63 chains [53]. In contrast, the 16 members of the OTU family appear to have specificity to one or a few linkages with members now characterised for each type of polyubiquitin chain e.g. OTUD3 cleaving K6 chains, OTUD1 cleaving K63 chains, Cezanne cleaving K11 chains, TRABID cleaving K29 and K33 chains, OTUB1 cleaving K48 chains, and OTULIN cleaving M1 chains [53, 57, 58]. The 12 JAMM family members appear to show specificity with four members being described to be K63 chain specific [53]. The most recently discovered four members of the MINDY DUB family also show specificity as all members exclusively hydrolyse K48 chains [54].

In addition to the six 'canonical' DUB families, a recent study has identified an additional family with only one, K63-specific, human member known as ZUFSP (also known as ZUP1 and C6orf113) [59]. The crystal structure of this DUB was solved and, in complex with propargylated ubiquitin, shows a fold similar to UFM1- and Atg8-specific proteases, but an active site similar to the canonical DUB families. These ZUFSP family members (observed between humans and yeast) show no inherent chain specificity from their catalytic domains but instead harbour a variety of specificities conferred by multiple UBDs [59].

Regulation of DUBs

DUBs can be subject to a variety of modifications to regulate their function including the conjugation of ubiquitin or Ubl modifiers. An example of this is Ataxin-3, a DUB which, following monoubiquitination, displays enhanced catalytic activity [60]. SUMOylation as a Ubl modifier also has been shown to be conjugated to DUBs. An example of this is SUMOylation of the first UIM of USP25, which acts to inhibit its DUB activity [61].

One of the simplest mechanisms to limit the function of DUBs is to limit their abundance through transcriptional regulation. This is exemplified by the cell-cycle-dependent translation of USP37, a DUB whose transcription is directed by E2F transcription factors and is present at high levels during the G1/S transition [62]. This cell cycle-dependent mechanism of transcriptional regulation is also true of other DUBS, particularly USP33, which has established roles in centrosome duplication [63]. Transcriptional regulation of A20 and CYLD has also been shown to be upregulated in response to NF-κB activation in a feedback loop where they then negatively regulate the pathway [64, 65].

Post-translationally, the regulation of DUB function can be achieved through their degradation. This can be achieved through their ubiquitination to target them to the proteasome and, in fact, some DUBs self-ubiquitinate to achieve this. An example of this is USP4, which auto-ubiquitinates and mediates its own degradation within the TGFβ signalling pathway [66].

Interaction partners of DUBs

Interaction partners of DUBs can have significant impact on their function. This was first described for all proteasome-associated DUBs responsible for cleaving ubiquitin (Rpn11, USP14, and UCH37), where their catalytic activity is significantly activated upon association with the 19S subunit [67]. UCH37 is present in an additional chromatin-remodelling complex, known as INO80, in which it is catalytically inactive [68]; however, the mechanism governing this control of its catalytic activity in different complexes was solved through the discovery of a DEUBAD

(deubiquitinase adaptor) domain in its interaction partners, Rpn13/ADRM1 in the proteasome, and INO80G/NFRKB in the INO80 complex, which induces particular structural rearrangements of UCH37 rendering it inactive or active in each respective complex [69].

The JAMM DUB, BRCC36 functions within two complexes in a similar manner, being incorporated into the nuclear ARISC complex (abraxas complex) and the cytosolic BRISC complex (BRCC36 isopeptidase complex) [70, 71]. Free-BRCC36 is predominantly inactive but, upon association with the BRISC complex, it is activated by Abo1, and, as part of the nuclear ARISC complex, it is activated by the Abraxas and RAP80 subunits [70, 71]. Whilst association with these complexes activates the catalytic activity of BRCC36, it also determines its cellular localisation. This allows activation of this DUB in particular cellular contexts to mediate a specific role i.e. the DNA damage repair pathway within the ARISC complex, and stabilisation of the type I interferon (IFN) receptor in the BRISC complex, through preventing its endocytosis and lysosomal degradation [72, 73].

The Spt-Ada-Gcn5-acetyl transferase (SAGA) complex controls the DUB function of USP22 [74]. Specifically, it acts as a transcriptional coactivator through catalysis of acetylation and ubiquitination of histone H2B. This deubiquitinating activity of the complex is controlled by USP22, which is the only DUB within the complex; however, additional subunits within the complex (collectively forming the deubiquitinating module (mDUB)) form extensive contacts with each other to stabilise USP22, allowing it to perform its DUB function [74].

Other DUBs also require interaction partners for activation of their function including USP1, USP12, and USP46, which are bound by USP1-associated factor 1 (UAF1; also known as WDR48) and WD-repeat containing proteins [75, 76]; USP10, which interacts with the Ras-GTPase-activating protein G3BP1 to modulate its catalytic activity [77]; and USP8 and AMSH interactions with signal transducing adaptor molecule 1 (STAM) and endosomal sorting complex required for transport III (ESCRT III) components to ensure appropriate cellular localisation of these DUBs for regulation of endocytosis [78].

CYLD has also recently been reported by numerous studies to interact with the adaptor protein, spermatogenesis associated protein 2, to module its function in NF-κB signalling and cell death (discussed in detail in chapter 4 and 6) [79–83].

1.1.6 Cellular functions of ubiquitin chains

The different chain topology of each ubiquitin modification allows for specific interactions with ubiquitin-binding proteins and thus creates particular cellular roles for each linkage type.

The most extensively studied of these are K48 chains. K48 linked chains are the most commonly occurring linkage within cells and are the classical signal for proteasomal degradation, with tetramers of K48 chains being the proposed requirement for efficient proteasomal targeting [84]. This tetraubiquitin requirement remained the dogma in the field even though structural studies of the 26S proteasome and its associated DUBs did not explain this requirement [85, 86]. Furthermore, some efficiently degraded proteins (such as Cyclin B1) show multiple short polyubiquitin chains of different linkages rather than a single, longer K48 chain and, moreover, K48 chains have been shown to be present on substrates that are not degraded (though K48 chain protection by UBDs likely plays a role here) [87–89]. Whilst K48 chains typically target chains for proteasomal degradation, it is important to note that this degradation of substrates plays important roles in a variety of cellular pathways including NF-κB signalling and cell cycle progression. Thus K48 chains are essential regulators of not only protein degradation, but many cellular pathways through this mechanism.

K63 chains serve non-proteolytic functions and have documented roles in a variety of cellular processes including endocytosis, vesicular trafficking, the DNA damage response, and immune signalling [9]. The most established role for this linkage lies within inflammatory signalling and NF-κB activation e.g. stimulation of the IL-1, NOD1/2, TNF, or toll-like receptor (TLR) pathways leads to the conjugation of K63 chains, which in turn recruit the TGFβ-activated kinase 1 (TAK1) via

the TAB2/3 ubiquitin-binding proteins, and leads to the phosphorylation and activation of the IKK complex [2].

M1 chains were first identified through the discovery of the only known E3 ligase to produce them, known as linear ubiquitin chains assembly complex (LUBAC), and since have emerged as important regulators of inflammatory signalling. In NF-κB signalling, the UBAN domain of the IKK subunit, NEMO (IKKγ), binds M1 chains to facilitate full activation of the IKK complex [16, 90]. This in turn facilitates transcriptional responses in response to a variety of stimuli including tumour necrosis factor (TNF) and IL-1 [91, 92].

In addition to these well characterised chain types, cellular roles for the other possible linkages have been described.

Next to K48, K63, and M1 chains, K11 chains are the most extensively studied. They have emerged as an additional proteasomal degradation signal used mostly in cell cycle regulation and are conjugated by the anaphase promoting complex/cyclosome (APC/C) [93, 94]. Furthermore, they have been implicated in various other cellular pathways including: inflammatory signalling via the TNF receptor; non-canonical NF-κB activation; T cell activation; and EGF receptor trafficking [95–97]; However, of note is that a direct link with these other pathways has not been established but has been inferred through the roles of the K11-specific DUBs, Cezanne and Cezanne2.

The cellular roles of K6, K27, K29, and K33 chains are less established but intriguing: K6 chains have documented roles in the DNA damage response, as reports suggest that the BRCA1 E3 complex conjugated K6 chains to its substrates [98]; K27 chains have reported functions in PARKIN-mediated regulation of mitophagy [99]; K29 chains has potential roles in lysosomal degradation but, through inferring its function via the K29 DUB, TRABID, has reported roles in Wnt-signalling and epigenetic regulation [100, 101]; and K33 chains have implicated roles in membrane trafficking as the BTB domain-containing adaptor protein, KLHL20, works with a Cullin-3 E3 complex to conjugate K33 chains on Coronin7 to promote its recruitment to the trans-golgi network (TGN) [102].

Branched and mixed chains

As K63 and M1 chains both have crucial roles in inflammatory signalling pathways,their relative importance was thoroughly debated within the field. This was resolved upon the discovery that K63 and M1 chains are able to form mixed or branched architectures in this system [103]. These mixed chains propose a solution as to how distinct signalling modules are recruited and brought in close proximity for their activation. For example, the IKK complex subunit NEMO, in addition to its M1-specific UBAN domain, contains a ZNF UBD that has been reported to preferentially bind to K63 chains. Having this dual specificity may allow the IKK complex to be targeted to M1/K63 chain junctions within the receptor complex for interaction with other signalling modules [104].

K48/K11 branched chains have been observed to be conjugated by the APC/C as a proteasomal signal and also some viral E3s assemble K11/K63 chains to facilitate MHC-I internalisation (though viral-induced branched chains of all linkage types have been observed) [105–108].

K48/K63 branched chains were also identified in a recent study whereby, in IL-1β signalling, the K48 chains on K63 chains protects them from deubiquitination by the DUB, CYLD, therefore acting to enhance NF-κB signalling [109]. Furthermore, K29 chains are consistently part of heterotypic chains when enriched from cells [11, 110–112].

1.2 The innate immune system and pattern recognition receptors (PRRs)

Multicellular organisms are constantly exposed to a variety of invading pathogens e.g. viruses, bacteria, and fungi. To maintain host-microbial homeostasis and defend against potential threats, evolution has provided us with two effector systems, which ensure the detection and eradication of pathogens: the innate and the adaptive immune system.

The innate immune system recognises invariant structures of invading microorganisms through a defined repertoire of germ-line encoded pattern recognition receptors (PRRs). In contrast, the adaptive immune system typically involves the generation of highly specific *de novo* receptors through somatic recombination, which requires massive expansion of responding T and B cell populations [113].

1.2.1 Pattern recognition receptors (PRRs)

PRRs are present on a variety of cell types but are heavily represented on cells of the innate immune system such as macrophages, dendritic cells, and neutrophils. These recognise conserved features of microbes known as pathogen-associated molecular patterns (PAMPS) [113]. However, in addition to the recognition of exogenous structures, PRRs can also recognise certain endogenous factors known as danger-associated molecular patterns (DAMPs), to activate the innate immune response [113].

The human genome encodes four main families of PRRs: The membrane-bound toll-like receptors (TLRs) and C-type lectin receptors (CLRs), and the cytosolic nucleotide-binding oligomerisation domain (NOD)-like receptors (NLRs), retinoic acid-inducible gene-I (RIG-I)-like receptors (RLRs) [114]. In addition to these, a set of cytosolic DNA-binding proteins have been identified as receptors for microbial DNA including DNA-dependent activator of interferon-regulatory factor (DAI) and members of the PYHIN family (IFI16 and IFI20X) [115]. Upon recognition of their respective ligands, PRRs induce a signalling cascade specific for the recognised pathogen, typically activating NF-κB transcription factors and/or interferon response factors (IRFs) (Figure 1.5).

Inflammation is the result of PRR activation and is a defined response of the body to tissue injury or infection. This process involves the immediate release of cytokines and chemokines from non-immune and resident immune cells within the damaged/infected tissue, which triggers an increase in local vascular permeability and attracts circulating immune cells such as neutrophils, monocytes, and lymphocytes. This leads to an accumulation of reactive plasma proteins

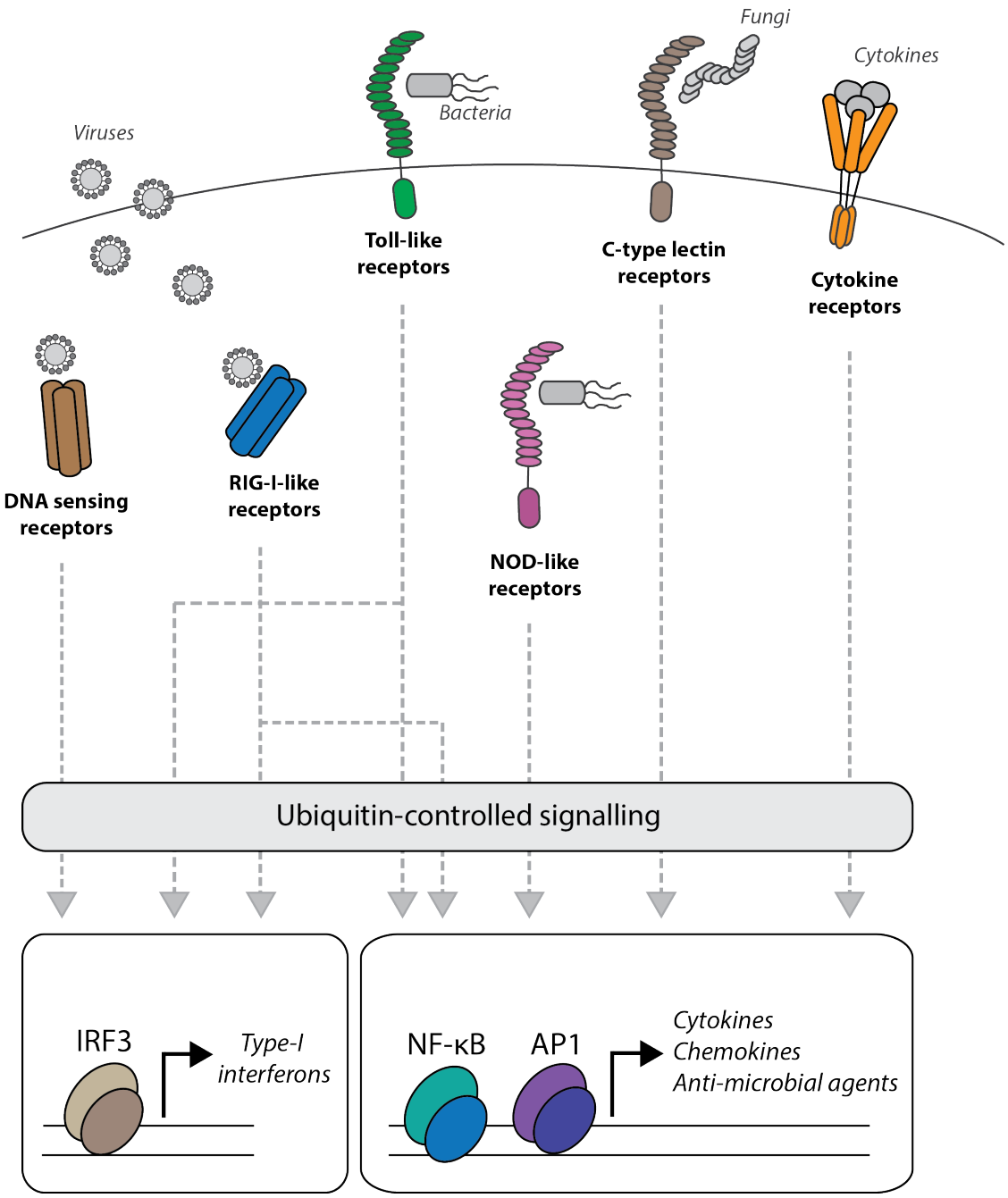


Figure 1.5: Pattern recognition signalling. Diagrammatic representation of each of the major types of pattern recognition receptors (PRRs), their respective ligands, and the main groups of transcription factors activated upon receptor stimulation. Importantly, all of these signalling events are reliant on ubiquitin-mediated signalling events.

and activated immune cells in the affected tissue that ultimately resolves the infection and/or injury.

One common downstream target of PRRs is the IKK complex, which together with MAPKs mediates the induction of the inflammatory response and, importantly, these are both reliant on ubiquitination events.

IKK specifically activates the NF-κB transcription factors - dimeric complexes of DNA-binding proteins including p50 (NF-κB1), p52 (NF-κB2), p65 (RelA), RelB, and c-Rel (Rel). The protein IκBα acts as an inhibitor of these complexes by sequestering them in the cytoplasm. However, in the canonical NF-κB pathway, the IKK-mediated phosphorylation of IκBα leads to its proteasomal degradation through conjugation of K48 chains, allowing NF-κB translocation to the nucleus [116]. This then leads to activation of genes required for induction of the inflammatory response including several cytokines/chemokines (TNF, IL-1β, IL-6, CXCL-8), immune receptors, and antigen presentation genes (CD48, MHC class I/II, ICAM-I) [64].

Early studies showed that activation of IKK is dependent on its binding to K63 chains assembled by TRAF6, TRAF2, cIAP1, and cIAP2; however, it also binds to M1 chains generated by the M1-specific E3, LUBAC. This is mediated by the ubiquitin binding subunit of the IKK complex, NEMO (IKKγ), as it contains a UBAN domain which binds M1 and K63 chains (though it has a reported 100-fold greater affinity for M1 chains) [116]. This binding facilitates the proximity-induced activation of the IKK complex by the ubiquitin-dependent kinase, TAK1, which exists in complex with TAB1 and TAB2/3 [117]. Mechanistically, the TAB2/3 subunit of the complex contains a UBD that preferentially binds K63 chains leading to its autophosphorylation and activation and ultimately to the phosphorylation-induced activation of IKK (figure 1.6) [118].

The functional significance of the NEMO subunit of IKK is highlighted by the fact that mutations in the UBAN of NEMO results in impaired NF-κB activation and X-linked ectodermal dysplasia with immunodeficiency [119].

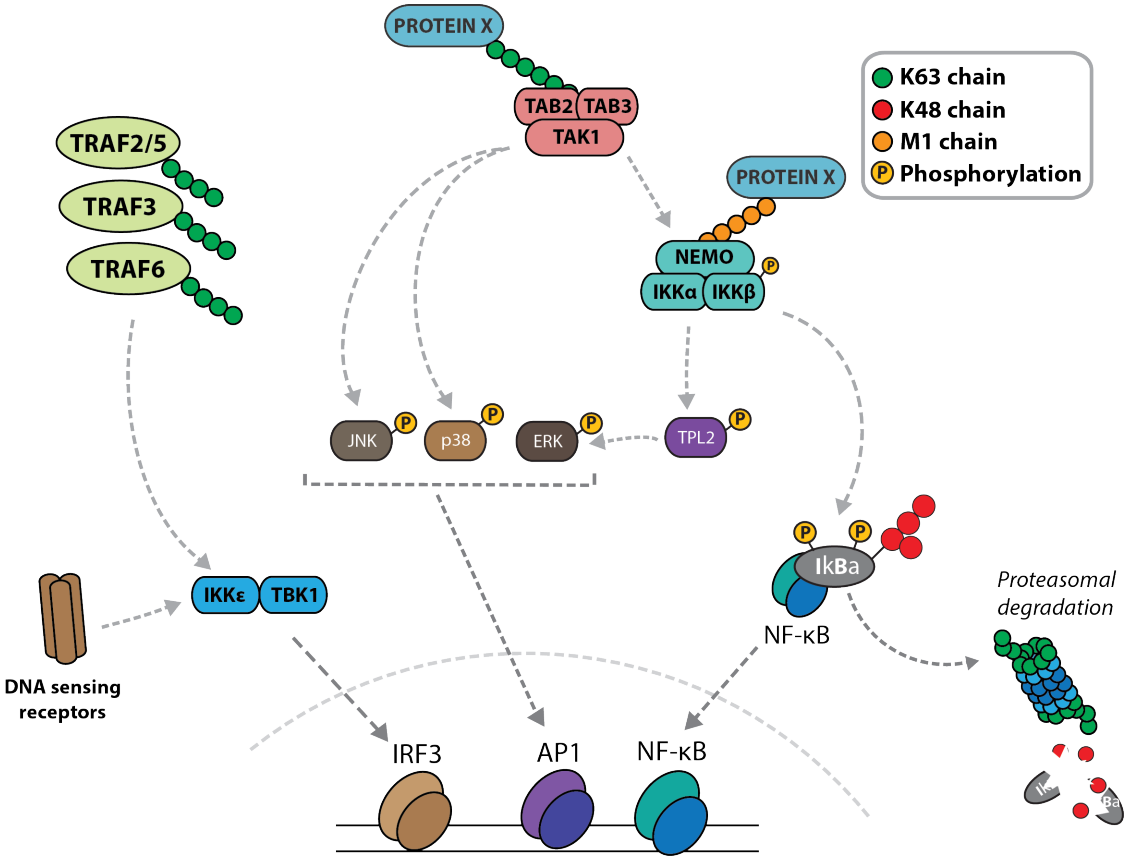


Figure 1.6: Signalling events mediated by PRR signalling modules. Diagrammatic representation of each of the PRR signalling modules, the IKK, TAK1, and IKK/TBK1 complexes, and their mode of activation.

Also activated by PRRs are the three major families of MAPKs which includes p38, JNK, and ERK. As with IKK, activation of p38 and JNK occur directly via TAK1; however, the TAK1-mediated activation of ERK occurs indirectly via IKK whereby TAK1-activated IKK phosphorylates and activates TPL2, an upstream activator of ERK [120]. These MAPKs activate the AP1 family members, which consist of heterodimers of the c-Jun and c-Fos family members that are involved in transcription of pro-survival and proliferative responsive genes (figure 1.6) [64].

The activation of IRF3 leading to type-I interferon production is reliant on the IKK-related kinase, TBK1 (tank binding kinase 1) and its homologue IKKϵ. This antiviral pathway is stimulated mainly by the TRIF-dependent TLRs (TLR3 and TLR4), RLRs, NLRs, and the cytoplasmic DNA sensing receptors [116]. Specifically, the K63 polyubiquitination of TBK1 and IKKϵ activates their catalytic

activity. Though the exact mechanism is unknown, it has been proposed that this ubiquitination may facilitate recruitment of an upstream kinase, which activates these kinases, or facilitate the association of TBK1 with NEMO to generate a higher order complex that leads to TBK1 activation (figure 1.6) [116].

1.2.2 NOD1 and NOD2 receptor signalling

The conserved NLRs, NOD1 and NOD2, recognise conserved features of bacterial cell walls known as peptidoglycan (PGN). Specifically, NOD1 recognises γ-$_D$-glutamyl-*meso*-diaminopimelic acid (iE-DAP), whereas NOD2 recognises muramyl dipeptide (MDP), (both constituents of PGN found in both gram-positive and gram-negative bacteria) [121].

Structurally, the NOD1 receptor is a multi-domain scaffolding protein consisting of a caspase activation and recruitment domain (CARD) domain, a NOD domain (aka the NACHT domain), and multiple leucine-rich repeats (LRRs). NOD2 is structurally similar to NOD1 but has an additional CARD domain (figure 1.7) [121].

The NOD domain is an evolutionary conserved domain consisting of seven distinct motifs and is involved in dNTPase activity and oligomerisation, the C-terminal LRR region is involved in ligand binding, and the CARD domain facilitates recruitment of the CARD-containing adaptor protein, Receptor-interacting serine/threonine-protein kinase 2 (RIPK2 (RICK/CARDIAK)). This recruitment is indispensable for productive signalling via activation of the mitogen activated protein kinase (MAPK) and IκB kinase (IKK) pathways [121, 122].

The adaptor RIPK2 is an essential regulator of NOD signalling and acts as a substrate for ubiquitination. Specifically, K63 chains (particularly on Lys 209 of RIPK2), likely conjugated by the TRAF2:cIAP1/2 (cellular inhibitor of apoptosis 1/2) complex, recruit the TAK1 complex [123]. Another IAP, known as X-linked inhibitor of apoptosis protein (XIAP), is crucial for productive NOD signalling as mutations compromising its function lead to impaired NOD1/2 signalling [124]. The importance of XIAP is further exemplified by a recent study showing that RIPK2 is an essential scaffold for XIAP binding [125]. Specifically, the kinase

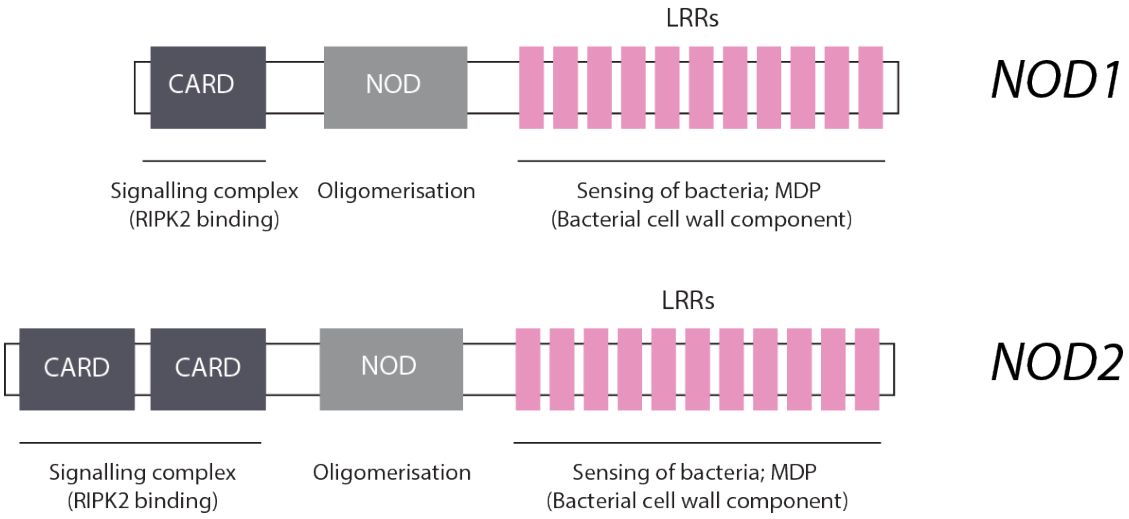


Figure 1.7: Diagrammatic representation of the NOD1/2 structure. The domain structure of NOD1 and NO2 highlights their similarity with NOD2 containing an extra CARD domain. NOD1/2 conformation resulting in an autoinhibited state is also shown.

activity of RIPK2 is dispensable for signalling, however small-molecule blocking of the ATP-binding site of RIPK2 interferes with XIAP interactions, resulting in impaired NF-κB signalling [125]. Once recruited, the E3 activity of XIAP is required for recruiting another essential component of NOD signalling, LUBAC [126]. The importance of XIAP is highlighted by mutations affecting its ligase activity being linked to X-linked lymphoproliferative syndrome type 2 (XLP-2), where the inability for XIAP to conjugate ubiquitin chains onto RIPK2 impairs LUBAC recruitment and leads to defective inflammatory signalling via the NOD2 receptor [126].

Though XIAP and LUBAC are indispensable for NOD2 function, additional E3s have been implicated that are dispensable for signalling including TNF receptor associated factor 2 (TRAF2), TRAF4, and TRAF5, RNF34, ITCH, Pellino3, and cIAP1/2 (figure 1.8) [123, 126–130]. In the case of cIAP1/2, this was shown via the use of SMAC (second mitochondrial activator of caspases) mimetics. SMAC mimetics are IAP antagonist compounds that bind the BIR domain of IAPs to trigger their autoubiquitination and degradation [131]. In NOD2 signalling, these act to degrade cIAP1/2 and, when used at high concentrations, block the association of XIAP with RIPK2 [124].

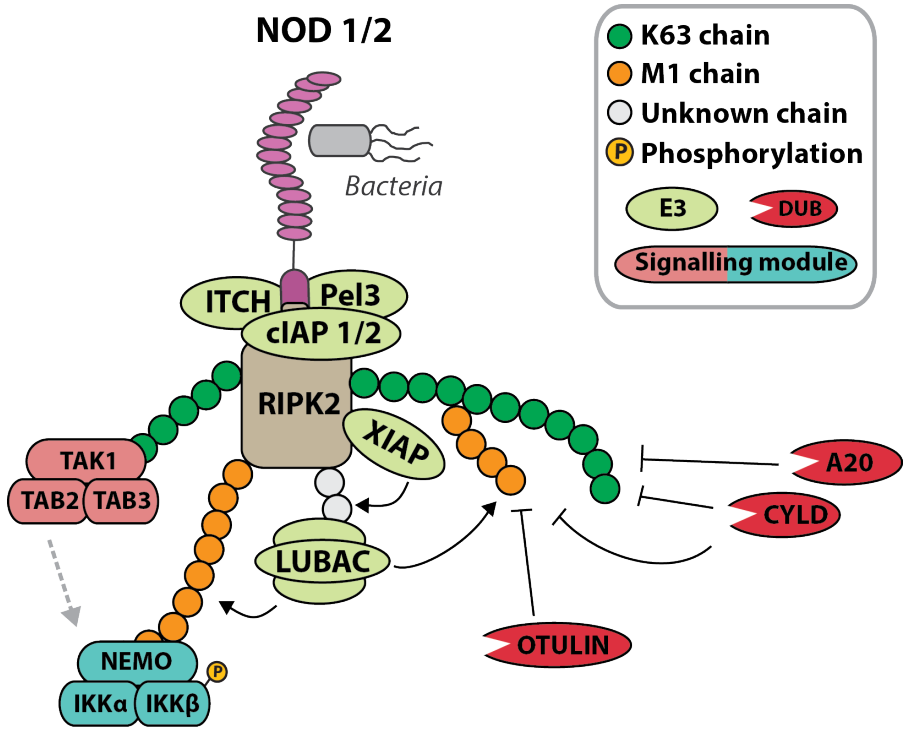


Figure 1.8: The NOD1/2 signalling cascade. Upon stimulation with muramyl dipeptide (MDP) constituents of peptidoglycan (a component of bacteria cell walls), RIPK2 is recruited to NOD2 along with numerous E3s to facilitate its polyubiquitination. The TAK1 and IKK signalling modules are recruited by these chains to facilitate the activation of the NF-κB and MAPK pathways for production of pro-inflammatory mediators. Various DUBs act throughout this process to hydrolyse the polyubiquitin chains and therefore negatively regulate signalling.

Collectively, the activity of these E3s leads to the recruitment and activation of the TAK1 and IKK complexes, and the subsequent downstream signalling events as discussed (figure 1.5) [116].

Regulation of the NOD2 receptor complex primarily involves the coordinated actions of three DUBs: CYLD, OTULIN, and A20 [132–134].

CYLD hydrolyses M1 and K63 chains (and to a lesser extent K11 and K48 chains) and is recruited to signalling complexes via LUBAC (discussed in detail later) [79–82, 135]. Once recruited, CYLD hydrolyses polyubiquitin chains formed on RIPK2 to control inflammatory signalling [132].

OTULIN (OTU DUB with linear linkage specificity) is an M1 chain-specific DUB, which hydrolyses M1 chains from LUBAC and its substrates [58, 134, 136, 137]. It is directly recruited to signalling complexes via LUBAC (Discussed later)

[137]; however, this direct association with signalling complexes is not an absolute requirement for OTULIN to function as it is not detected within the TNFR complex I, but retains the ability to negatively regulate receptor components, likely via its strong M1 chain binding activity [58, 133, 134]. In addition to directly inhibiting NF-κB signalling via its DUB function, OTULIN also suppresses through binding to M1 chains, as expression of catalytically dead OTULIN results in decreased NF-κB activation [58]. In line with this, *Fiil et al* provided evidence that a double mutant of OTULIN abolishing its DUB and ubiquitin binding functions no longer suppresses signalling [134].

A20 (also known as TNFAIP3) is an OTU DUB, which is upregulated following NF-κB activation and directly recruited to signalling complexes via its ZF4 and ZF7 domains (binding K63 and M1 chains respectively) [138, 139]. *In vitro* data reported that it hydrolyses K48 and K11 chains and, to a lesser extent, K63 chains; however, in cells it facilitates the hydrolysis of K63 chains [140]. IKKβ-mediated phosphorylation of A20 at Ser381 increases the *in vitro* DUB activity of A20 towards K63 chains; however, it is unclear if this increase in activity is limited to this chain type.

A20 displays E3 ligase activity as it has been shown to ligate K48 chains, which leads to proteasomal degradation [140]. Direct evidence for this ligase activity was shown by *in vitro* studies with recombinant A20 demonstrating E3 ligase activity mediated by its ZF4 domain, which was enhanced by IKKβ-mediated phosphorylation [140]. However, in cells, the A20-associated ubiquitin ligases, RNF11 and Itch, have been reported to be involved in mediating K48 ubiquitination [141, 142].

The presence of A20 also results in the accumulation of M1 chains, most likely due to its direct binding to them. In addition to increasing M1 chain substrates for recruitment of the IKK complex (via NEMO), this binding has been shown to protect the chains from hydrolysis by CYLD [133].

Taken together, CYLD and OTULIN mediate the early events of receptor signalling through editing of the ubiquitin landscape of the NOD2 signalling complex. In contrast, A20 is primarily considered to be a later regulator as it is upregulated following stimulation.

1.2.3 TNF receptor signalling

One of the most extensively studied cytokine receptor systems is the tumour necrosis factor (TNF) receptor due to the many context-dependent cellular responses that can be mediated from a single stimulus such as pro-inflammatory and cell survival/cell death signalling. Under normal conditions, TNF is not detectable in the serum, but it is produced in response to a variety of PAMPs, DAMPs, and other pro-inflammatory cytokine signalling. It is initially expressed as a homotrimeric type II trans-membrane protein, which is cleaved by a metalloprotease known as TNF-converting enzyme (TACE) to facilitate its secretion (producing a homotrimeric soluble cytokine) [143]. As not all TNF is immediately cleaved for secretion, it can exist in both a membrane-bound and soluble form, which have two receptors, TNF receptor 1 (TNFR1), which is constitutively expressed in most tissues, and TNFR2, which is expressed only within the lymphoid compartment [144]. TNFR1 displays high affinity for both the soluble and membrane-bound forms of TNF and is readily activated by both, whereas TNFR2 displays a much lower affinity for TNF and is more efficiently activated by membrane-bound TNF due to the low affinity interaction allowing only transient interactions with soluble TNF [145]. TNFR1 and TNFR2 also differ in their domain structure with TNFR1 containing a death domain (DD) whereas TNFR2 does not [144].

Binding of soluble TNF to TNFR1 leads to a conformational change and the recruitment of the adaptor protein, TNFRSF1A-associated via death domain (TRADD), via a homotypic interaction between C-terminal death domains (DD) [146]. Similarly, the adaptor protein RIPK1 is recruited to the receptor complex via a homotypic DD interaction; however, its interaction with the DD of the TNFR is relatively weak in comparison to TRADD. TRADD also serves as a platform further recruiting TRAF2/6 and cIAP1/2 (figure 1.9) [91, 147, 148].

TRAF proteins are recruited to serve a scaffolding function (as their E3 activity has been shown to be dispensable) whereas cIAP1/2 conjugates K63 and K11 chains (also K48 chains to a smaller extent) to various targets, which is an absolute requirement for productive pro-inflammatory signalling - exemplified by the fact

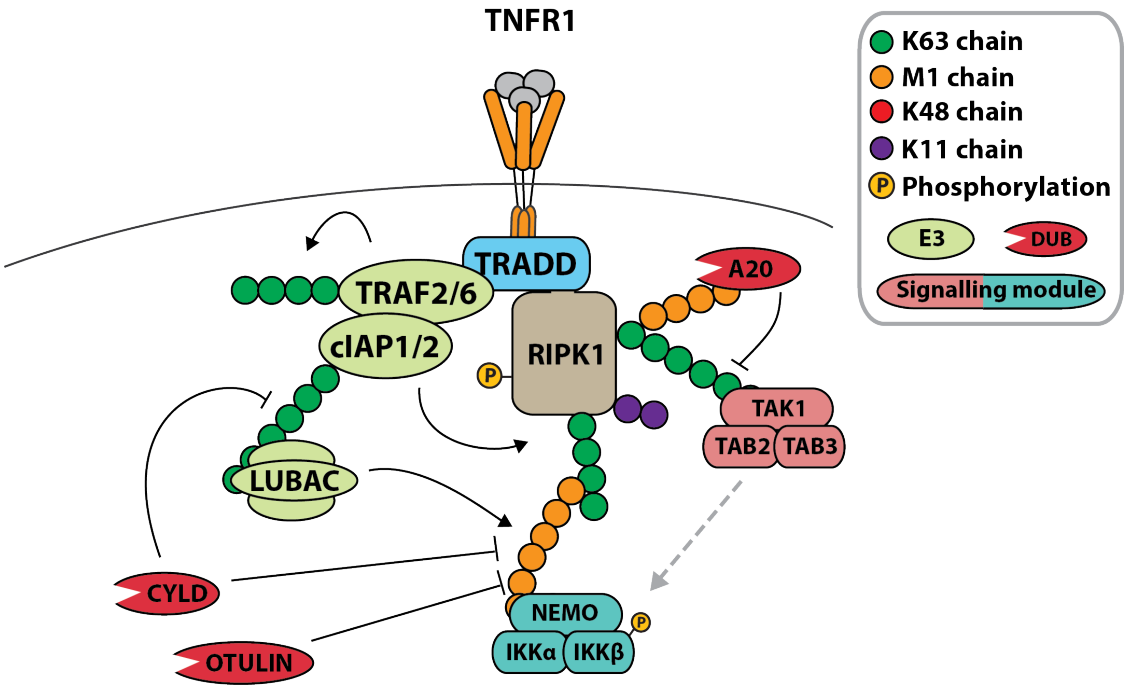


Figure 1.9: The TNF receptor complex I signalling cascade. Following TNFR1 activat5ion, the adaptors TRADD and RIPK1 are recruited and ubiquitinated by numerous E3s resulting in activation of the TAK1 and IKK signalling modules. E3 act on this complex to negatively regulate it and promote its instability, which may lead to the formation of cell death-inducing complexes as shown in figure **??**.

that their depletion almost completely removes polyubiquitin chains from RIPK1 [91, 147, 149, 150]. The cIAP1/2-mediated conjugation of K63 and K11 chains to TNFR complex I components facilitates the recruitment of the E3 complex, LUBAC, which is essential for productive NF-κB and MAPK signalling [91, 126, 151]. The conjugation of these polyubiquitin linkages recruits the TAK1 and IKK complexes which, as discussed, facilitates pro-inflammatory/pro-survival signalling.

TNFR complex I is subject to regulation by DUBs with USP21 being the first described to deubiquitinate RIPK1 [152]. CYLD was also shown to be a crucial regulator through cleavage of K63 and M1 chains from a variety of components including TRAF2, NEMO, and RIPK1 [132, 133, 153–155]. Though not associated with complex I, OTULIN can also mediate the early signalling events of TNF [58, 81, 136].

In contrast to USP21 and CYLD, which are constitutively expressed, the DUBs A20 and Cezanne also regulate TNFR1 signalling and are predominantly upregulated

in response to NF-κB activation to deubiquitinate RIPK1 [140, 156]. In this context, A20 has been shown to deubiquitinate RIPK1 and subsequently conjugate K48 chains for its proteasomal degradation [140].

Destabilisation of complex I by removal of ubiquitin can lead to the formation of a secondary cytoplasmic complex, known as complex II, consisting of RIPK1, FADD, caspase-8, and cFLIP (cellular FLICE inhibitory protein). This complex can also include RIPK3 and, in the case of humans, caspase-10. The relative abundance of caspase-8 and RIPK3 in this complex leads to the activation of cell death by apoptosis (characterised by membrane blebbing, chromatin condensation, DNA laddering, and lack of induction of an inflammatory response in the surrounding environment) or necroptosis (characterised by cytoplasmic swelling (oncosis) and the rupturing of the plasma membrane, leading to the release of DAMPs) [157, 158].

Apoptosis is initiated by the activation of caspase-8 within complex II, which cleaves and activates caspase-3 to initiate apoptotic signalling events [117, 159, 160].

Necroptosis occurs when disassociated RIPK1 binds to RIPK3, forming large amyloid structures leading to a high MW (>2MDa) complex [161]. Mechanistically, RIPK1 phosphorylates itself, which facilitates its binding to RIPK3 via a homotypic RHIM (RIP homotypic interaction motif) [162]. Upon binding, RIPK1 phosphorylates RIPK3, which recruits the pseudo kinase, MLKL (mixed lineage kinase domain-like). RIPK3 phosphorylates and activates MLKL, which facilitates the formation of homotrimers that translocate to the plasma membrane to form pores. A loss of membrane integrity then occurs and an influx of ions leads to membrane rupturing as part of the necroptotic cell death [163].

1.3 The Linear ubiquitin chain assembly complex (LUBAC)

To date, LUBAC is the only E3 ligase complex capable of generating M1 chains and consists of three subunits known as Heme-oxidised IRP2 ubiquitin ligase 1 (HOIL-1/RBCK1), Shank-associated RH domain-interacting protein (SHARPIN),

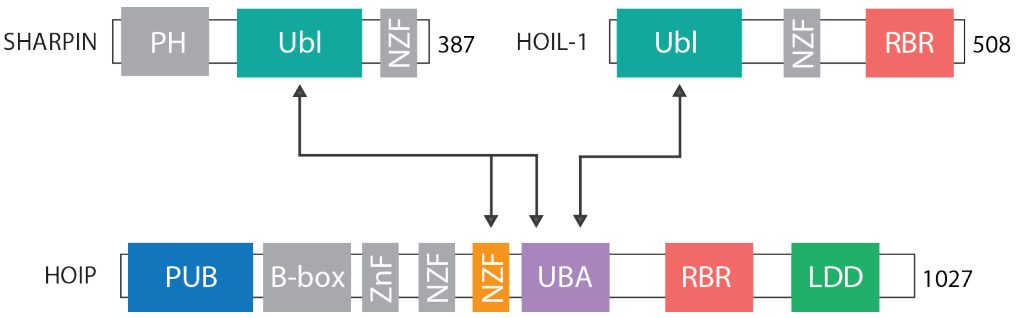


Figure 1.10: Diagrammatic representation of the structure of LUBAC. The domain structure of the constituent components of LUBAC (HOIP, HOIL-1, and SHARPIN) are shown with arrows indicating the known domains required to allow them to form the LUBAC complex. Domains shown in colour are discussed further within this chapter and are important for the function of LUBAC. Adapted from [165].

and HOIL-1 interacting protein (HOIP/RNF31), which is the main catalytic core of the complex (figure 1.10) [16, 91, 151]. The complex exists in a tripartite state where HOIP is constitutively bound to the regulatory components, SHARPIN and HOIL-1 and, though the exact stoichiometry of the complex is unclear, it has been estimated to have a mass of around 600kDa [164].

Though all LUBAC subunits are required for its full activity, this section will focus on the activities of the HOIP subunit, as it relates more specifically to data presented in chapter 4 and is also the main component of the complex required for recruitment of the associated DUBs, CYLD and OTULIN.

1.3.1 The structure and function of HOIP

HOIP is an RBR domain-containing DUB, which conjugates chains in a HECT-like mechanism where it transfers the ubiquitin to its catalytic cysteine prior to conjugation. HOIL-1 is also an RBR E3 but its ligase activity is very low compared to HOIP and, as of yet, has no characterised *in vivo* ligase function [166, 167]; however, it has been shown *in vitro* to conjugate M1 chains [167].

As HOIP is the catalytic subunit of the complex, much work has gone into investigating how it associates with the other components of LUBAC. It has been shown that the interaction between HOIP and HOIL-1 occurs via their respective UBA and Ubl domains, which form a non-canonical UBA:Ubl interaction (figure

1.10). Specifically, the Ubl of HOIL-1 adopts a classical Ubl fold whereas the UBA of HOIP forms a nine-helix bundle containing a three-helix bundle consisting of α6, α7, and α8, similar to typical UBA domains. Studies addressing the stoichiometry of this interaction in solution found that the α6, α7, α8, and α9 helices of HOIPs UBA recognise an interface on HOIL-1s Ubl opposite the canonical UBA-binding interface [168]. Studies investigating the interactions between HOIP and SHARPIN are less clear but have suggested that both the UBA and NZF2 domains of HOIP are mediating the interaction with SHARPINs Ubl (figure 1.10) [151, 164, 169].

Interactions with these proteins is essential for LUBAC function as unbound HOIP (*in vitro*) is retained in an auto-inhibited state through binding of its UBA domain with the N-terminal portion of the protein and the RBR region [167]; however, its E3 activity is fully activated when complexed with SHARPIN or HOIL-1 [170]. MS analysis of the protein levels of each component shows similar abundance, which may suggest their levels are coordinated, and, in line with this, loss of one or more components of LUBAC leads to its instability and loss of function [151, 164, 169, 171–175].

HOIP alone contains the required domain structure to conjugate ubiquitin chains to substrates, namely the RBR domain and a C-terminal extension known as the catalytic in-between-RING (CBR) domain, which includes the RING2 and linear ubiquitin chain determining domain (LDD)) (figure 1.10) [167, 170]. One curiosity previously unknown about HOIP was its unique ability to conjugate M1 chains to substrates; however, a structural study investigating this C-terminal portion of HOIP in complex with both the donor and acceptor ubiquitin moieties has revealed the underlying mechanism [166]. The acceptor ubiquitin sits within a surface created by the RING2-LDD fragment and is orientated such that the N-terminal α-amino group is in close proximity to the catalytic cysteine residue (3.5 Å), whilst none of the seven Lys residues are in close enough proximity to compete for a nucleophilic attack on the thioester intermediate. This structure also highlights that the LDD domain consists of a ZF domain, which is integrated into the RING2 of HOIP with a helical extension. Furthermore, whilst the interaction with the donor ubiquitin is

primarily mediated by the RING2 domain (involving hydrophobic interactions with the C-terminal of ubiquitin), it is further stabilised by the β-hairpin located within the helical base of the LDD, which orientates gly76 of the ubiquitin towards the active site of HOIP. This highlights the LDD extension to be a specific requirement for the M1 specificity of HOIP, indicating that the extension could not simply be integrated into another E3 to confer M1 specificity [166].

Further to the domains required for its ligase activity and ability to enter a complex with HOIL-1 and SHARPIN, HOIP also contains a conserved N-terminal PUB domain, which facilitates the association of the two LUBAC-associated DUBs, CYLD and OTULIN [79–82, 135].

1.3.2 The association of CYLD and OTULIN with LUBAC

The PUB domain of HOIP has been well established to contain a conserved PIM-binding pocket, which mediates its interaction with both OTULIN and CYLD [132, 133, 137, 176, 177]. OTULIN contains a PIM that is highly specific for this PUB domain and binds to create a high-affinity interaction that is essential for OTULIN to counteract auto-ubiquitination of LUBAC under basal conditions [137, 176]. CYLD does not contain such a PIM but still requires the same PIM binding pocket of HOIP to facilitate this interaction and to perform its function of regulating polyubiquitin chains generated by LUBAC on receptor components [132, 133, 177]. Instead, CYLD interacts with an adaptor protein known as SPATA2, which mediates the interaction with LUBAC through its own PUB domain and PIM that are highly specific for this interaction [79–82, 135] (data for this interaction also shown in chapter 4).

1.3.3 Cellular functions of LUBAC

LUBAC has been implicated in a variety of signalling pathways including the NOD2, IL-1, CD40, TLR3, Wnt, RIG-I, and TNF pathways [90, 91, 126, 132, 134, 136, 173, 178–180]. In the TNF receptor complex I, it is recruited through polyubiquitin chains generated by cIAP1/2, where it conjugates M1 chains onto various receptor components to recruit and activate the IKK complex [151, 173].

This deposition of M1 chains facilitates full NF-κB signalling as shown by a deficiency in LUBAC, or failure to recruit it to the signalling complex, leading to a weaker NF-κB response [90, 126, 180].

Impaired LUBAC function

Studies in mice and humans have shown that impaired LUBAC function, through deletion or mutation of one or more its components, can result in pathology.

HOIP KO mice, or mice with catalytically inactive HOIP, die at midgestation, displaying abnormal heart development and defects in vascularisation of the yolk sac [172, 181]. This is partly caused by excessive TNF-dependent apoptosis of endothelial cells; however, lethality is not rescued by deletion of TNFR1, suggesting that LUBAC regulates embryogenesis by other means [172]. Met1 chains have been shown to negatively regulate Wnt signalling but whether this underlies embryonic lethality has yet to be determined [136, 177]. A recent study by *Peltzer et al* shows that, contrary to previous reports, HOIL-1 KO in mice is embryonic lethal due to its contribution to LUBAC stability [182]. Together, these models reflect human pathology as a hypomorphic mutation of HOIP or truncating mutations of HOIL-1 leads to severe pathology including multi-organ autoinflammation, polyglucosan storage myopathy and cardiomyopathy (aka muscular amylopectinosis), and immunodeficiency [171]. Studies on SHARPIN have been facilitated by the spontaneous autosomal recessive mutation in the Sharpin gene, which leads to loss of SHARPIN and destabilisation of the LUBAC complex in homozygous mice. Phenotypically, this leads to the early onset of chronic proliferative dermatitis (cpdm; mice are referred to as SHARPIN^{cpdm} mice) and multi-organ inflammation [164, 169, 183]. The skin phenotype of the SHARPIN^{cpdm} mice is driven by TNFR1 signalling as it has been shown that the absence of SHARPIN results in the increased susceptibility of keratinocytes to TRADD-, FADD-, and caspase-8- mediated apoptosis [151, 184, 185]. TNFR1-mediated cell death also contributes to organ inflammation in SHARPIN^{cpdm} mice but, in contrast to the skin phenotype, this also involves necroptosis [184–186].

Enhanced LUBAC function

In addition to the impairment of LUBAC, enhanced function also results in pathology. A recent study by *Damgaard et al* demonstrates, in mice, that depletion of the LUBAC regulator, OTULIN, within the immune compartment results in cell-type-specific defects: constitutive NF-κB signalling in myeloid cells, and down-regulation of M1-specific signals in T and B cells from LUBAC degradation [187]. This phenotype matches the features of human patients with OTULIN deficiency known as OTULIN-related autoinflammatory syndrome (ORAS; also otulipenia) [187, 188].

Enhanced function of LUBAC has also been implicated in susceptibility to certain blood cancers. Specifically, SNPs within HOIP that enhance LUBAC activity and leads to an increase in NF-κB signalling are increased 8-fold in patients with ABC DLBCL relative to the general population [189]. In line with this, oncogenic mutations in the CARD11 component of the CBM complex have been found to promote its spontaneous association with LUBAC, resulting in the activation of NF-κB [190].

LUBAC and pathogenic infection

LUBAC is a core component of ubiquitin-mediated immune signalling and, as a result, is targeted by a variety of pathogens that modulate its function.

As part of a broad immune-evasion strategy, *Shigella flexneri* targets LUBAC via its type III secretion system [191]. Specifically, the bacterial ubiquitin ligases IpaH1.4 and IpaH2.5 conjugate K48 chains on HOIP, leading to its proteasomal degradation; whereas the OspG protein indirectly targets LUBAC through sequestration of the E2 it utilises for M1 chain synthesis, UBE2L3 [192, 193]. Disruption of the LUBAC complex itself is seen by the Porcine reproductive and respiratory syndrome virus (PRRSV). Here, the virulence factor, Non-structural protein 1 (NP1), impairs the interaction between HOIP and SHARPIN to inhibit NF-κB signalling [194].

In contrast to impairing LUBAC function, the oncogenic Epstein-Barr virus (EBV) activates LUBAC to evade cellular anti-virus responses and mediate NF-κB-dependent cellular transformation. Specifically, LMP1, an EBV-encoded member of

the TNF superfamily, recruits LUBAC where it ubiquitinates and inactivates IRF7, to inhibit production of type I interferon [195]. Furthermore, LMP1 also facilitates the interaction between LUBAC and TRAF1/2, leading to the conjugation of K63 and M1 chains on LMP1 and TRAF1, which activates the NF-κB pathway [196]. HBV also utilises LUBAC to dampen antiviral responses via its HBx protein, which recruits LUBAC to disrupt mitochondrial antiviral signalling (MAVS) protein signallosome formation, leading to impaired IRF3-mediated type I interferon production [197].

1.4 The deubiquitinase, CYLD

CYLD was first identified as the causative gene in patients suffering from familial cylindromatosis, a disease resulting in the development of large, benign tumours manifesting in areas of hair growth [198, 199]. Whilst patients usually carry a heterozygous germline mutation in the CYLD gene (mainly in the USP domain affecting its catalytic activity), it is the deletion of the WT allele that leads to disease [199]. Mice with full CYLD deficiency have no tumour development but are more susceptible to chemically and DSS-induced colitis-associated tumourigenesis; however, mice expressing a truncated form of CYLD (exon 9 truncation resulting in a shortened USP domain and therefore no catalytic activity), die shortly after birth due to lung failure [200–202]. CYLD has also been implicated in other diseases including hepatocellular/uterine/cervical carcinoma, and also in multiple myeloma patients [202, 203]. Taken together, this implicates CYLD in processes maintaining tissue homeostasis as well as defining it as a bona fide tumour suppressor.

1.4.1 Structure and function of CYLD

CYLD is a 956 amino acid protein, though a smaller isoform is produced through alternative splicing events, which lacks exon 7 [65, 199]. Both isoforms are expressed in almost all tissues (figure 1.11).

In its C-terminal, CYLD possesses a USP domain, which mediates the cleavage of K63 and M1-linked polyubiquitin chains and, within this domain, there is a

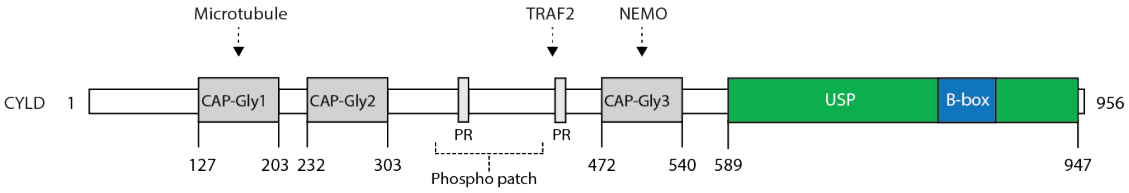


Figure 1.11: Cartoon representation of the domain structure of CYLD. The domain structure of CYLD showing each CAPGly domain and the USP domain (with the embedded B-box domain). Also annotated is the binding areas for microtubule association, TRAF2, and NEMO.

zinc-binding B-box domain [204]. CYLD also contains three CAPGly (cytoskeleton-associated protein glycine rich) domains. The first CAPGly domain has been implicated in mediating interactions with microtubule-associated proteins, suggesting a role for CYLD in cell motility and cell cycle progression, whilst the other domains were identified as interaction motifs for the binding of immune receptor signalling complex components including TRAF2 and NEMO [153, 205]. CYLD also contains a serine cluster, which is a target site for multiple phosphorylation events (figure 1.11) [65].

1.4.2 CYLD in immune signalling

CYLD has been implicated in a variety of cellular pathways including: activation and regulation of immune cells (T cells, B cells, and macrophages); mediating the inflammatory response to pathogens including *Streptococcus pneumonia*, *Escherichia coli*, and viral infection; controlling apoptosis in the process of spermatogenesis; cell cycle progression; and the prevention of bone disorders, including osteoporosis, though its negative regulation of TRAF2 [65, 153, 154, 202, 206–211].

As discussed previously in the NOD2 and TNF pathways, CYLD represents an important negative regulator of NF-κB and MAPK signalling, which in turn makes it a positive regulator of PRR and cytokine receptor-mediated cell death, via its ability to deubiquitinate signalling complex components. In addition to targeting RIPK1, TRAF2, and NEMO for deubiquitination, CYLD has also been reported to hydrolyse

polyubiquitin chains from TRAF6/7 and TAK1 and, in fact, the deubiquitination of TAK1 by CYLD prevents its spontaneous activation in T cells [65, 206].

1.4.3 Regulation of CYLD function

A number of reports exist regarding regulation of CYLD via PTMs. One study suggests that ubiquitination of CYLD by E6, one of the major oncoproteins of the human papilloma virus (HPV), mediates its degradation, ultimately leading to enhanced NF-κB responses [212]. In addition, CYLD has been reported to be regulated by the Ubl modification SUMO in a study showing that, in neuroblastoma cells, SUMOylation of CYLD leads to inhibition of its deubiquitinase activity against TRAF2/6, resulting in enhanced NF-κB signalling [213]. CYLD has also been shown to be phosphorylated in NF-κB signalling. Two conflicting reports regarding the activatory/inhibitory roles of this modification exist [214, 215]. In one study, phosphorylation of CYLD at S418 is reported to be mediated by the IKK complex and acts to suppress TRAF2 deubiquitination by CYLD; whereas the second study, in a screen for IKKϵ substrates, identified CYLD as a target and concluded that S418 phosphorylation decreases CYLDs activity.

Additionally, CYLD has also been reported as a substrate for caspase-8 cleavage at position D215, which acts to inactivate CYLD [216]. In agreement with the cell death-promoting activities of CYLD through deubiquitination of complex I (discussed previously), prevention of this cleavage by D215N mutation leads to an increase in the susceptibility towards TNF-induced cell death [216].

Further to these PTMs, the activity of CYLD has also been reported to be regulated via induced gene expression e.g. in osteoclastogenesis, and also by downregulation of CYLD mRNA expression in patients with irritable bowel disease (IBD) [65, 211, 217].

1.5 Spermatogenesis-associated protein 2

Spermatogenesis-associated protein 2 (SPATA2) was first identified in 1999 as a novel human testicular protein with an approximate size of 60kDa. Initially named

PD1, it was shown to be highly expressed in the cytoplasm of Sertoli cells but also at lower levels in spleen, thymus, and prostate tissue [218]. As Sertoli cells are important for the process of spermatogenesis, *Onisto et al* investigated a potential role for SPATA2 in this process and showed a correlative relationship between testicular development and SPATA2 expression in rats, with maximum expression shown when sexual maturity was reached [218, 219]. This group also showed that SPATA2 mRNA levels were reduced in individuals with hypospermatogenesis, which ultimately lead to the renaming of the protein to SPATA2 [220]. Strengthening the link to Sertoli cell function, SPATA2 expression was reported to be induced by follicle-stimulating hormone (FSH), which is essential for Sertoli cell function [221, 222]. SPATA2 expression was also shown to be upregulated in zebrafish development and also pancreatic development, as well as being reported in a screen for psoriasis susceptibility genes [222–224].

Whilst these studies show correlative roles for SPATA2 in tissue function and development, no studies had, as of 2016, reported any function of SPATA2 in inflammatory signalling. However, prior to the work presented in this thesis, two studies existed that clearly demonstrated an interaction between SPATA2 and CYLD. The first study by *Sowa et al* was a global analysis of the interactome of DUBs and showed a direct interaction between CYLD and SPATA2, and the second study used an siRNA screen to identify factors regulating the process of necroptosis and found that, similar to CYLD, SPATA2 knockdown resulted in a protective effect against TNF-induced apoptosis and necroptosis [56, 225].

Since 2016, a further five studies have been published on the function of SPATA2 in TNF-mediated NF-κB signalling and induced cell death [79–82, 135]. As I will detail in chapter 4, SPATA2 has become a protein of interest in NF-κB signalling due to being critical for CYLD function in NOD2 and TNF-mediated signalling.

1.6 Aims of the study

LUBAC is an essential mediator of TNF and NOD2 signalling through the generation of M1 chains and recruitment of CYLD and OTULIN to receptor complexes. Whilst the association of OTULIN with LUBAC is well characterised, it is unclear how CYLD is recruited by LUBAC as they do not interact *in vitro*. Furthermore, upon association with receptor complexes following stimulation, CYLD is modified by a PTM, which results in an increase in its MW.

Therefore, the aims of this study were two-fold:

1/ Investigate how CYLD and LUBAC interact

1a/ Identify potential binding partners of CYLD based on existing data about requirements for its recruitment to LUBAC
1b/ Characterise the mechanism by which such a protein may bridge the CYLD:HOIP interaction
1c/ Investigate the functional consequences of loss of such a mediator

2/ Determine the factors mediating activation of CYLD

2a/ Characterise the post translational modification of CYLD following activation
2b/ Determine the functional consequences of inhibition of the modification

2 Materials

Contents

2.1 Materials 39
2.1.1 Chemicals, reagents, and consumables 39
2.1.2 Buffers and solutions 42
2.1.3 Commercial kits 43
2.1.4 Antibodies 43
2.1.5 Plasmids 44
2.1.6 Oligos 45
2.1.7 Cell lines 46

2.1 Materials

2.1.1 Chemicals, reagents, and consumables

Table 2.1: Reagents used in this study .

Reagent	Supplier	Code
2-mercaptoethanol	Gibco	31350-010
45μm filter (low protein binding)	Sartorius stedim	16555-K
Acetic Acid	Fisher	A/0360/PB17
Acetone	Fisher	A/0600/17
Acrylamide	Severn Biotech	20-210-10
Agarose	Web Scientific	AGR-500
Ammonium peroxide sulphate (APS)	-	-
Ampicillin	Sigma-Aldrich	A9518

Continuation of Table 2.1

Reagent	**Supplier**	**Code**
Anchored oligoes	Sigma	$T^{18}VN$
Anti-c-MYC magnetic beads	Thermo	88842
Anti-V5 agarose	Sigma	A7345
BamHI-HF	NEB	R3136S
Biotin-TNF	R%D	BT210
Blotting paper	GE healthcare	3030-917
Bovine serum albumin (BSA)	Sigma	A9647
Brefeldin A	BioLegend	420601
Bromophenol blue	Fisher	BP510-500
cOmplete protease inhibitor cocktail	Roche	04 693 124 001
Culturplate - 96	PerkinElmer	6005680
Cutsmart buffer	NEB	B7204S
Dimethyl sulphoxide (DMSO)	Sigma	D2650
Dithiothreitol(DTT)	Sigma	43819
DMEM media	Gibco	31966-021
dNTPs	NEB	N0446S
ECL developing solution	Amersham	RPN2209
ECL enhancer solution	Amersham	RPN2235
Ethanol	Merck	32221
Ethylendiaminetetraacetic acid (EDTA)	Fluorochem	239931
Foetal bovine serum (FBS)	Labtech	FCS-SA
FLAG M2 affinity agarose beads	Sigma	A2220
FLAG peptide	Sigma	F3290
FLAG-TNF	Enzo	ALX-522-008-C050
Fugene 6	Promega	E2692
Fugene HD	Promega	E2312
Gel Filtration Markers Kit	Sigma	MWGF1000
Glutathione Sepharose 4 Fast Flow	GE healthcare	17-5132-02
Glycerol	Honeywell	G7757
Glycine	Fisher	G/0800/60
Hydochloric acid (HCl)	Fisher	H/1200/PB15
Hygromycin B	Invitrogen	10687010
IC fixation buffer	Biolegend	420801
IKK inhibitor VII	Millipore	401486
IKK inhibitor XII	Millipore	401491
IPEGAL CA-630 (NP-40)	Sigma-Aldrich	I3021
Isopropanol	Merck	24137
L18-Muramyldipeptide (L18-MDP)	Invivogen	tlrl-lmdp
Lambda phosphatase	NEB	P0753S
Lipofectamine RNAiMAX	Invitrogen	100014472
MES running buffer	Invitrogen	NP0002-02
Methanol	Honeywell	32213

Continuation of Table 2.1

Reagent	**Supplier**	**Code**
Micro BioSpin columns	BioRad	7326204
Milk powder	Marvel	3023034
Manganese Chloride ($MnCl_2$)	NEB	B1761S
Monensin	BioLegend	420701
MOPS running buffer	Invitrogen	NP0001-02
N-Ethylmaleimide (NEM)	Sigma	E1271
NheI-HF	NEB	R3131S
Nitrocellulose membrane	GE Healthcare	10600002
NotI-HF	NEB	R3189S
NuPAGE 4-12% Bis-Tris midi gels	Invitrogen	WG1403BX10
OptiMEM	Gibco	31985
Oxozeaeonol	Tocris	3604
PBS (10x)	Fisher	BP399-20
PBS (Sterile)	Gibco	14190-094
Penicillin/Streptomycin (P/S)	Gibco	15070
Pentadecamers	IDT	169190224
peqGREEN DNA dye	Peqlab	37-5010
PhosSTOP inhibitors	Roche	04 906 837 001
Phusion polymerase	NEB	M0530L
Phusion polymerase reaction buffer (5x)	NEB	B0518S
PMP buffer	NEB	B0761S
Polyethylene glycol (PEG)	Aldrich	P2139
Ponceau stain	Sigma	P7170
Potassium chloride (KCl)	Sigma	P9541
Protein A/G PLUS beads	Santa cruz	sc-2003
Puromycin	Invivogen	ant-pr
PVDF membrane	GE healthcare	10600023
RevertAID reverse transcriptase	Thermo	EP0441
RiboLock	Thermo	EO0381
RPMI medium	Gibco	42401-018
RT buffer (5x)	Thermo	LT-02241
S.O.C. medium	Invitrogen	15544-034
SalI-HF	NEB	S3138S
Saponin	Fluka	47036
SeeBlue protein standard	Invitrogen	LC5925
Sodium azide	Sigma	S2002
Sodium chloride (NaCl)	SLS	CHE3316
Sodium dodecyl sulphate (SDS)	Fisher	1281-1680
Sodium phosphate dibasic heptahydrate (Na_2HPO_4)	Sigma-Aldrich	S9390
Sodium phosphate monobasic monohydrate (NaH_2PO_4)	Sigma-Aldrich	S9638
Sodium pyruvate	Gibco	11360-039

Continuation of Table 2.1

Reagent	Supplier	Code
Streptavidin magnetic beads	Thermo	88817
T4 DNA ligase	NEB	M0202L
T4 ligation buffer (10x)	NEB	B0202S
Tetramethylendiamine (TEMED)	Amresco	0761
TNF (recombinant human)	Peprotech	300-01A
Tris base	Fisher	BP152-1
Triton X-100	Sigma	T9284
Trypsin-EDTA	Gibco	25300-054
Tween-20	Fisher	BP337-500
X-ray film	Fujifilm	47410 19289

2.1.2 Buffers and solutions

Table 2.2: Buffers used in this study .

Buffer	Composition
1 % agarose gel	1 % w/v agarose powder in 1 x TAE buffer (boiled until homogenous) plus 2-3 μl/50 ml peqGREEN
Blocking solution	5 % Milk powder in PBS-Tween
IP buffer (sucrose gradients)	150 mM NaCl, 50 mM Tris (pH 7.4), 5 mM EDTA, 1 mM PMSF
Laemmli sample buffer	50 mM Tris (pH 6.8), 10 % Glycerol, 100 mM DTT, 2 % SDS, 0.1 % Bromophenol blue
Perm/wash buffer	2 % FBS, 0.1 % saponin, 0.1 %NaN_3 in PBS
Phosphate buffered saline (PBS)	1.47 mM KH_2PO_4, 2.68 mM KCl, 136.9 mM NaCl, 7.97 mM Na_2HPO_4
PMP buffer (no salt)	50 mM HEPES, 2 mM DTT, 0.01 % Brij 35, pH 7.5
RIPA lysis buffer	20 mM Tris-HCl (pH 7.5), 150 mM NaCl, 1 mM EGTA, 1 % NP-40, 1 % Sodium deoxycholate, 1 mM β-glycerophosphate supplemented with 5 mM NEM, 1 mM DTT, cOmplete protease inhibitor cocktail and phosSTOP
SDS running buffer	192 mM Glycine, 25 mM Tris base, 0.1 % SDS
TAE buffer	40 mM Tris base, 1 mM EDTA-Na, 20 mM acetic acid, pH 8.5
TBS + 0.5 % NP-40 lysis buffer	TBS and 0.5 % NP-40 supplemented with 5 mM NEM, 1 mM DTT, cOmplete protease inhibitor cocktail and phosSTOP

Continuation of Table 2.2

Reagent	Supplier
TNF lysis buffer	30 mM Tris HCl (pH 7.4), 120 mM NaCl, 2 mM EDTA, 2 mM KCl, 1 % Triton X-100 supplemented with 5 mM NEM, 1 mM DTT, cOmplete protease inhibitor cocktail and phosSTOP.
Transfer buffer	25 mM Tris, 192 mM glycine, 10 % ethanol
Tris-buffered saline	50 mM Tris-Cl (pH 7.5), 150 mM NaCl
TUBE lysis buffer	20 mM Na_2HPO_4, 20 mM NaH_2PO_4, 1 % NP-40, 2 mM EDTA supplemented with 5 mM NEM, 1 mM DTT, cOmplete protease inhibitor cocktail and phosSTOP

2.1.3 Commercial kits

Table 2.3: Commercial kits used in this study .

Kit	Supplier	Code
MycoAlert mycoplasma detection kit	Lonza	LT07-318
Nucleospin gel and PCR clean-up	Machery-Nagel	740609.250
Nucleospin plasmid	Machery-Nagel	740588.250
Purelink HiPure Midiprep kit	Invitrogen	K210014
Qiaprep spin miniprep kit	Qiagen	27106
Quick-gDNA Blood prep Microprep	Zymo research	D3071
Realtime-Glo MT cell viability assay	Promega	G9712
RNase-free DNase set	Qiagen	79254
RNeasy Mini kit	Qiagen	74106
SYBR Select master mix	Applied Biosystems	4472908

2.1.4 Antibodies

Table 2.4: Antibodies used in this study .

Antibody	Host species	Supplier / Code
anti-Actin	Mouse	Millipore / MAB1501
anti-cIAP1	Rat	Enzo / ALX-803-335
anti-CYLD	Mouse	Santa cruz / sc- 74435
anti-CYLD	Rabbit	Cell signaling / 8462
anti-pCYLD (S418)	Rabbit	Cell signaling / 4500
anti-p44/42 MAPK (ERK1/2)	Rabbit	Cell signaling / 4370
anti-HOIP/RNF31	Rabbit	Aviva / ARP43241
anti-HOIP/RNF31	Sheep	R&D / AF8039
anti-IκBα	Rabbit	Cell signaling / 9242
anti-IKKγ/NEMO	Rabbit	Santa cruz / sc-8330

Continuation of Table 2.4

Antibody	Host species	Supplier / Code
anti-IL8 (APC conjugated)	Rabbit	BioLegend / 511410
anti-K63 ubiquitin	Rabbit	Millipore / 05-1308
anti-M1 ubiquitin	Rabbit	Millipore / MABS199
anti-Myc	Mouse	Cell signaling / 2276
anti-OTULIN	Rabbit	Cell signaling / 14127
anti-p38 MAPK	Rabbit	Cell signaling / 9212
anti-phospho-p38 MAPK	Rabbit	Cell signaling / 4511
anti-p65	Rabbit	Cell signaling / 8242
anti-phospho p65	Rabbit	Cell signaling / 3033
anti-RIPK1	Rabbit	Cell signaling / 3493s
anti-RIPK2	Rabbit	Santa cruz / sc-22763
anti-SHARPIN	Rabbit	Protein tech / 14626-1-AP
anti-SPATA2	Rabbit	Bethyl / A302-493A
anti-SPATA2	Rabbit	Bethyl / A302-494A
anti-TNFR1	Rabbit	Cell signaling / 3736
anti-Ubiquitin (P4D1)	Mouse	Cell signaling / 3936
anti-V5	Mouse	AbD serotech / MCA1360
anti-mouse-HRP	Goat	Dako / P0447
anti-rabbit-HRP	Goat	Bio-Rad / 1706515
anti-rat-HRP	Goat	ThermoFisher / 31470
anti-sheep-HRP	Donkey	R&D systems / HAF016

2.1.5 Plasmids

Table 2.5: Plasmids used in this study .

Insert	Backbone	Source
FLAG-CYLD	CMV2	Gyrd-Hansen lab
FLAG-CYLD^{C601A}	CMV2	Gyrd-Hansen lab
FLAG-CYLD	pBABE	Gyrd-Hansen lab
FLAG-CYLD^{C601A}	pBABE	Gyrd-Hansen lab
FLAG-CYLD^{L475P}	pBABE	Gyrd-Hansen lab
FLAG-CYLD$^{L475P/S418A}$	pBABE	Gyrd-Hansen lab
FLAG-CYLD$^{L475P/S568A}$	pBABE	Gyrd-Hansen lab
FLAG-CYLD$^{L475P/S418A/S568A}$	pBABE	Gyrd-Hansen lab
FLAG-CYLD^{S418A}	pBABE	Gyrd-Hansen lab
FLAG-CYLD^{S568A}	pBABE	Gyrd-Hansen lab
FLAG-CYLD$^{S418A/S568A}$	pBABE	Gyrd-Hansen lab
His-OTULIN	pcDNA5	Gyrd-Hansen lab
His-OTULIN^{C129A}	pcDNA5	Gyrd-Hansen lab
MYC-SPATA2	pcDNA3.1	Gyrd-Hansen lab
MYC-SPATA2^{R212X}	pcDNA3.1	Gyrd-Hansen lab
MYC-SPATA2^{V357X}	pcDNA3.1	Gyrd-Hansen lab

Continuation of Table 2.5

Insert	Backbone	Source
MYC-SPATA2^{Y338A}	pcDNA3.1	Gyrd-Hansen lab
MYC-SPATA2^{Y338F}	pcDNA3.1	Gyrd-Hansen lab
pMD.G	pMD.G	B. Jordan (Einstein, NY)
V5/H13 HOIL1	pcDNA3	Walczak lab
V5/H13 HOIP	pcDNA3	Walczak lab

2.1.6 Oligos

Table 2.6: Oligos used in this study for template amplification .

Name	Sequence
FLAG-CYLD amplification	F - 5'-GAGGGATCCGCCACCATGGACTACAAAGACGAT-3' R - 5'-GAGGTCGACGCCACCTATTTGTACAAACTCATT-3'
MYC-SPATA2 amplification	F - 5'-GAGGCTAGCGCCACCATGGAGCAGAAGCTGATCTC... ...AGAGGAGGACCTGGGAAGCTTGGGTACCATGGGCAGCA... ...GCTCGCTG-3' R - 5'-GAGGCGGCCGCGCCACCCTAGGGCCGGGCCCCG-3'

Oligos for site-directed mutagenesis

Table 2.7: Oligos used in this study for site-directed mutagenesis .

Name	Sequence
CYLD^{C601A}	F - 5'-AGAATAAGGTTGAGTCTAAGTAAGCAGAATTGTAATG... ...ACCCTGGATGC-3' R - 5'-GCATCCAGGGTCATTACAATTCTGCTTACTTAGACTCA... ...ACCTTATTCT-3'
CYLD^{L475P}	F - 5'-CTCCTTAACTTCAGCCGGTGAGCCCACTTCTAGACCA... ...TGTG-3' R - 5'-CACATGGTCTAGAAGTGGGCTCACCGGCTGAAGTTA... ...AGGAG-3'
CYLD^{S418A}	F - 5'-GAGACTGAATGGTAAAGCGTGGAATCTGTTCTCGG-3' R - 5'-CCGAGAACAGATTCCACGCTTTACCATTCAGTCTC-3'
CYLD^{S568A}	F - 5'-AGTATTTTCTTCTACTACTTCAGCTAAGTAGCCTCCAA... ...ATGCTAAAGAGTT-3' R - 5'-AACTCTTTAGCATTTGGAGGCTACTTAGCTGAAGTAG... ...TAGAAGAAAATACT-3'
SPATA2^{R212X}	F - 5'-CTCTGCCCGCCGCTACAGGGCGTCCGAG-3' R - 5'-CTCGGACGCCCTGTAGCGGCGGGCAGAG-3'
SPATA2^{V357X}	F - 5'-CTGAGCAGCTACTAATCCGGCCGCAGAGCA-3' R - 5'-TGCTCTGCGGCCGGATTAGTGGCTGCTCAG-3'
SPATA2^{Y338A}	F - 5'-CTGGGTTCAGAGTCTGTGGCCAGATCCACGTCATC...

Continuation of Table 2.7primers

Name	Sequence
	...CTG-3' R - 5'-CAGGATGACGTGGATCTGGCCACAGACTCTGAACC... ...CAG-3'
SPATA2^{Y338F}	F - 5'-GATGACGTGGATCTGTTCACAGACTCTGAACCC-3' R - 5'-GGGTTCAGAGTCTGTGAACAGATCCACGTCATC-3'

Oligos for qRT-PCR

Table 2.8: qRT-PCR oligos used in this study .

Name	Sequence
HPRT	F - 5'-AGCCAGACTTTGTTGGATTTG-3' R - 5'-TTTACTGGCGATGTCAATAGG-3'
TNF	F - 5'-TGCTGCAGGACTTGAGAAGA-3' R - 5'-GAGGAAGGCCTAAGGTCCAC-3'
CXCL8	F - 5'-TCTGGCAACCCTAGTCTGCT-3' R - 5'-AAACCAAGGCACAGTGGAAC-3'
A20	F - 5'-ATGCACCGATACACACTGGA-3' R - 5'-GGATGATCTCCCGAAACTGA-3'
NFKBIA	F - 5'-GCTGATGTCAATGCTCAGGA-3' R - 5'-CCCCACACTTCAACAGGAGT-3'

2.1.7 Cell lines

Parental cell lines

Cell line	Cell type	Source
HCT116	Human colonic cell line	Gyrd-Hansen lab
HEK293T	Human embryonic kidney cells	Gyrd-Hansen lab
HEK293 Phoenix cells	Human embryonic kidney cells	Gyrd-Hansen lab
U2OS/NOD2	Osteosarcoma cells	Gyrd-Hansen lab

Table 2.9: Parental cell lines used in this study

Genetically modified cell lines

Table 2.10: Self-generated genetically modified cell lines .

Cell line	Cell type
CYLD KO U2OS/NOD2	U2OS
CYLD KO U2OS/NOD2 + FLAG-hCYLD^{C601A}	U2OS
CYLD KO U2OS/NOD2 + FLAG-hCYLD^{L475P}	U2OS
CYLD KO U2OS/NOD2 + FLAG-hCYLD$^{L475P/S418A}$	U2OS
CYLD KO U2OS/NOD2 + FLAG-hCYLD$^{L475P/S568A}$	U2OS
CYLD KO U2OS/NOD2 + FLAG-hCYLD$^{L475P/S418A/S568A}$	U2OS
CYLD KO U2OS/NOD2 + FLAG-hCYLD^{S418A}	U2OS
CYLD KO U2OS/NOD2 + FLAG-hCYLD^{S568A}	U2OS
CYLD KO U2OS/NOD2 + FLAG-hCYLD$^{S418A/S568A}$	U2OS
CYLD KO U2OS/NOD2 + FLAG-hCYLD$^{S418A/S568A}$	U2OS
SPATA2 KO U2OS/NOD2	U2OS

3

Methods

Contents

3.1 Cell biology 49
3.1.1 Cell culture 49
3.1.2 Transient transfection of cells 49
3.1.3 Stable transduction by γ- retrovirus 50
3.1.4 Flow cytometry 51
3.1.5 RNA isolation, cDNA synthesis, and qRT-PCR 51
3.2 Protein biochemistry 53
3.2.1 Immunoblotting 53
3.2.2 Immunoprecipitation of tagged proteins 54
3.2.3 Pulldown of the TNFR1 complex 54
3.2.4 Purification of endogenous ubiquitin conjugates 55
3.2.5 Protein dephosphorylation by lambda phosphatase . . . 56
3.2.6 Identifying phosphorylation sites by mass spectrometry 56
3.2.7 Sucrose gradient sedimentation 58
3.3 Molecular biology 59
3.3.1 Generation of knock-out cell lines with CRISPR/Cas9 . 59
3.3.2 Plasmid preparation 59
3.3.3 Cloning and mutagenesis 60
3.4 Statistical analyses 63

3.1 Cell biology

3.1.1 Cell culture

Cultivation of cell lines was performed under sterile conditions at 37 ^{o}C and 5 % CO_2. U2OS/NOD2 cells, HEK 293 cells, mouse embryonic fibroblasts (MEFs), and all genetically modified variants of these lines were grown as a monolayer using Dulbecco's Modified Eagle Medium (DMEM) supplemented with 10 % v/v foetal calf serum (FCS) and 60 μg/ml penicillin / 100 μg/ml streptomycin (P/S). Cells were passaged every 2-4 days to maintain them at a density not exceeding 95 % confluency in the flask (T 75 or T 175).

Splitting of cells consisted of discarding existing media, washing with phosphate-buffered saline (PBS) and adding Trypsin/EDTA solution (4 ml / T 175 or 15 cm plate, 2 ml / T 75 or 10 cm plate). Cells with trypsin solution were incubated for up to 10 min in the 37 ^{o}C incubator to allow detachment from the plate followed by resuspension in DMEM medium for experimental use or re-plating at a ratio between 1:6 and 1:20. Once per month, all cell lines were re-plated into fresh flasks.

3.1.2 Transient transfection of cells

Transfection of DNA with FuGENE 6/HD reagents

FuGENE 6 (Promega) was used for transfection of U2OS/NOD2 cell lines whereas FuGENE HD (Promega) was used for the transfection of HEK293 cells. For both FuGENE 6 and FuGENE HD, the transfection reagent to DNA ratio was kept consistent at 3:1 for the number of cells transfected (see table 3.1).

Plate	**DNA (μg)**	**FuGENE 6/HD (μl)**	**OptiMEM (μl)**
12 well	0.2	0.6	2 x 50
6 well	1	3	2 x 100
10 cm	3.5	10	2 x 500

Table 3.1: Volumes/concentrations of FuGENE 6/HD transfection mix

For transfection, cells were plated to allow for around 60 % confluency on the day of transfection. The transfection mix was prepared through the separate dilution of DNA and FuGENE 6/HD to optiMEM and each were thoroughly mixed. After

incubation for 5 min, the two solutions were mixed and incubated for a further 10 min at room temperature before dropwise addition to the cells. Fresh media was added after 24 h. 48 h after initial transfection cells were stimulated/harvested for experimental use.

Transient knockdown of genes by siRNA

siRNA-mediated gene silencing was performed through reverse transfection of the targeting siRNA with the reagent, lipofectamine RNAiMax (See table 2.1). For transfection, siRNA and lipofectamine RNAimax were separately diluted in optiMEM and incubated at room temperature for 5 min before being mixed together and incubated for a further 15 min at room temperature (RT). Cells were then plated at the desired concentration in fresh media and the lipofectamine/siRNA mix was added (for concentrations see table 3.2). Fresh media was added after 24 h and, following a period of 72 h for knockdown, cells were stimulated and/or harvested for experimental use.

Plate	**100 μM siRNA (μl)**	**Lipofectamine(μl)**	**OptiMEM (μl)**
12 well	0.4	2	2 x 100
6 well	1	5	2 x 250
10 cm	5	25	2 x 1000
15 cm	10	50	2 x 2000

Table 3.2: Volumes/concentrations of Lipofectamine RNAiMAX transfection mix

3.1.3 Stable transduction by γ- retrovirus

Production of γ-retrovirus

Retroviral particles were used to induce the stable expression of a variety of FLAG-hCYLD-based constructs into CYLD KO (9E-8) U2OS/NOD2 and

CYLD KO (9E-8) U2OS/NOD2 or *Cyld*$^{-/-}$ MEF cells were plated into 6 well plates and grown to around 60 % confluency. At this point, titrations of 200 μl to 1000 μl from the filtered viral supernatant (detailed above) were applied directly to cells alongside polybrene (5 μg/ml final conc.). After 24 h, fresh media was

added and selection was started using puromycin at a concentration of 1 μg/ml, which continued until control cells had all died.

3.1.4 Flow cytometry

Flow cytometry was used for the detection of intracellular CXCL8. U2OS/NOD2 cells and CYLD KO (9E-8) U2OS/NOD2 cells (and all FLAG-hCYLD expressing variants) were cultured in 12 well plates and grown to 90 % confluency. Cells were then stimulated for 5 h with L18-MDP at 200 ng/ml in the presence of 5 μg/ml brefeldin A and 2 μM monensin protein transport inhibitors. Following stimulation, cells were washed once with PBS, dissociated with Trypsin/EDTA solution and collected by centrifugation of 300 g for 5 min. Cells were then fixed with 150 μl of IC fixation buffer (Biolegend) O/N at 4 ^{o}C, washed with PBS, and permeabilised with Perm/wash buffer. After a further centrifugation of 600 g for 3 min at 4 ^{o}C, cells were incubated for 1 h at RT with perm/wash buffer containing anti-IL8/APC antibody (Biolegend: 100 x). Following incubation, cells were washed once with perm/wash buffer and resuspended in PBS for analysis by flow cytometry (FACS Canto Flow cytometer, BD Biosciences, San Jose, CA). Analysis of the data was performed with FlowJo software (TreeStar, Ashland, OR) and statistical analysis by two-way ANOVA in Prism 6 (GraphPad Software Inc).

3.1.5 RNA isolation, cDNA synthesis, and qRT-PCR

U2OS/NOD2 cells (and all derived variants) were plated into 12 well plates and, at around 90 % confluency, stimulated with 20 ng/ml TNF or 200 ng/ml L18-MDP for 3 h. Lysis of cells and extraction of RNA was performed using an RNeasy Mini kit (Qiagen) and on-column DNase digestion was performed with the RNase-free DNase Set (Qiagen) according to the manufacturer's protocol. Following extraction, total RNA was reverse transcribed using RevertAid^{TM} reverse transcriptase (Thermofisher) and a mixture of anchored oligo $(dT)_{20}$ primers and random pentadecamers alongside RiboLock (Thermofisher) as per table 3.3. As indicated, 3.5 μl of mix 1 was added to 10 μl of extracted RNA and incubated at

65 ^{o}C for 5 min. Samples were immediately put on ice and 6.5 μl of mix 2 was added followed by heating to 25 ^{o}C for 10 min, 42 ^{o}C for 60 min, and 70 ^{o}C for 10 min. Resulting cDNA was diluted and qPCR was performed using the SYBR Select Master Mix (Applied Biosystems), primer pairs for genes of interest (plus HPRT for the internal control) as detailed in table 2.8, and RNase free water as per table 3.3.

Mix (per sample)	Reagent	Volume
cDNA mix 1 (3.5 μl)	Pentadecamers (10 μM)	1 μl
	Anchored oligo dT primes (100 μM)	0.5 μl
	dNTPs (10 mM)	2 μl
cDNA mix 2 (6.5 μl)	RT buffer (5 x)	4 μl
	RiboLock	0.5 μl
	RevertAid^{TM} reverse transcriptase	0.5 μl
	RNase-free H_2O	1.5 μl
qPCR mix	cDNA	1 μl
	SYBERGreen mix	5 μl
	Primer pairs (Forward and reverse - 20 μM)	0.5 μl
	RNase-free water	3.5 μl

Table 3.3: Volumes/quantities of reagents used for cDNA synthesis and qPCR

The qPCR mix was pipetted into 384 well plates and run as per table 3.4 on a Lightcycler® 480 II qPCR machine (Roche). The resulting cycle values (Ct values) were analysed by calculating the deltaCt and deltadeltaCt values through normalisation to the HPRT control and subsequently the parental or WT unstimulated condition. Graphpad Prism 6 was used for plotting the relative fold changes as well as performing statistical tests. For all qRT-PCR data, Two-way ANOVA tests were used to determine significance.

Name	Temp.	Duration	Ramp rate	Cycles	Acquisition
Warming	50 ^{o}C	2 min	4.4 ^{o}C/sec	1	None
Melting	95 ^{o}C	2 min	4.4 ^{o}C/sec	1	None
Amplification	95 ^{o}C	15 sec	4.4 ^{o}C/sec	40	-
	60 ^{o}C	1 min	2.2 ^{o}C/sec		Quant
Melting curve	95 ^{o}C	1 min	4.4 ^{o}C/sec	1	-
	55 ^{o}C	30 sec	2.2 ^{o}C/sec		-
	95 ^{o}C	-	0.11 ^{o}C/sec		Continuous (5/1 ^{o}C)

Table 3.4: Details of the qPCR programme used on the Lightcycler 480

3.2 Protein biochemistry

3.2.1 Immunoblotting

Samples prepared for immunoblotting were heated with Laemmli's sample buffer (LSB) (to a final 1 x conc.) to 95 ^{o}C for 5 min to ensure complete denaturing. Two electrophoresis systems were used: the BioRad mini system and the Invitrogen Novex system. For the BioRad system, self-cast 10 % Bis-Tris gels were placed into the tank with 1 x running buffer and samples were loaded into the wells with one well of SeeBlue pre-stained protein ladder (Invitrogen) to indicate the molecular weight (MW) of identified proteins. The gel tank was topped up with buffer and run at a constant 140 V until the dye front had run off the gel. For the Invitrogen system, samples were loaded into 4-12 % gradient gels (Invitrogen) with 1 x MOPS or 1 x MES buffer with one well of SeeBlue pre-stained protein ladder (Invitrogen). After loading, gels were run at a constant 190 V until the dye front had run off the gel.

Gels were equilibrated in 1 x transfer buffer for 10 min followed by transfer using a semi-dry system (OWL HEP1, Thermo) to transfer protein to nitrocellulose or PVDF membrane (GE Healthcare). A constant current of 100 mA/gel (BioRad) or 150 mA/gel (Invitrogen), with a maximum voltage of 24 V, was applied for a duration of 1 h. Protein transfer efficiency was checked through the addition of Ponceau stain to the membrane for 5 min, after which the gel was washed 2 x with dH_2O. Nonspecific interactions were blocked through the addition of 5 % w/v milk in PBS-Tween (PBST) for 1 h at RT, followed by 1 x with PBST and incubation O/N at 4 ^{o}C with the primary antibody diluted in 1 % Bovine serum albumin (BSA).

After incubation with the primary antibody, membranes were washed 2 x with PBST and incubated with the appropriate secondary antibody diluted in PBST with 1 % BSA for 1 h at RT. After 3-6 x 5 min washes with PBST the membranes were incubated with ECL solution for 1.5 min for developing. For low abundance or difficult to detect proteins, 10 % enhancer solution was added to the ECL solution to increase signal.

3.2.2 Immunoprecipitation of tagged proteins

For MYC-immunoprecipitation (MYC-IP), constructs encoding proteins possessing a MYC-tag were transiently expressed in cells as described in 3.1.2. Cells were grown in 10 cm plates and stimulated and/or harvested for experimental use at 90 % confluency. Cells were washed 1 x with ice-cold PBST and lysed in 500 μl TBS + 0.5 % NP40 lysis buffer. The lysate was incubated on ice for 20 min and precipitates were cleared by centrifugation at 21,000 g, 4 ^{o}C for 10 min before being transferred to new tubes. An input fraction was removed from the lysate and the remainder was incubated with 10 μl (per sample) of anti-c-MYC magnetic beads (Thermo) for 4 h at 4 ^{o}C, rotating. Beads were washed 5 x with ice-cold PBST using an Invitrogen DynaMag^{TM}-2 and elution was performed through the addition of 40-60 μl 1 x LSB and heating for 10 min, shaking, at 70 ^{o}C. Samples were placed back on the DynaMag^{TM} and the eluate was transferred to a new tube for analysis by immunoblotting.

For V5-immunoprecipitation (V5-IP), constructs encoding V5-tagged proteins were transiently expressed in cells as described in 3.1.2. Cells were grown, harvested and prepared as described for MYC-IP. After clearing, the lysate was incubated with anti-V5 agarose beads (5 μl per sample) for 4 h at 4 ^{o}C, rotating. Lysate and beads were subsequently transferred to a Biorad micro-spin column, centrifuged for 1 min at 900 g, and washed 5 x with ice-cold PBST (centrifuging between washes as previous) before elution with 2 x lithium dodecyl sulphate (LDS) at RT for 20 min. The spin column was centrifuged again at 1200 g for 1 min and DTT was added to 1 mM final conc. The eluate was analysed by immunoblotting.

3.2.3 Pulldown of the TNFR1 complex

U2OS/NOD2 cells (and all derived variants) were grown in 15 cm dishes until around 90 % confluent. Per condition, 2 x 15 cm plates were used and prior to stimulation, the existing DMEM was changed for 10 ml of fresh pre-warmed DMEM. Cells were then stimulated for 15 min with either 100 ng/ml of FLAG-TNF or 50 ng/ml of Biotin-TNF. Following stimulation, cells were washed 1 x with ice-cold

TBS before lysis with 1 ml of TNF lysis buffer. The lysate was incubated on ice for 20 min and precipitates were cleared by centrifugation at 21,000 g, 4 ^{o}C for 10 min before being transferred to new tubes. Input fractions were taken and either 1 μg of FLAG-TNF or 500 ng of Biotin-TNF was added to the cleared zero time point lysates. 10 μl of M2 affinity anti-FLAG agarose beads (FLAG-TNF pulldown) or 10 μl of streptavidin magnetic beads (Biotin-TNF pulldown) were added to the lysates and incubated at 4 ^{o}C, rotating for 2 h. For the FLAG-TNF pulldown, the beads were pelleted at 900 g, 4 ^{o}C for 1 min and washed 5 x with ice cold TBST (centrifuging between washes) before the addition of 80 μl of 100 μg/ml FLAG peptide diluted in TBS. Samples were incubated on ice before additional centrifugation and the supernatant was carefully transferred to a new tube for analysis by immunoblotting. For Biotin-TNF pulldowns, the samples were placed on an Invitrogen DynaMag^{TM}-2 magnet and washed 5 x with ice-cold TBST (allowing resuspension of the beads between washes). Following the final wash, 80 μl of 1 x LSB was added to the samples which were then heated to 70 ^{o}C for 10 min. Samples were then placed back on the DynaMag^{TM}-2 magnet and the eluate was transferred to a new tube for analysis by immunoblotting.

3.2.4 Purification of endogenous ubiquitin conjugates

Ubiquitin conjugates were purified from U2OS/NOD2 cells (and all derived variants in this study) through the use of a GST-1 x UBA^{ubq} ubiquitin affinity reagent (TUBE), generated from the 4 x GST-1 x UBA^{ubq} TUBE in the Gyrd-Hansen lab by Katrin Bagola. Prior to cell stimulation, 30 μg of the GST-1 x UBA^{ubq} TUBE was prebound to 15 μl Glutathione Sepharose 4B beads per sample and incubated at 4 ^{o}C on a rotating wheel for a minimum of 2 h to allow for pre-binding of the TUBE to the beads. Meanwhile, cells which have grown to around 90 % confluency in 10 cm plates were stimulated with 200 ng/ml L18-MDP for 1 h with or without pre-treatment for 30 min with 1 μM Compound A (CpA), a SMAC mimetic which shuts down L18-MDP signalling. Following stimulation, cells were lysed in 500 μl of TUBE lysis buffer and incubated on ice for 20 min. Lysates

were cleared by centrifugation at 21,000 g, 4 ^{o}C for 10 min before input fractions were taken and the remaining lysate was mixed with the Glutathione sepharose beads pre-bound with the GST-1 x UBA^{ubq} TUBE. The lysate and beads were incubated at 4 ^{o}C O/N on a rotating wheel before being washed 3 x with 500 μl of ice-cold PBST. The bound material was eluted from the beads with 50 μl of 1 x LSB and analysed by immunoblotting.

3.2.5 Protein dephosphorylation by lambda phosphatase

For the dephosphorylation of whole protein lysates, 10 x PMP buffer without salt (as the lysis buffer contains salt: see 2.2) was added to lysate where the buffer used was TBS + 0.5 % NP40 (without the phosSTOP supplement) plus 10 x MnCl to give a final 1 x conc. of each. Lambda phosphatase was then added to the lysate (1 μl per 100 μl lysate) and samples were incubated at 30 ^{o}C, shaking for 30 min before the addition of 4 x LSB to give a final 1 x conc. and further heating at 70 ^{o}C for 10 min.

For the dephosphorylation of the TNFR1 pulldown, the streptavidin magnetic beads were washed 3 x after the 2 h pulldown incubation with ice-cold TBSTween (TBST) as described in 3.2.3, before the addition of PMP buffer (NEB) and MnCl to a total volume of 50 μl at 1 x conc. Lambda phosphatase (NEB) was added (1 μl per pulldown from 15 cm plate) and samples were incubated at 30 ^{o}C, shaking for 30 min. Following incubation with the phosphatase, the beads were washed a further 2 x with ice-cold TBST before elution with 80 μl of 1 x LSB with heating to 70 ^{o}C for 10 min, shaking. Samples were analysed by immunoblotting.

3.2.6 Identifying phosphorylation sites by mass spectrometry

Note: The digestion and preparation of samples for mass spectrometry (MS) was performed by Georgina Berridge of the Kessler lab, Target Discovery Institute, University of Oxford. All other preparation and analysis of samples was performed by myself.

CYLD KO (9E-8) U2OS/NOD2 cells with a virally reintroduced FLAG-tagged WT CYLD were grown in 15 cm plates using 20 plates per condition (stimulated and unstimulated: roughly 2.5x10^8 cells). To identify phospho-CYLD sites resulting from TNF stimulation, cells were stimulated with 20 ng/ml TNF for 15 min at 37 ^{o}C. After stimulation, cells were washed 1 x in ice-cold TBS and lysed in 750 μl of TBS + 0.5 % NP40 lysis buffer (15 ml total lysate volume per condition). The lysate was incubated on ice for 20 min and precipitates were cleared by centrifugation at 21,000 g, 4 ^{o}C for 10 min before being transferred to new tubes. An input fraction was removed from the lysate and the remainder of each condition was incubated with 300 μl of M2 FLAG agarose beads (Sigma) for 2 h at 4 ^{o}C, rotating. Samples were washed 5 x with ice-cold TBST (1 ml wash and centrifugation of 900 g, 1 min, 4 ^{o}C) and elution was performed with 750 μl of 100 μg/ml FLAG peptide diluted in TBS on ice for 15 min. Samples were centrifuged (900 g, 1 min, 4 ^{o}C) and a fraction was taken for testing by immunoblotting.

The remaining eluate was digested O/N with elastase. Following this, samples were desalted using SepPak reverse phase columns and peptides were subsequently eluted with 1 M Glycolic acid in 80 % Acetonitrile containing 5 % TFA. Eluted peptides were enriched using 10 μM TiO_2 spin columns as described in [226]. The enriched peptides were dried and injected into an LC-MS/MS platform consisting of Dionex Ultimate 3000 nano LC and Orbitrap Fusion Lumos instruments. Sample separation was achieved with a 60 min gradient of 2-35 % acetonitrile in 0.1 % formic acid and 5 % DMSO and 250 nl/min flow rate with an EasySpray column (ES803, Thermo Fisher) of 50 cm length and 75 µm inner diameter. MS1 spectra were acquired with a resolution of 120.000 and an ion target of 400.000, followed by a top speed duty cycle of up to 3 s for MS/MS acquisition. Precursor ions were isolated in the quadrupole with a mass window of 1.6 Th and fragmented with HCD @ 28 % normalized collision energy. MS/MS data was acquired in the ion trap with rapid scan mode and an ion target of 4000.

LC-MS/MS data was analysed using PEAKS Server V.7 and V.8.5 (Bioinformatics Solutions) and a Uniprot/Trembl database. Variable modifications were

set to Phosphorylation (S, T, Y), Oxidation (M) and Deamidation (N, Q). Mass tolerance was 10 ppm for precursor and 0.5 Da for fragment mass. The false discovery rate was set to 1 % at peptide level.

3.2.7 Sucrose gradient sedimentation

Note: The preparation of the gradient and the velocity sedimentation was performed by Norbert Volkmar from the Christianson lab, University of Oxford. Samples were otherwise prepared and analysed by myself.

CYLD KO (9E-8), SPATA2 KO (S2-4), and parental U2OS/NOD2 cells were grown to 90 % confluency in 15cm plates and lysed in 1 ml of TBS + 0.5 % NP40 lysis buffer plus supplements as described in table 2.2. Samples were incubated on ice and precipitates cleared by centrifugation at 21,000 g, 4 ^{o}C for 10 min before being transferred to new tubes.

Continuous 10-40 % (w/v) sucrose gradients in a physiological salt solution (150 mM NaCl, 50 mM Tris pH 7.4, 5 mM EDTA, 1 mM PMSF) were generated using a Gradient MasterTM 108 (Biocomp) and 500 μg of protein lysate was subjected to velocity sedimentation at 36,000 rpm (OptimaTM L-100 XP (SW41 rotor), Beckman-Coulter), 4 ^{o}C, for 16 h. 13 fractions were collected in total and protein was precipitated with trichloracetic acid at a concentration of 8.4 %, incubated on ice for 60 min, and centrifuged at 14,000 g for 5 min. The resulting pellet was washed 2 x with acetone and resuspended in 2 x LSB. To approximate the hydrodynamic radii of individual protein complexes, a mixture of purified, native gel filtration standards (Sigma) was subjected to sucrose gradient sedimentation. Fractions were collected and processed as described above. The sedimentation pattern of each protein standard was determined by SDS-PAGE and subsequent silver staining (Silver Stain for Mass Spectrometry, Pierce). To assess shift in the MW of complexes containing CYLD, samples were subjected to immunoblotting as described above. Resulting blots were analysed by densitometry whereby the intensity of each fraction, minus

background signal, was quantified in ImageJ. The resulting values were normalised and plotted relative to the highest intensity value in each blot.

3.3 Molecular biology

3.3.1 Generation of knock-out cell lines with CRISPR/Cas9

Knock-out (KO) cell lines were generated through the use of the Santa cruz one-plasmid CRISPR/Cas9 system. Plasmids were purchased as a pool of three targeting sequences with a GFP selection marker. To identify the targeting sequence, a transformation of the pool was performed into TOP10 *E.coli* whereby the selection marker was ampicillin. Single colonies were picked and sequenced to separate out each targeting sequence. Cells which were to be targeted for KO were plated into 6 well plates and at around 60 % confluency, a forward transfection of each of the single targeting sequences was performed (mix as per 3.1). After 48 h for expression of the Cas9, targeting sequences, and GFP, cells were sorted by FACS (top 10 % GFP-positive cells) at the core sorting facility in the Jenner Institute, University of Oxford. For sorting, cells were trypsinised and centrifuged for 5 min at 200 g before being transferred to a 15 ml falcon tube containing 5 % FCS (to avoid blocking the FACS) and 1 x Gentamicin. Approximately 4000-10,000 cells were returned from the sorting facility which were diluted to 100 cells / 10 ml and 100 μl of this was plated into each well of a 96 well plate. Wells were regularly checked for cell growth and media was changed every three days. When wells had reached confluency, they were expanded to a 6cm plate for initial analysis by immunoblotting.

3.3.2 Plasmid preparation

For small scale plasmid prep (mini-prep), TOP10 competent *E.coli* were incubated with the plasmid of interest on ice for 5 min. Heat shock was performed for 1 min at 42 ^{o}C before being placed back on ice. 500 μl of S.O.C media was added to each transformation, mixed, and 250 μl was pipetted on to agar plates containing ampicillin at a conc. of 100 μg/ml. After allowing the mix to dry into the plate at RT, the plate was placed into a 37 ^{o}C incubator O/N to allow for bacterial

growth. The following day, 5-10 colonies were carefully picked from the plates and cultured O/N at 37 ^{o}C in 4 ml of L-broth containing 100 μg/ml ampicillin (this is also a starter prep for midis). Following this, 1 ml of the culture was taken for purification of plasmid DNA with a Qiagen spin miniprep kit or Machery-Nagel nucleospin plasmid kit as per manufacturer's protocol.

For large scale plasmid production (midi-prep), the Machery-Nagel Purelink HiPure midiprep kit was used. Samples were prepared for extraction firstly through the addition of 150 μl of a starter prep (as detailed above) to 100 ml of L-broth containing ampicillin at a conc. of 100 μg/ml and subsequent O/N incubation at 37 ^{o}C, shaking. Following incubation, all 100 ml of culture was used for midi-prep as per manufacturer's protocol. For both mini- and midi-preps, the extracted plasmid was eluted in RNase and DNase-free dH_2O.

3.3.3 Cloning and mutagenesis

SPATA2 cloning and mutagenesis

For the creation of a pcDNA3.1 MYC-hSPATA2, the hSPATA2 sequence was amplified from template cDNA using primers allowing a continuous open reading frame (ORF) which included the MYC tag and full length hSPATA2 (see table 2.6). The PCR performed for template amplification is detailed in table 3.5 and table 3.6. The resulting PCR product was run on a 1 % agarose gel with 2.5 μl of peqGREEN (per 50 μl of agarose gel mix) at 90 V for 20 min and the resulting band was excised and purified using a Machery-Nagel nucleospin gel and PCR clean-up kit as per manufacturer's protocol.

Component	**Volume (μl)**
5 x Phusion buffer	4
dNTPs (10 mM)	0.4
Forward primer (10 μM)	0.5
Reverse primer (10 μM)	0.5
Template (100 ng/μl)	0.4
Phusion DNA polymerase	0.2
dH_2O	up to 20

Table 3.5: Reaction mix for SPATA2 template PCR

Step	Temperature (^{o}C)	Time (mm:ss)
Denaturing	98	01:00
Amplification (25 cycles)	98 55 72	00:15 00:45 01:30
Final extension	72	05:00

Table 3.6: Details of the PCR cycles for SPATA2 template amplification

pcDNA 3.1 (+ve) plasmid and the PCR product were digested with NheI-HF and NotI-HF restriction enzymes in CutSmart buffer for 3 h at 37 ^{o}C before being re-purified with the Nucleospin gel and PCR clean-up kit. The resulting purified product concentrations were measured by Nanodrop and a ligation reaction was set up as per table 3.7 at a 3:1 molar ratio of SPATA2 insert to pcDNA3.1 vector and incubated at RT for 10 min before transformation into TOP10 *E.coli* as detailed in 3.3.2.

Component	Volume/Amount
10 x T4 ligation buffer	1 μl
DMSO	0.5 μl
pcDNA3.1	3:1 molar ratio with SPATA2
SPATA2 insert	3:1 molar ratio with pcDNA3.1
T4 DNA ligase	0.3 μl
dH_2O	up to 20 μl

Table 3.7: Ligation mix for SPATA2 into pcDNA3.1/CYLD into pBABE

For the generation of the MYC-hSPATA2 Y338A, Y338F, R212X, and V357X mutants, the template was the pcDNA 3.1 MYC-hSPATA2. For details of primers used see table 2.7 and for details of the reaction mix and cycles, see table 3.8 and 3.9.

Following the PCR reaction, clean-up was performed and the samples were transformed, grown, and prepped as described previously. To confirm the presence of the mutation, sequencing was performed with Eurofins (3 clones sent for each mutation).

CYLD cloning and mutagenesis

For cloning of CYLD into the pBABE vector, the pFLAG CMV2-CYLD vector was used. Amplification of the CYLD ORF (including FLAG tag) was performed

Component	Volume (μl)
5 x Phusion buffer	10
dNTPs (10 mM)	1
Forward primer (10 μM)	1
Reverse primer (10 μM)	1
Template (100 ng/μl)	1
DMSO	1.5
Phusion DNA polymerase	0.5
dH_2O	up to 50

Table 3.8: Reaction mix for SPATA2/CYLD mutagenesis PCR

Step	Temperature (^{o}C)	Time (mm:ss)
Denaturing	98	01:00
Amplification (18 cycles)	98	00:30
	55	01:00
	72	05:00
Final extension	72	10:00

Table 3.9: Details of the PCR cycles for SPATA2 mutagenesis

using primers as per table 2.6 and the reaction mix and pcr programme is outlined in table 3.10 and table 3.11.

Component	Volume (μl)
5 x Phusion buffer	4
dNTPs (10 mM)	0.4
Forward primer (10 μM)	0.5
Reverse primer (10 μM)	0.5
Template (100 ng/μl)	0.4
Phusion DNA polymerase	0.2
dH_2O	up to 20

Table 3.10: Reaction mix for FLAG-CYLD PCR

Ligation of the amplified FLAG-CYLD was performed by digestion of the pBABE vector and the FLAG-CYLD insert with BamHI-HF and SalI-HF in cutsmart buffer for 3 h at 37^{o}C. Following this, PCR cleanup was performed and a ligation reaction was set up as per table 3.7. The ligated construct was transformed into TOP10 *E.coli* and resulting colonies were picked and grown for mini-prep as previously described.

For the generation of pBABE FLAG-CYLD with S418A, S568A, C601A, L622D, I790D, and L475P mutations, primers from table 2.7 were used and the pcr was

Step	Temperature (^{o}C)	Time (mm:ss)
Denaturing	98	01:00
Amplification (25 cycles)	98 58 72	00:15 00:45 02:00
Final extension	72	05:00

Table 3.11: Details of the PCR cycles for FLAG-CYLD amplification

performed as per table 3.9. As previous, several colonies were picked, grown for mini prep, and sequenced with Eurofins to confirm the presence of the mutation.

3.4 Statistical analyses

All statistical analyses shown in this thesis were calculated by two-way ANOVA (analysis of variance) tests. Two-way ANOVA tests calculate the mean differences between groups with two independent variables (in this study, the cell type) on one dependent variable (stimulation).

In each case, the standard error of the mean (SEM) was used to indicate the error bars of replicates as multiple technical replicates were used in each experiment to generate a mean value. This sampling distribution was calculated for each experiment and the SEM refers to the change in the mean over each set of biological replicates (for each experiment n$\geq$3).

4

SPATA2 links CYLD and HOIP to regulate immune signalling

Contents

4.1 Introduction 65
4.2 SPATA2 interactions with CYLD and HOIP 65
4.2.1 SPATA2 binds CYLD in a B-box-dependent manner . . 65
4.2.2 SPATA2 interaction with CYLD 66
4.2.3 SPATA2 interaction with HOIP 70
4.2.4 SPATA2 links CYLD to LUBAC 73
4.3 SPATA2 bridges CYLD to receptor complexes 75
4.3.1 SPATA2 is required for CYLD recruitment to the TNFR complex I 75
4.3.2 Loss of SPATA2 leads to a loss of CYLD in high molecular weight complexes 76
4.4 SPATA2 regulates CYLD-mediated NF-κB responses . 78
4.4.1 SPATA2 controls the ubiquitin landscape of TNFR1 and NOD2 adaptor proteins 78
4.4.2 Loss of SPATA2 leads to less ubiquitinated substrates within the TNFR complex I but little effect on downstream signalling 81
4.4.3 Loss of SPATA2 leads to enhanced NF-κB activity in the NOD2 signalling pathway 84
4.5 CYLD does not regulate auto-ubiquitination of the LUBAC complex 86
4.6 Discussion 87

4.1 Introduction

OTULIN harbours a PIM that associates with the PUB domain of HOIP to create a high-affinity interaction, which is essential for OTULIN to regulate the auto-ubiquitination of LUBAC [137, 176]. A study by *Takiuchi et al* demonstrated that CYLD is also recruited to LUBAC and that this is dependent on the B-box domain of CYLD [177]. Furthermore, ongoing work within the Gyrd-Hansen lab identified that a single point mutation within the PIM-binding pocket of the PUB domain of HOIP (N102D) is sufficient to abrogate the association of both CYLD and OTULIN with the complex. CYLD does not contain a PIM, therefore how it is recruited to LUBAC in a HOIP PUB domain-, and CYLD B-box- dependent manner was unknown.

To address this question, a collaboration was formed with Paul Elliott of the Komander lab in Cambridge, who solved the structures presented within this chapter. *In vitro* data from Paul demonstrated that CYLD and HOIP do not directly interact so it was concluded that a third protein may be mediating this interaction. The identification and characterisation of this mediator will be the focus of this chapter.

4.2 SPATA2 interactions with CYLD and HOIP

4.2.1 SPATA2 binds CYLD in a B-box-dependent manner

To investigate the B-box-dependent recruitment of CYLD to LUBAC, FLAG-tagged WT CYLD ($CYLD^{WT}$) and CYLD with a deletion of its B-box domain ($CYLD^{DB-box}$) were purified and subjected to LC-MS/MS to identify interaction partners [80].

Several previously identified CYLD-interacting proteins identified validated the study (TAK1 [206], TRAF2 [153]), however, the most enriched protein identified in the WT CYLD IP relative to the ΔB-box CYLD IP was SPATA2 (figure 4.1b). To validate this interaction, $CYLD^{WT}$ and $CYLD^{DB-box}$ were transiently transfected into U2OS/NOD2 cells and immunoprecipitated to identify interacting partners.

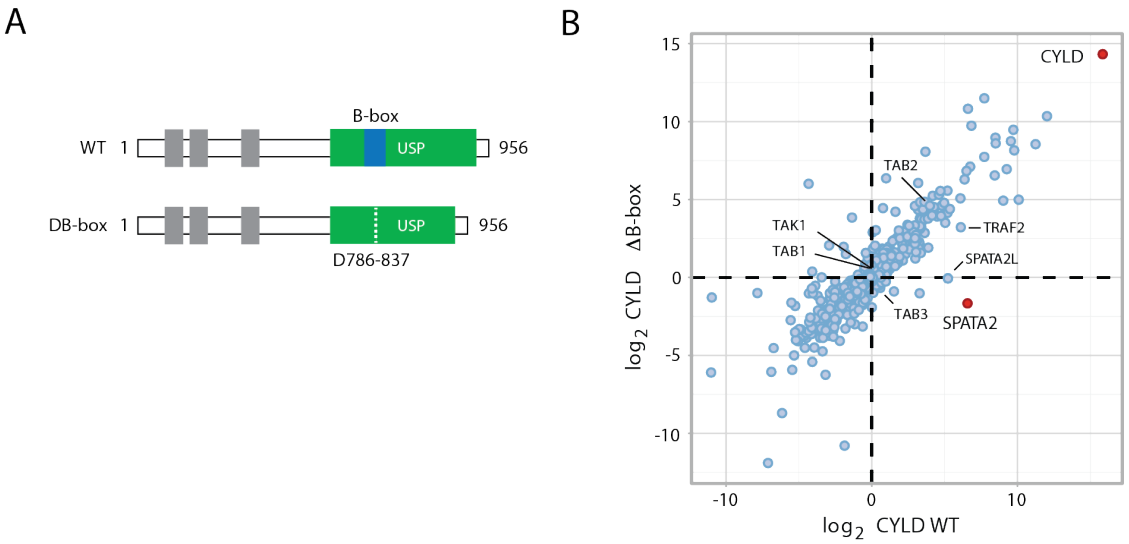


Figure 4.1: WT/ΔB-box CYLD structure and LC-MS/MS analysis. (A) A cartoon of the structure of Flag-tagged CYLD, showing the B-box region deleted for LC-MS/MS analysis. (B) A $\log_2$ plot of WT CYLD against ΔB-box CYLD showing identified interacting proteins. ***This LC-MS/MS experiment was performed by Matous Hrdinka of the Gyrd-Hansen lab, including analysis of the resulting data.*** Figure from [80].

$CYLD^{WT}$ interacts with HOIP and also SPATA2, whereas these interactions were completely lost with the $CYLD^{DB-box}$ mutant (figure 4.2A). The specificity of the antibody targeting SPATA2 was validated by two siRNA, which effectively reduce protein levels of SPATA2 compared to the mismatch (MM) control (figure 4.2B)

4.2.2 SPATA2 interaction with CYLD

Following its identification as a CYLD interacting partner, domain conservation analysis was performed for SPATA2. This found that it contains an N-terminal PUB domain, putative PIM, and C-terminal ZnF domain (figure 4.3A).

To address how CYLD interacts with SPATA2, CRISPR/Cas9 mediated knock-out of SPATA2 was performed within U2OS/NOD2 cells and several viable clones were obtained in which SPATA2 was not detected upon immunoprecipitation of endogenous CYLD (figure 4.4). The clone S2-4 was selected for use for further experiments and is hence force referred to as SPATA2 KO U2OS/NOD2 cells.

Myc-tagged constructs were generated for WT SPATA2 ($SPATA2^{WT}$) and a truncation mutant of only its PUB domain by the insertion of an early stop codon

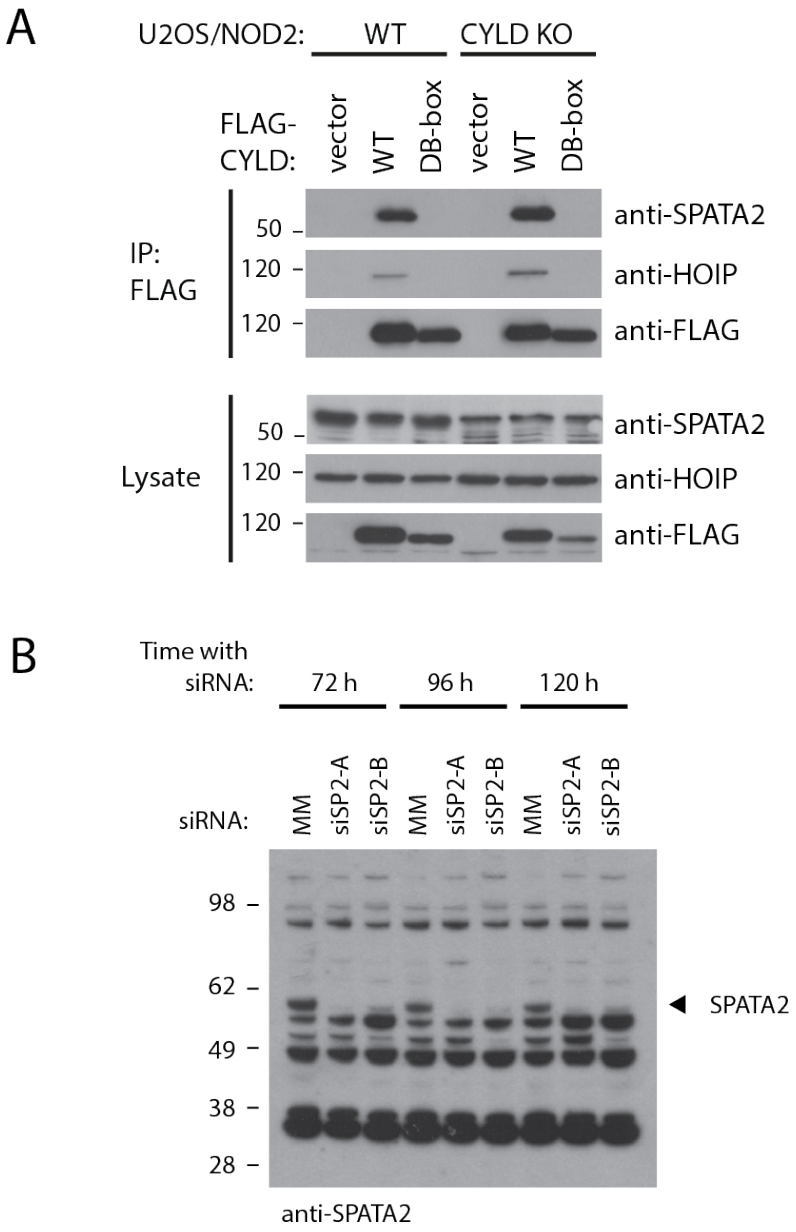


Figure 4.2: CYLD B-box is required for SPATA2:HOIP interactions. (A) Shown is a western blot from an IP of WT/ΔB-box CYLD highlighting the B-box dependent interaction with SPATA2. (B) Confirmation of the specificity of the SPATA2 (Bethyl, A302-494A) antibody using two siRNA targeting SPATA2. Figure from [80].

via site-directed mutagenesis ($SPATA2^{R212X}$)(figure 4.3B). These were transiently transfected into the SPATA2 KO cells and purified by immunoprecipitation on the Myc tag of the SPATA2 constructs. Both $SPATA2^{WT}$ and $SPATA2^{R212X}$ showed an interaction with CYLD at steady state, indicating that CYLD and SPATA2 interact at steady state, but also that CYLD associates with the PUB

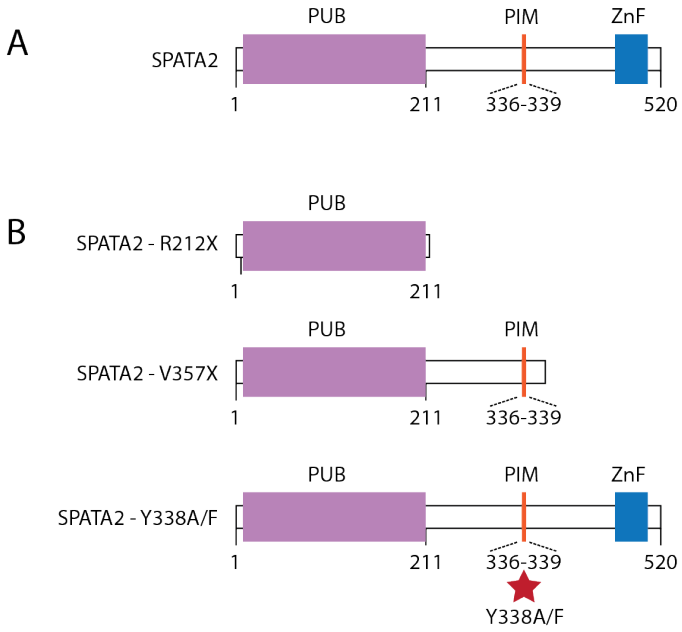


Figure 4.3: The domain structure of SPATA2. (A) The domain structure of SPATA2 showing the corresponding amino acid residues for the PUB domain and PIM (B) Constructs of SPATA2 generated for this study. Figure from [80].

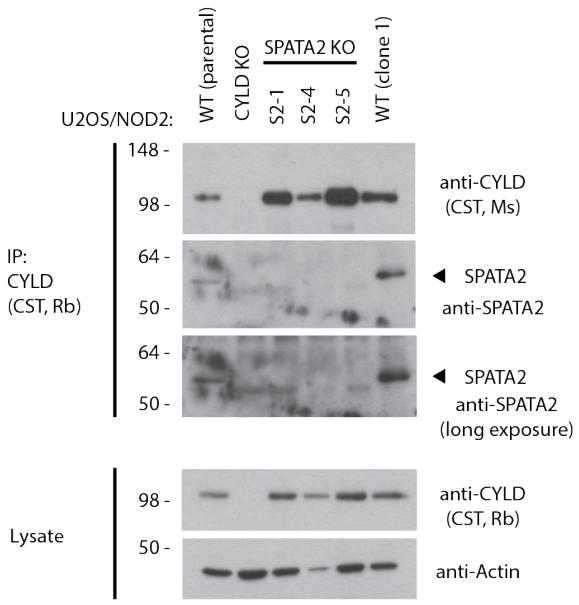


Figure 4.4: Confirmation of SPATA2 KO U2OS/NOD2 cells. Shown is an IP of endogenous CYLD, blotting for SPATA2, on several SPATA2 KO clones. Figure from [80].

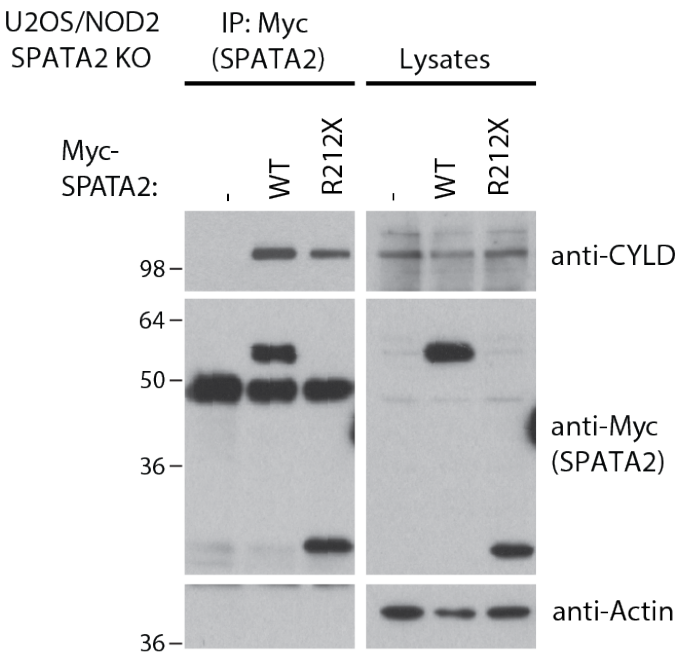


Figure 4.5: The SPATA2 PUB domain interacts with CYLD. IP of Myc-tagged WT and R212X SPATA2 constructs in SPATA2 KO U2OS / NOD2 cells. Figure from [80].

domain of SPATA2 (figure 4.5).

As CYLD associates with the PUB domain of SPATA2, but not that of HOIP, we sought to determine how this interaction occurs. Structural analysis of the PUB domain of SPATA2 showed that it contains a fold structure similar to that of HOIP and also the smaller PUB domain of PNGase (figure 4.6). Previously mapped PUB-PIM interactions consist of a conserved Asp-Leu/Met-Tyr for the PIM where the Leu and Tyr insert into a hydrophobic pocket on the PUB surface [137]. Whilst the fold structure of the SPATA2 PUB domain is similar to that of HOIP and PNGase, the hydrophobic binding pocket is significantly different and does not bind any known PIM; however, mutations within the PIM binding pocket of the SPATA2 PUB abrogated the interaction with CYLD, showing that CYLD interacts with the PUB domain of SPATA2 in a PIM-independent manner.

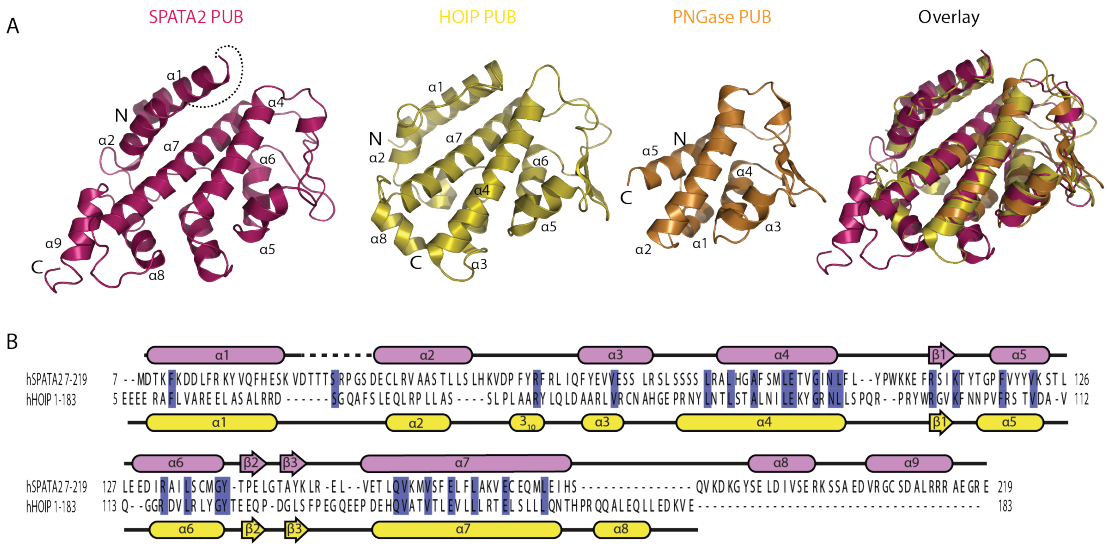


Figure 4.6: Fold structure of the SPATA2 PUB domain (A) A comparison of the fold structure of the SPATA2 PUB domain with that of HOIP and PNGase. (B) Sequence overlay of the amino acid sequences of the SPATA2 and HOIP PUB domains. ***The crystal structures of the SPATA2 PUB domain and alignment were performed by Paul Elliott of the Komander lab, LMB, Cambridge.*** Figure from [80].

4.2.3 SPATA2 interaction with HOIP

Species conservation analysis of the sequence of SPATA2 revealed that it also contains a highly conserved PIM (Asp-Leu-Tyr-Thr) between amino acids 336 and 339, similar to that of OTULIN [137, 176] (figure 4.7).

SPATA2 and OTULIN PIMs are similar in their sequence alignment but differ with the presence of the Leu-337 in SPATA2 compared to the Met-55 in OTULIN; Furthermore, the SPATA2 PIM closely resembles that of the originally derived p97 PIM sequence (Asp-Leu-Tyr-Gly-COO^-) [137, 176, 227].

Given that SPATA2 has a PIM similar to that of OTULIN, I investigated if it could bind HOIP and if this domain is important for the interaction. I generated a truncation mutant of SPATA2 at position 357 ($SPATA2^{V357X}$; the PUB domain and putative PIM) and, together with the $SPATA2^{WT}$ and $SPATA2^{R212X}$ constructs previously generated, this was transiently expressed in SPATA2 KO cells. An immunoprecipitation of the MYC-SPATA2 constructs was performed at steady state to assess interactions with these mutants (figure 4.8). $SPATA2^{WT}$ was shown to interact with HOIP whereas the $SPATA2^{R212X}$ mutant did not, indicating that the

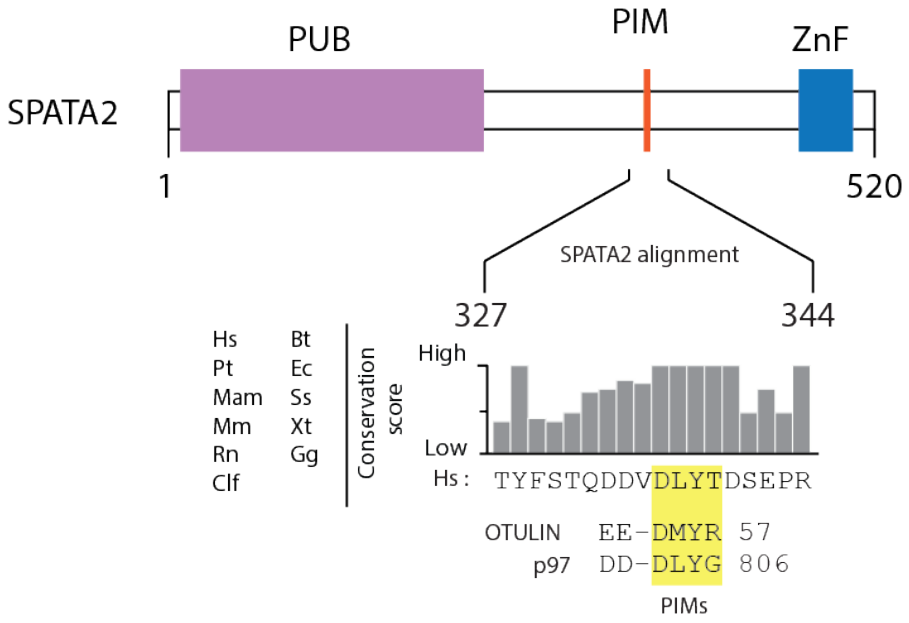


Figure 4.7: SPATA2 contains a conserved PIM. Conservation analysis of the SPATA2 PIM with the OTULIN and p97 PIMs. Figure from [80].

interaction occurs outside of the PUB domain. Notably, the SPATA2^{V357} mutant, which includes the PIM of SPATA2, was able to interact with HOIP, suggesting that the PIM is required for the SPATA2:HOIP interaction (figure 4.8).

To confirm whether the binding of SPATA2 to HOIP requires the conserved PIM, and not another region between the PUB domain and PIM, I mutated the conserved Tyr of the SPATA2 PIM to alanine (SPATA2^{Y338A}) and phenylalanine SPATA2^{Y338F} (figure 4.3). These constructs were transiently expressed in SPATA2 KO cells alongside SPATA2^{WT} and SPATA2^{R212X} as controls. Immunoprecipitation by the MYC tag was performed and the purified material was examined for HOIP interactions by western blot analysis (figure 4.9). As shown previously, SPATA2^{WT}, containing an intact PIM, interacted with HOIP; however, mutation of the key Tyr residue within the PIM (SPATA2^{Y338A}/SPATA2^{Y338F}) completely abrogated the interaction, akin to not having the PIM present at all (SPATA2^{R212X}). In contrast, the association of CYLD with SPATA2 was not affected by any mutation of the PIM.

Confirming the observation that the PIM of SPATA2 is required for the interaction with HOIP, the crystal structure of the HOIP PUB domain containing the SPATA2 PIM was solved (figure 4.10: 2.7Å). The interaction of the SPATA2 PIM

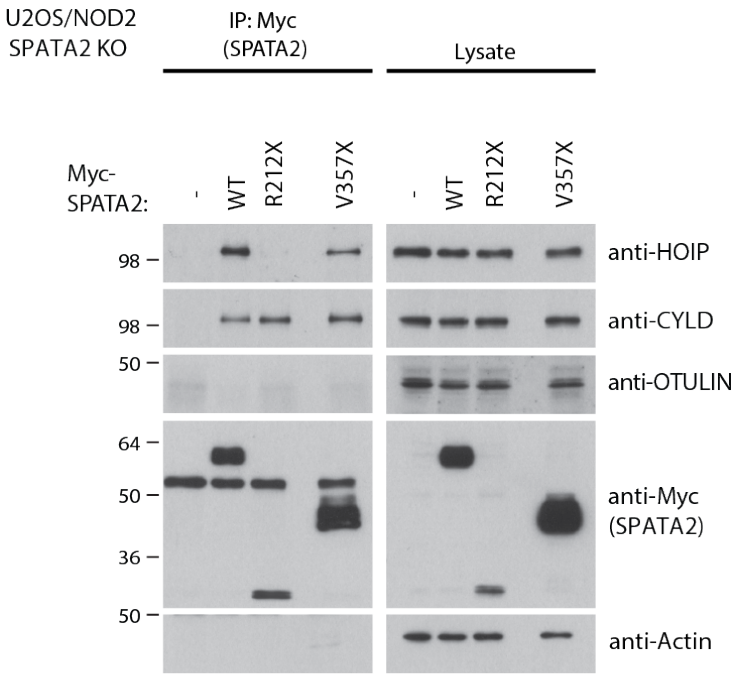


Figure 4.8: The SPATA2 PIM is required for binding to HOIP. IP of full length (WT), R212X truncation (PUB only), and V357X truncation (PUB and PIM) SPATA2 to assess binding to HOIP. Figure from [80].

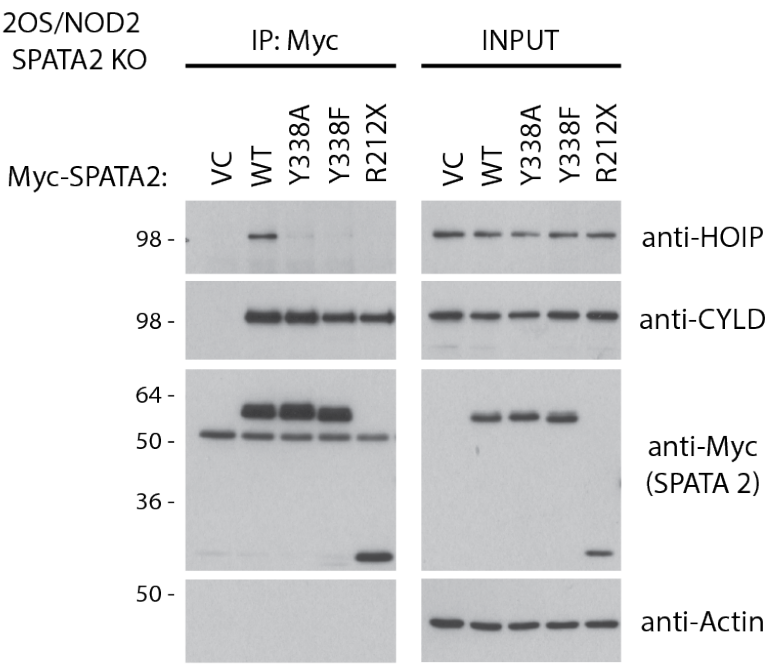


Figure 4.9: Mutating the SPATA2 PIM abrogates HOIP interactions. IP of Myc-tagged WT, or PIM-mutated (Y338A/F) SPATA2 to assess HOIP binding. Figure from [80].

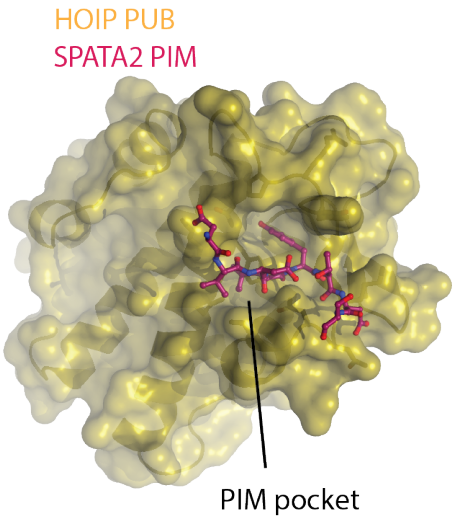


Figure 4.10: The SPATA2 PIM binds HOIP PUB domain. Crystal structure of the HOIP PUB domain binding the SPATA2 PIM (2.7 Å resolution). ***The crystal structure of the SPATA2 PIM bound to the HOIP PUB domain was performed by Paul Elliott of the Komander lab, LMB, Cambridge.*** Figure from [80].

with the HOIP PUB domain is identical to that of OTULIN and highlights the exclusivity of CYLD and OTULIN recruitment to LUBAC.

4.2.4 SPATA2 links CYLD to LUBAC

Having confirmed that SPATA2 binds CYLD (non-canonical PUB interaction) and also HOIP (classical PUB:PIM interaction), I investigated whether it is able to bridge the interaction of CYLD and LUBAC.

WT, CYLD KO, and SPATA2 KO U2OS/NOD2 cells were transiently transfected with V5-tagged HOIP and, after 48 h, HOIP was immunoprecipitated by the V5 tag to assess interactions with CYLD (figure 4.11). In WT cells, HOIP showed an interaction with CYLD; however, this interaction was lost in the SPATA2 KO cells, indicating that, at steady state levels, SPATA2 can bridge the interaction between CYLD and HOIP.

To ensure that the lack of interaction observed between CYLD and HOIP in the SPATA2 KO U2OS/NOD2 cells was due to the loss of SPATA2 and not any other factors resulting from the CRISPR/Cas9 KO process, I repeated the V5-HOIP immunoprecipitation with WT and SPATA2 KO U2OS/NOD2 cells with the

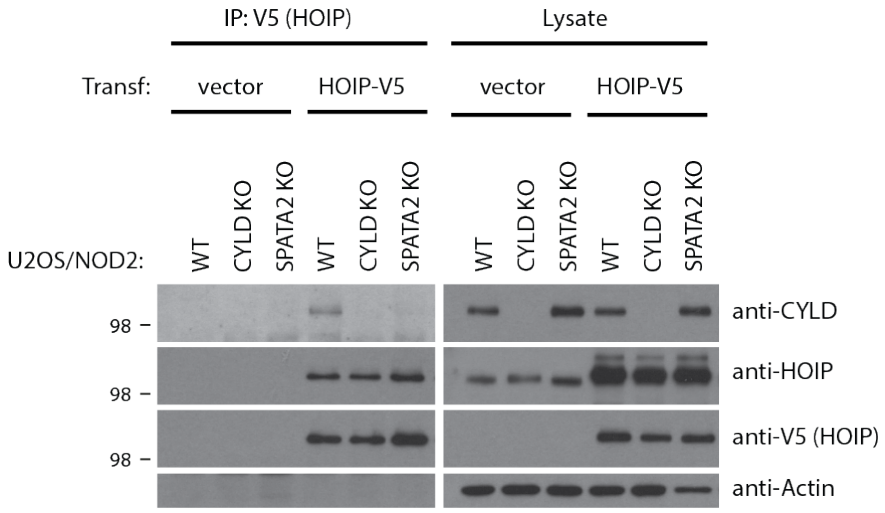


Figure 4.11: SPATA2 KO inhibits CYLD:HOIP interactions. IP of reintroduced V5-tagged HOIP into WT, CYLD KO, and SPATA2 KO U2OS/NOD2 cells to assess the requirement of SPATA2 for CYLD recruitment to LUBAC. Figure from [80].

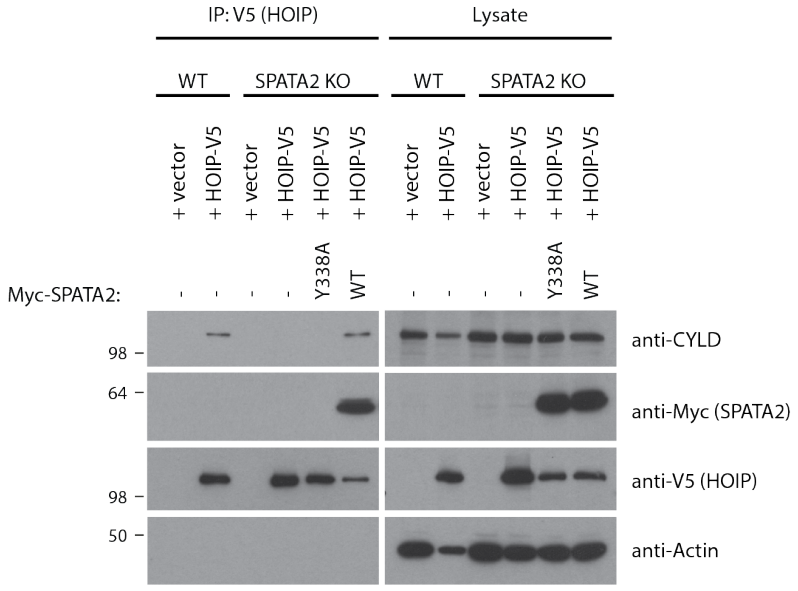


Figure 4.12: WT SPATA2 restores CYLD:HOIP interactions. IP of V5 - HOIP in SPATA2 KO background with the transient reintroduction of WT or PIM-mutated (Y338A/F) SPATA2. Figure from [80].

additional transient expression of Myc-tagged SPATA2^{WT} or SPATA2^{Y338A} in the SPATA2 KO cells (figure 4.12). V5-HOIP immunoprecipitation in WT U2OS/NOD2 cells showed an interaction with CYLD, which was lost in SPATA2 KO U2OS/NOD2 cells; however, reintroduction of SPATA2^{WT}, but not SPATA2^{Y338A}, restored the interaction between HOIP and CYLD. This confirmed that SPATA2 is the main factor mediating the association of HOIP and CYLD and that the PIM of SPATA2 is crucial for this interaction.

4.3 SPATA2 bridges CYLD to receptor complexes

4.3.1 SPATA2 is required for CYLD recruitment to the TNFR complex I

It has previously been shown that immunoprecipitation of TNFR complex I recruits LUBAC components and also CYLD [91]; Thus, I investigated whether the association of CYLD with the TNFR complex I is dependent on SPATA2. Purification of the TNFR complex I can be achieved by stimulation of cells with FLAG-tagged TNF for given time points. Following stimulation, cells are washed and an immunoprecipitation is performed on the FLAG tag of TNF to purify the TNFR-bound complex I and, with it, its associated components.

WT and SPATA2 KO U2OS/NOD2 cells were stimulated with FLAG-tagged TNF for 5 and 15 minutes before purification of the TNFR complex I (figure 4.13). In WT U2OS/NOD2 cells, both HOIP and CYLD were recruited to the complex. However, in SPATA2 KO U2OS/NOD2 cells, the association of CYLD with the complex was completely lost, though HOIP remained associated. This result is in line with the previous data showing that SPATA2 is bridging the interaction between HOIP and CYLD and introduces a role for SPATA2 in mediating CYLD recruitment to the TNFR complex I via LUBAC.

As previously reported, OTULIN was not found to be a part of the TNFR complex I [91]. Furthermore, this association was not present even in the absence of SPATA2.

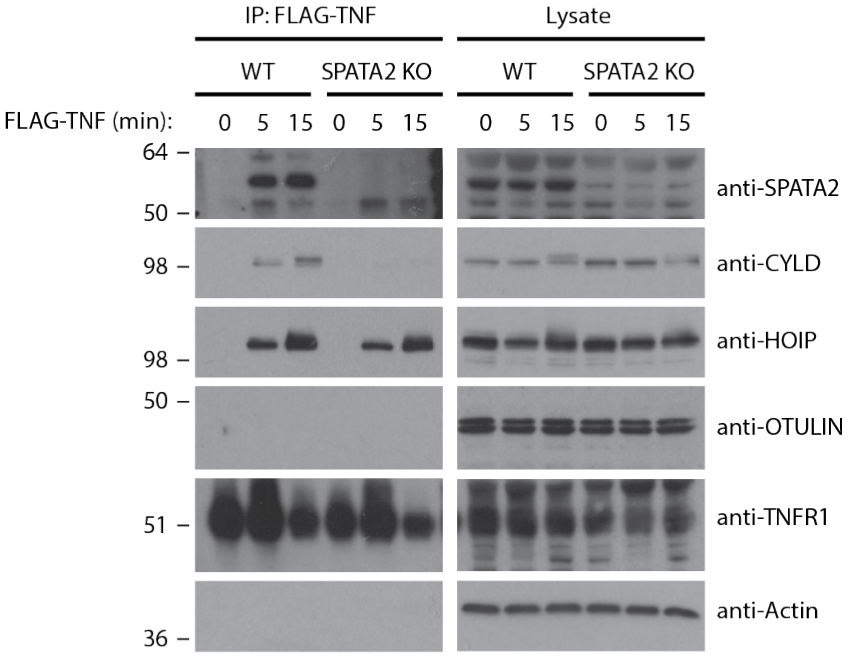


Figure 4.13: SPATA2 is required for CYLD recruitment to TNFR complex I. FLAG-TNF IP of the TNFR complex I, with 1 μg of FLAG-TNF per IP, to assess binding of CYLD in the absence of SPATA2. Figure from [80].

4.3.2 Loss of SPATA2 leads to a loss of CYLD in high molecular weight complexes

As SPATA2 associates with CYLD and HOIP at steady state levels as well as following TNF receptor stimulation, I investigated how SPATA2 affects the recruitment of CYLD to high MW complexes in the cell as a whole. Sucrose density gradient ultracentrifugation was utilised to investigate this as it is a powerful technique that fractions macromolecules such as DNA, RNA, and proteins by their MW. This is achieved by the layering of a sample containing different sizes of macromolecules onto the surface of a sucrose gradient where the density increases linearly from top to bottom.

Whole cell lysates from unstimulated WT, CYLD KO, and SPATA2 KO

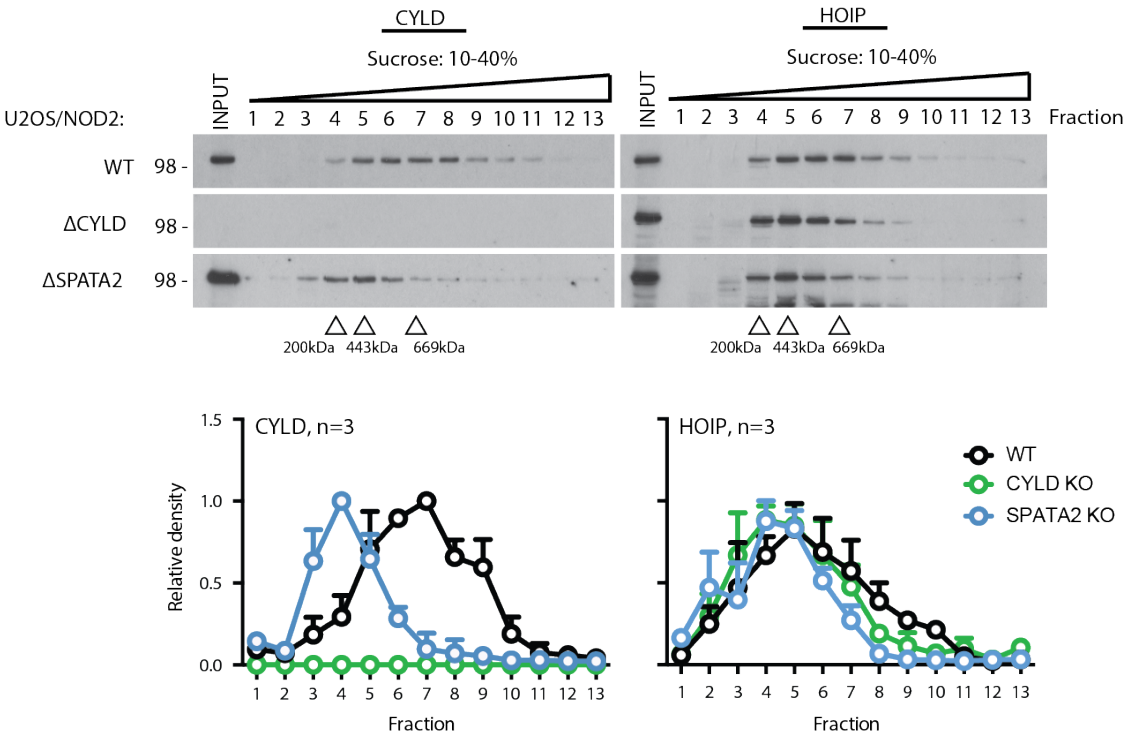


Figure 4.14: SPATA2 links CYLD to high MW complexes. Sucrose gradient sedimentation of CYLD in WT, CYLD KO, and SPATA2 KO U2OS/NOD2 cells. ***The sucrose gradient sedimentation step was performed by Norbert Volkmar of the Christianson lab, Oxford. All other steps were performed by myself.*** Figure from [80].

U2OS/NOD2 cells were layered onto a 10-40 % sucrose gradient and subjected to ultracentrifugation. The resulting sample was separated into 13 different fractions, where each sample reflected a particular MW range, and the material was subjected to western blot analysis where the presence of a protein within a sample reflects its presence in a MW complex within the mass range of the sample (figure 4.14). CYLD in WT U2OS/NOD2 cells was present in fractions 4 through 11, with a peak MW density of around 600-700 kDa. In contrast, CYLD in SPATA2 KO U2OS/NOD2 cells was present in lower MW fractions with a peak density of around 200-300 kDa. Taken together, this suggested that the majority of CYLD within the cell, at steady state, is bound with SPATA2, which links it to LUBAC and potentially other high MW complexes.

The sedimentation pattern of HOIP upon loss of SPATA2 also underwent a minor downwards shift in the MW fractions it was present within (difference in

densitometry peak of around 250-300 kDa). As the SPATA2 KO and CYLD KO sedimentation patterns of HOIP were similar compared to parental cells, it is possible that this smaller shift was representative of the loss of SPATA2:CYLD dimers from the LUBAC complex. This hypothesis is supported by data from Paul Elliott showing that SPATA2 and CYLD both function and bind each other as homodimers, giving a quaternary complex consisting of two SPATA2 and two CYLD proteins (Data not shown). As the predicted MW of such a complex is around 330 kDa, it is possible that the loss of SPATA2:CYLD may be causing this shift as it closely matches the observed densitometry peak difference of 250-300 kDa.

4.4 SPATA2 regulates CYLD-mediated NF-κB responses

4.4.1 SPATA2 controls the ubiquitin landscape of TNFR1 and NOD2 adaptor proteins

Upon stimulation with their respective ligands, the TNF and NOD2 adaptor proteins, RIPK1 and RIPK2 respectively, are heavily ubiquitinated, which can be detected through pulldown with a TUBE (Tandem Ubiquitin Binding Entity) to enrich for ubiquitinated substrates and subsequent immunoblotting with anti-RIPK1 or anti-RIPK2 antibodies. The resulting blot shows a 'smear' representing the ubiquitin-conjugated form of the adaptor protein.

Ongoing work within the lab identified CYLD as a major regulatory component of the ubiquitination of RIPK1 and RIPK2. Thus, a loss of CYLD from these systems represents a loss of regulation of the E3 enzymes in the systems, which leads to an unregulated deposition of polyubiquitin chains. This is detectable in this assay through the presence of higher MW ubiquitin species than the WT control.

To assess how the loss of SPATA2 affects the ubiquitination landscape of these complexes, WT, CYLD KO, and three SPATA2 KO clones (S2-1, S2-4, and S2-5) were stimulated with TNF or L18-MDP (for NOD2 receptor activation), and a TUBE pulldown was performed (figure 4.15). As discussed, the CYLD KO cells compared to the WT U2OS/NOD2 cells showed a higher MW smear for both RIPK1

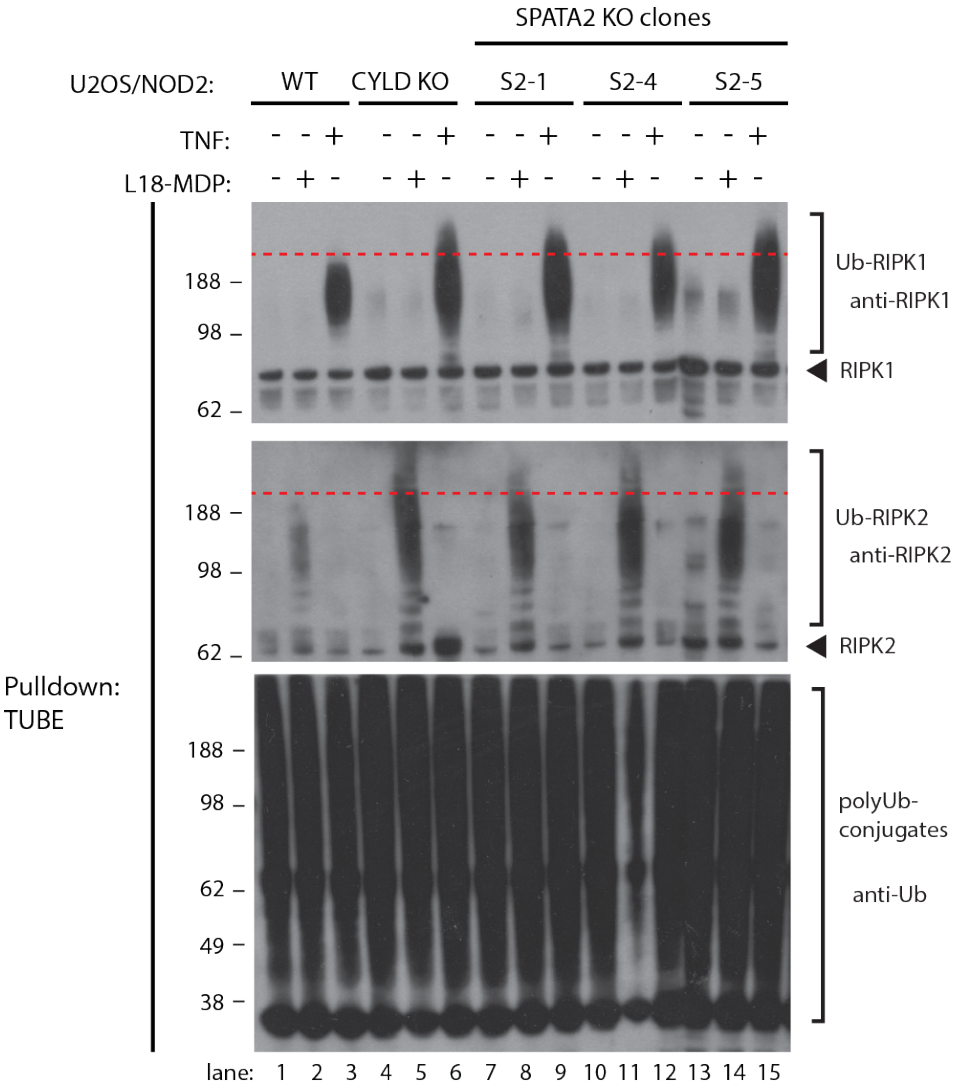


Figure 4.15: SPATA2 regulates CYLDs ability to control ubiquitination. TUBE pulldown from parental (WT), CYLD KO, and SPATA2 KO U2OS/NOD2 cells following stimulation with 5 ng/ml TNF for 15 min and 200 ng/ml L18-MDP for 1 h to assess ubiquitination of their key adaptor proteins, RIPK1 and RIPK2. Figure from [80].

and RIPK2, indicating a loss of regulation of the deposition of polyubiquitin chains. Phenocopying the CYLD KO, all SPATA2 KO clones also showed a deregulation of the ubiquitin chain deposition on these receptors. This is in line with previous data in this study showing that CYLD is recruited to the TNFR complex I via SPATA2 but also indicates an important role for SPATA2 for the CYLD-mediated regulation of the NOD2 adaptor, RIPK2.

The ubiquitination status of these receptor complexes is a constant balance between the rate of deposition and the removal of polyubiquitin chains. Therefore, to more precisely investigate the role of factors affecting the disassembly of ubiquitin chains, it is possible to remove factors that are contributing to the deposition of chains. This was achieved through the use of SMAC mimetics which, as discussed, are small molecules degrading IAPs. In the NOD2 system, cIAP1/2 are degraded and XIAP is blocked from interacting with RIPK2 following addition of the SMAC mimetic, compound A (CpA). This removal of several E3s from the system limits the rate of ubiquitin deposition and, as the rate of the removal of these chains is not affected, this results in a complete loss of ubiquitination from the adaptor and blocks productive signalling [124].

CYLD is a major regulator of RIPK2 ubiquitination and ongoing work within the lab identified that its loss can 'rescue' the polyubiquitin smear seen on RIPK2 following NOD2 stimulation in the presence of CpA. This indicates that the residual E3 activity for the NOD2 receptor system remaining following CpA treatment is sufficient for productive signalling if the major regulator of the system, CYLD, is not present.

To more clearly investigate if SPATA2 is mediating this CYLD-mediated regulation of RIPK2 following CpA, a TUBE pulldown was performed on WT, CYLD KO, and three SPATA2 KO clones following NOD2 receptor stimulation with or without pretreatment with CpA (figure 4.16). As expected, pre-treatment of WT cells with CpA prior to L18-MDP stimulation lead to the abolishment of the ubiquitin smear on RIPK2 and a lack of productive signalling, as shown by the lack of IκB degradation; whereas, CpA treatment prior to stimulation in CYLD KO cells lead to the retention of the previously observed higher MW ubiquitin smear. As with CYLD KO, SPATA2 KO also resulted in the retention of the deposition of ubiquitin on RIPK2 following CpA pre-treatment prior to L18-MDP stimulation., indicating an important role for SPATA2 in controlling the CYLD-mediated regulation of NOD2 signalling.

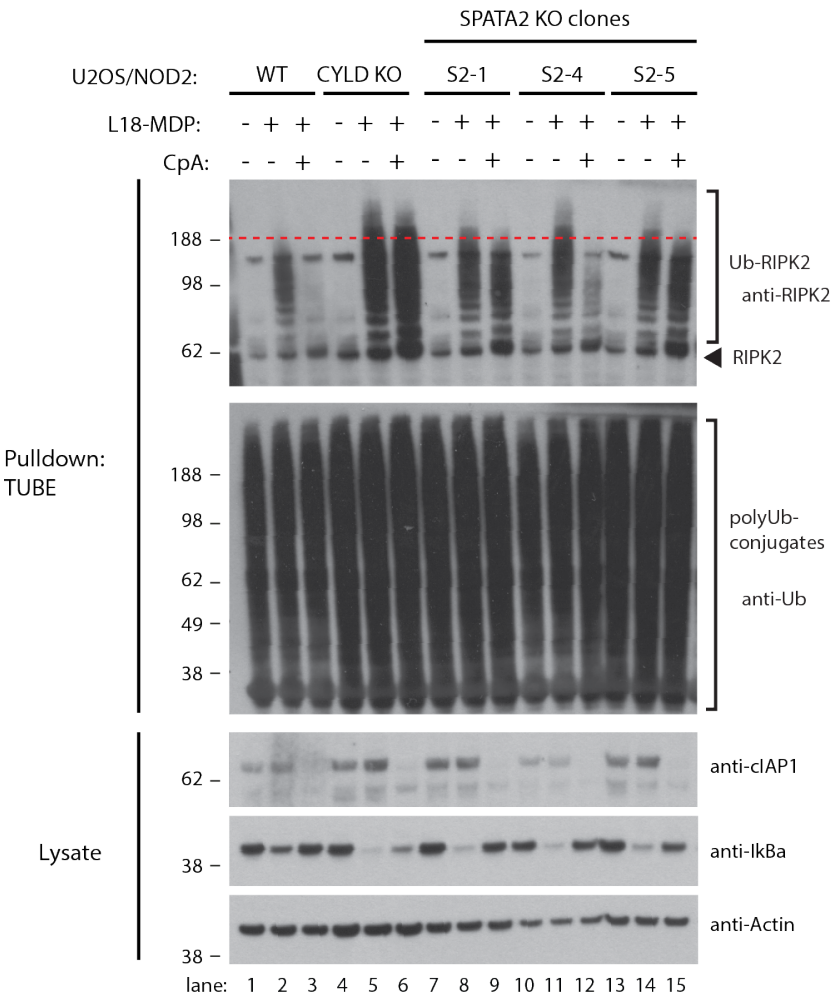


Figure 4.16: SPATA2 regulates RIPK2 ubiquitination following CpA/MDP. TUBE pulldown from parental (WT), CYLD KO, and SPATA2 KO U2OS/NOD2 cells following stimulation with 1 μM CpA for 30 min prior to 200 ng/ml L18-MDP for 1h to assess ubiquitination of RIPK2. Figure from [80].

4.4.2 Loss of SPATA2 leads to less ubiquitinated substrates within the TNFR complex I but little effect on downstream signalling

Pulldown of the TNFR complex I by FLAG-TNF allows for the detection of individual components of the complex, thus I sought to investigate how loss of SPATA2 affected the ubiquitination of these.

WT and SPATA2 KO U2OS/NOD2 cells were stimulated with FLAG-tagged TNF before FLAG immunoprecipitation for pulldown of complex I. Purified material

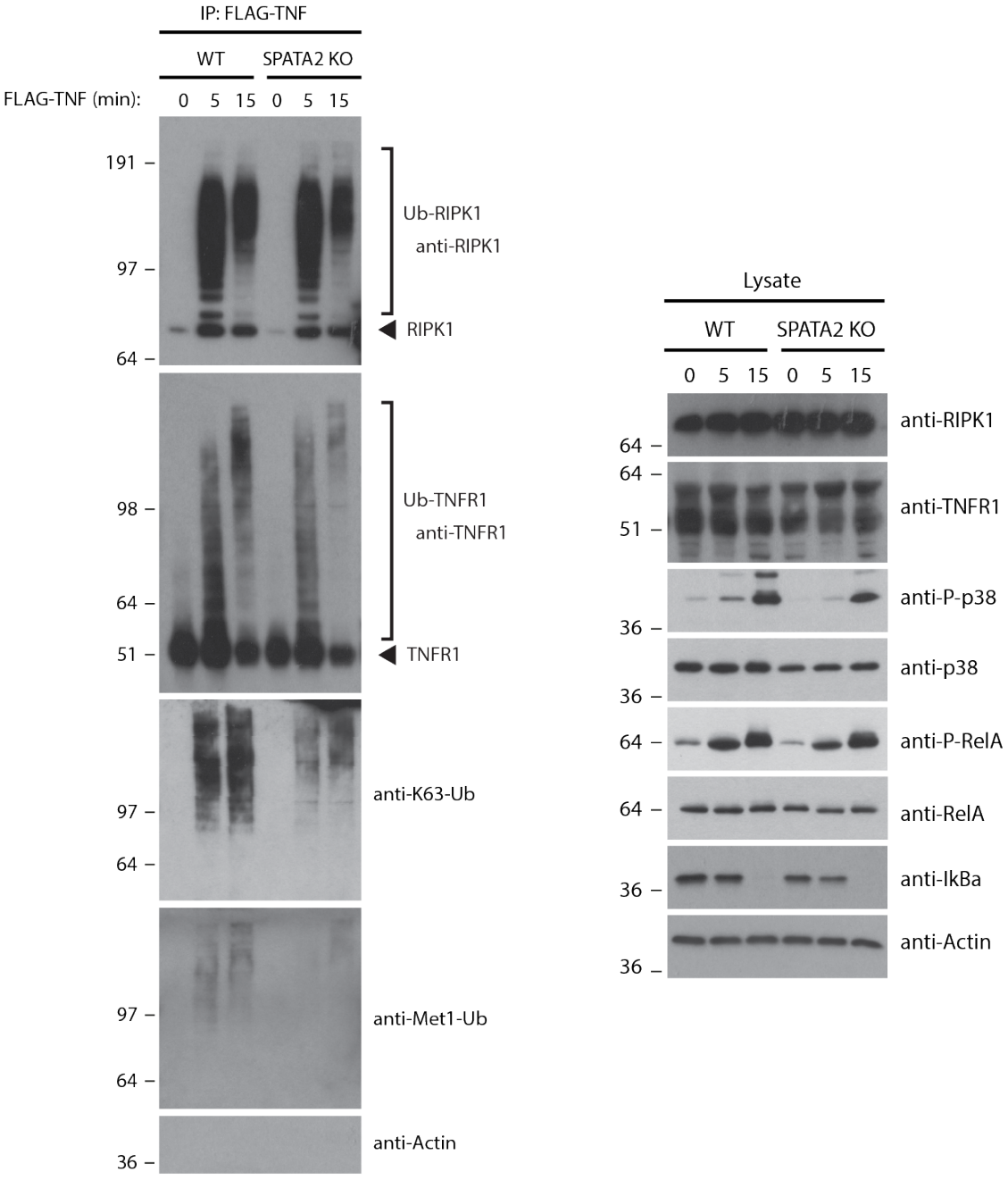


Figure 4.17: SPATA2 KO affects ubiquitination of TNFR complex I substrates. FLAG - TNF pulldown of the TNFR complex I, with 1 μg of FLAG-TNF per IP, in parental (WT) and SPATA2 KO U2OS/NOD2 cells to assess how SPATA2 affects ubiquitination of the complex. Figure from [80].

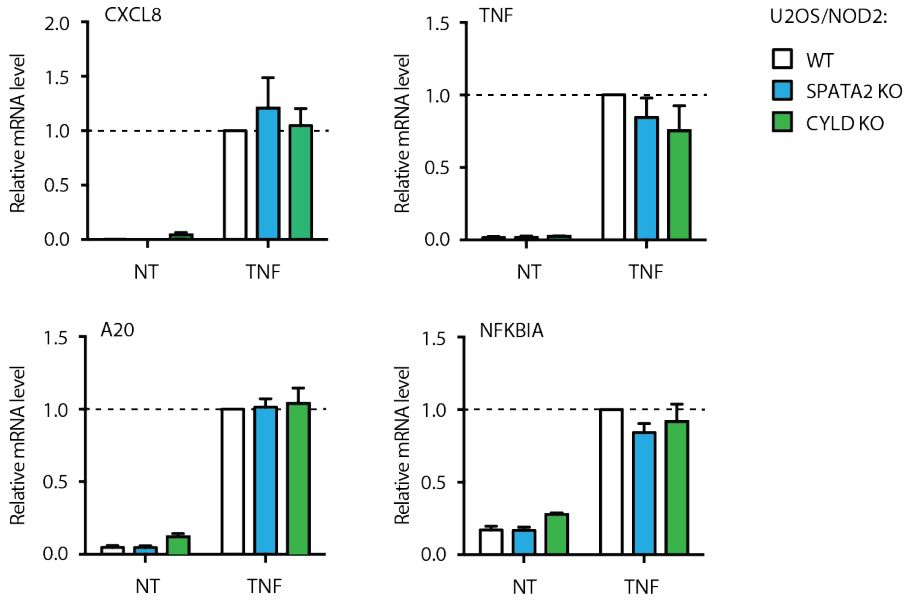


Figure 4.18: SPATA2 and CYLD do not regulate TNF signalling. qRT- PCR performed on parental (WT), CYLD KO, and SPATA2 KO U2OS/NOD2 cells following stimulation with 5 ng/ml TNF for 3 h. Data normalised to HPRT control and subsequently the $CYLD^{WT}$ stimulated condition. Data was collated from three experiments and analysed in Graphpad prism 6 with statistic tests by two-way ANOVA. Figure from [80].

was subjected to analysis by western blot to assess the ubiquitination of RIPK1 and TNFR1 (figure 4.17). SPATA2 KO cells displayed a reduction in the levels of polyubiquitin on TNFR1 when compared to WT cells. Furthermore, since CYLD is a reported M1 and K63 DUB, I probed all purified material for total levels of K63 and M1 ubiquitin. As with TNFR1, SPATA2 KO cells showed a marked reduction in the levels of ubiquitin when compared to WT cells. This suggested that SPATA2 not only regulates the ubiquitination of LUBAC substrates but also contributes to the retention of ubiquitinated proteins within the complex.

Ongoing work within the lab suggested that CYLD has little effect on the downstream signalling of TNF with regards to activation of the MAPK p38, phosphorylation of the NF-κB subunit RelA, or the degradation of IκB. In accordance with this, SPATA2 KO cells showed little effect on the activation/degradation of these factors.

To confirm this observation, qRT-PCR analysis of the NF-κB target genes CXCL-8, TNF, A20, and NFKBIA was performed following stimulation with TNF for 3 h

(figure 4.18). Relative to WT cells, SPATA2 and CYLD KO cells showed no significant difference in the level of transcription for these proinflammatory mediators.

Taken together, this highlights a role for SPATA2 in mediating the ubiquitin landscape of the TNFR complex I, but that SPATA2 KO or CYLD KO has no major effects on downstream signalling events.

4.4.3 Loss of SPATA2 leads to enhanced NF-κB activity in the NOD2 signalling pathway

The loss of SPATA2 leads to increased production of pro-inflammatory transcripts

As the loss of SPATA2 also affected the ubiquitination landscape of the NOD2 receptor, I investigated whether its absence has a major role in the downstream signalling events of NOD2 signalling. To do so, I performed qRT-PCR analysis investigating NF-κB target genes following stimulation with L18-MDP for 3 h (figure 4.19). In contrast to the TNFR stimulation, SPATA2 KO cells displayed higher levels of CXCL-8, TNF, A20, and NFKBIA transcripts (similar to CYLD KO) when compared to WT cells. In addition to confirming that CYLD negatively regulates downstream transcriptional events of NOD2 signalling, this also highlighted a role for SPATA2 in mediating this regulation.

The loss of SPATA2 leads to an increased production of CXCL-8

As SPATA2 and CYLD KO both negatively regulate downstream signalling events in NOD2 signalling, I investigated whether this effect translated to the production of the proinflammatory mediator, CXCL-8. To investigate this, WT, CYLD KO, SPATA2 KO, and the parental U2OS/NOD2 cells from which the SPATA2 and CYLD KO cells were produced, were stimulated with L18-MDP in the presence of brefeldin A and monensin for 5 h (figure 4.20). Brefeldin A and monensin are protein transport inhibitors which prevent the cellular secretion of CXCL-8 following L18-MDP stimulation. After 5 h, cells were fixed, permeabilised, and stained with an anti-CXCL-8 fluorescent antibody prior to analysis by flow cytometry to determine the percentage of cells which were positive for CXCL-8 production.

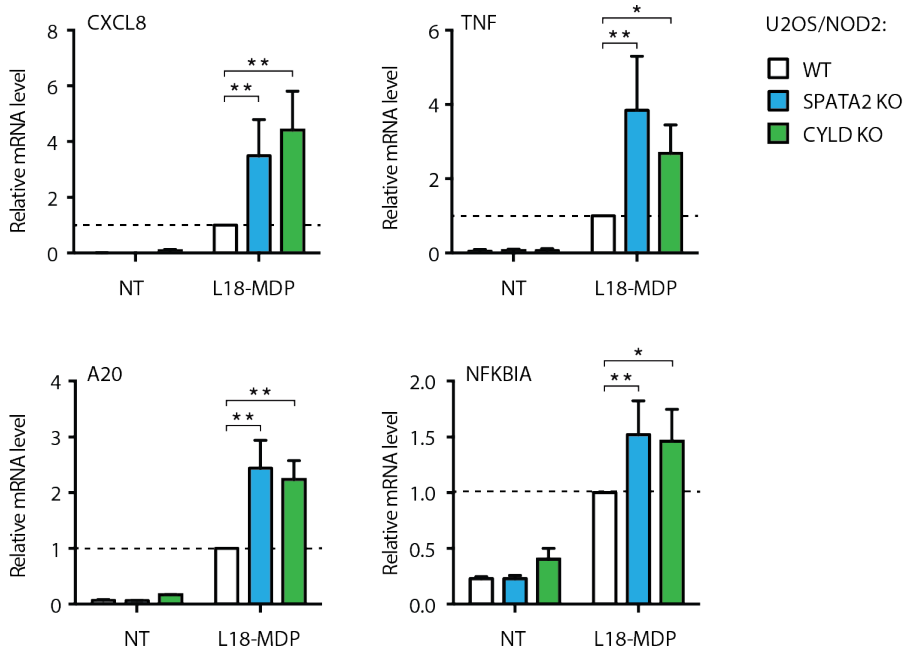


Figure 4.19: SPATA2 is important for the regulation of NOD2 signalling. qRT-PCR performed on parental (WT), CYLD KO, and SPATA2 KO U2OS/NOD2 cells following stimulation with 200 ng/ml L18-MDP for 3 h. Data normalised to HPRT control and subsequently the $CYLD^{WT}$ stimulated condition. Data was collated from three experiments and analysed in Graphpad prism 6 with statistical tests by two-way ANOVA. Figure from [80].

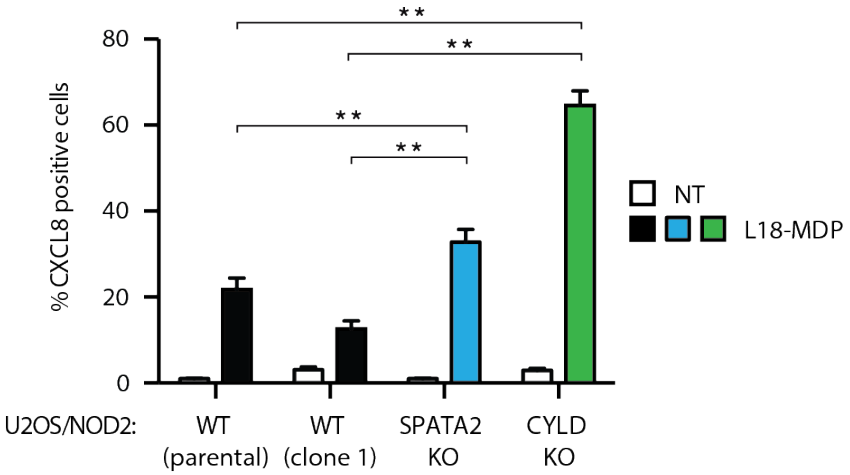


Figure 4.20: SPATA2 regulates CXCL8 production from NOD2 signalling. Flow cytometry analysis to assess CXCL-8 production performed on parental (WT), CYLD KO, and SPATA2 KO U2OS/NOD2 cells following stimulation with 200 ng/ml L18-MDP for 5 h the presence of 5 μg/ml brefeldin A and 2 μM monensin. Data was collated from 15 biological replicates and analysed in Graphpad prism 6 with statistical tests by two-way ANOVA. Figure from [80].

Similar to that observed with transcript production, SPATA2 KO and CYLD KO cells displayed a greater percentage of CXCL-8-positive cells when compared to WT cells (albeit SPATA2 KO cells showed a lower responding percentage when compared to CYLD KO cells).

Nonetheless, taken together, these data highlighted a role for SPATA2 in the CYLD-mediated regulation of the NOD2 receptor system.

4.5 CYLD does not regulate auto-ubiquitination of the LUBAC complex

OTULIN and the SPATA2:CYLD complex occupy the same PIM binding pocket of the LUBAC catalytic subunit, HOIP, and can both regulate NF-κB activation via their DUB activity [137, 176, 177]. LUBAC is constitutively active and, in the absence of OTULIN regulation, autoubiquitination of its components can be observed. Together with initial *in vitro* reports that CYLD can cleave both M1- and K63-polyubiquitin chains, this suggested that CYLD may also have an ability to regulate the auto-ubiquitination of the LUBAC complex [29, 228].

To address this question, U2OS/NOD2 cells with stable virally introduced shRNA targeting OTULIN, CYLD, or a non-specific (NS) control were generated. To observe the ubiquitination of HOIP, an M1-specific TUBE was used (M1-SUB) to enrich for substrates modified with M1 chains. Subsequent western blot analysis with an anti-HOIP antibody allowed for the identification of dysregulated LUBAC, through the presence of a polyubiquitination 'smear' on HOIP (figure 4.21). Knockdown of OTULIN leads of the removal of LUBAC regulation and thus leads to its auto-ubiquitination. In contrast, knockdown of CYLD did not result in the spontaneous ubiquitination of LUBAC.

In addition to highlighting the importance of OTULIN in regulating LUBAC function to prevent its auto-ubiquitination, this demonstrates that CYLD does not regulate LUBAC at steady state levels, but instead controls the ubiquitination of LUBAC substrates and other receptor components.

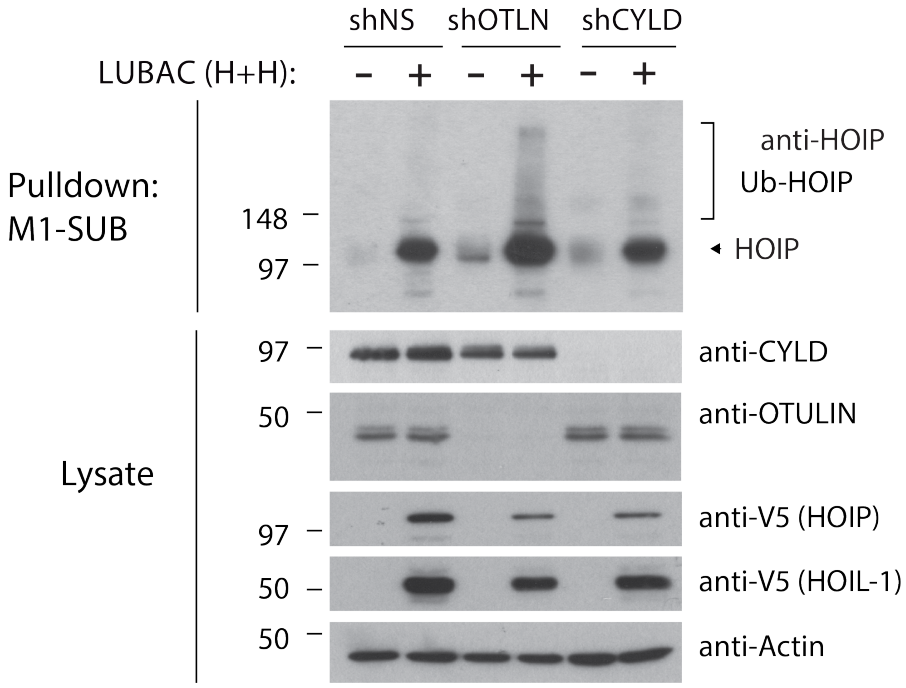


Figure 4.21: OTULIN controls steady-state LUBAC activation. Immunoblot of an M1-specific TUBE pulldown from U2OS/NOD2 cells with a stable virally-expressed shRNA targeting a NS control, OTULIN, or CYLD. Blotting with anti-HOIP (sigma antibody) shows ubiquitination of HOIP at steady state levels. Figure from [132].

4.6 Discussion

In this chapter, I detailed how I identified SPATA2 as a new regulatory factor bridging the interaction between HOIP and CYLD to regulate the ubiquitination landscape of the TNFR1 and NOD2 pathways. Furthermore, SPATA2 also negatively regulated the downstream signalling of the NOD2 receptor, as CRISPR/Cas9-mediated genetic knockout of SPATA2 resulted in an increase in proinflammatory transcript and protein production (akin to CYLD KO).

CYLD was previously described as a regulator of M1 and K63 chains within these pathways and, as such, this places SPATA2 as an important secondary factor for mediating CYLDs ability to control signalling events [132, 133, 177].

Since the publication of the work within this chapter, four further studies have emerged, which confirm the observations that place SPATA2 as an important mediator of TNF and NOD2 signalling [79–82, 135]; however, each paper shows discrepancies with regards to the ubiquitination of components within the TNFR

complex I. In this study, a reduction of the ubiquitination of the TNFR1 was observed with SPATA2 as well as CYLD KO, which was also observed by *Wagner et al* and *Wei et al* [81, 135]. In contrast, *Schlicher et al* and *Kupka et al* observe an increase in ubiquitinated substrates within the TNFR complex I in SPATA2$^{-/-}$ MEFs or CYLD KO A549 cells [79, 82].

Importantly, the interaction of CYLD with the LUBAC complex is governed by a PUB:PIM interaction, in the same manner as has been reported for OTULIN [137]. An important question is therefore if these DUBs can co-exist in the same signalling complex or form distinct complexes which exclude each other. From my data, CYLD but not OTULIN is lost from LUBAC in SPATA2 KO cells and immunoprecipitation of SPATA2 pulls down LUBAC and CYLD but not OTULIN. Furthermore, *Draber et al* report that OTULIN and CYLD do not co-purify together, but both interact with LUBAC [133].

Another remaining question arising from this data is that of the composition of the LUBAC complex as a whole. Whilst previous studies have attempted to address this, no concrete answer is available. At present, it is known that both HOIP and SHARPIN exist as dimers and furthermore, Paul Elliott also identified that CYLD and SPATA2 forms a 2:2 complex [80, 137, 229]. The result of these interactions is that two SPATA2 PIMs are placed in close proximity to each other, poised to bind the PUB domains of a HOIP dimer for a high avidity interaction. Whilst one would assume that a lack of cellular SPATA2 would open up the PUB domain of HOIP for binding by OTULIN, this did not appear to be the case. This is unlikely due to a lack of availability of OTULIN for binding, as cellular levels of OTULIN have been observed to be in excess of HOIP, but potentially that OTULIN is actively kept out of the complex by other means e.g. by phosphorylation of its PIM or exclusion by other interacting partners [137, 227].

OTULIN has been described to mainly act in a regulatory capacity, restricting LUBAC auto-ubiquitination, which is detected on HOIP, HOIL-1, and SHARPIN when OTULIN is depleted or enzymatically inactive (figure 4.21) [58, 132, 133,

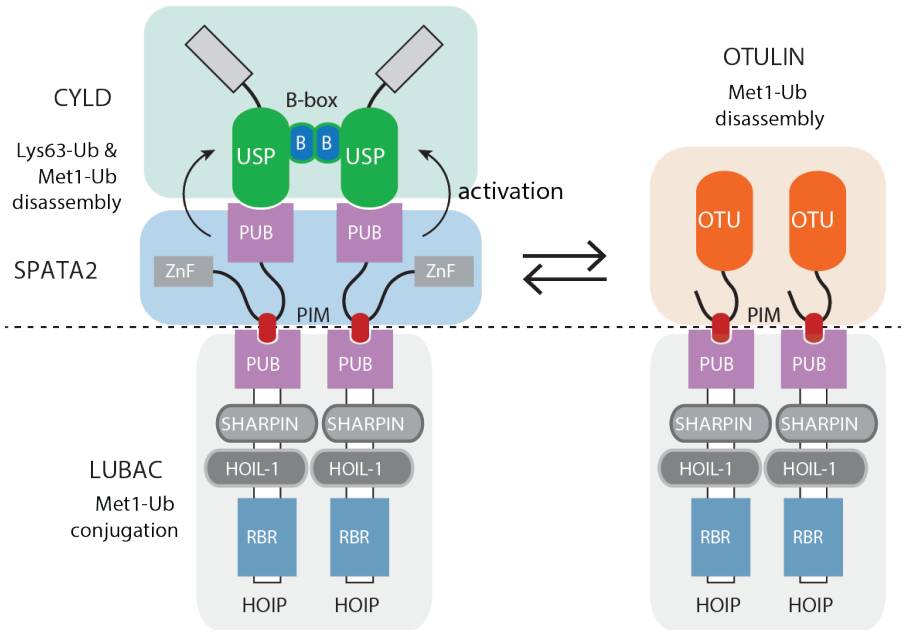


Figure 4.22: Schematic representation of the structure of LUBAC. Cartoon representation of the dynamic structure of LUBAC with OTULIN or SPATA2:CYLD bound via the HOIP PUB domain. Figure from [80].

137]; whereas CYLD has mainly been described to regulate inflammatory signalling through deubiquitination of LUBAC substrates (e.g. RIPK2 and components of the TNFR complex I) [132, 133]. It may be that the LUBAC complex exists within a dynamic state where, depending on the situation, the regulatory DUB OTULIN is bound to regulate its autoubiquitination or CYLD is bound to regulate the ubiquitination of its substrates.

My functional data indicates that SPATA2 is an essential regulator of LUBAC-mediated signalling, in particular in response to NOD2 signalling, where loss of SPATA2 resulted in an increase of ubiquitinated substrates and productive signalling. Of note is that loss of SPATA2 had a less pronounced effect on the production of CXCL8 in response to L18-MDP than loss of CYLD. It is possible that this reflects an ability of CYLD to regulate signalling events independent of LUBAC binding, however this may be a cell specific feature of U2OS/NOD2 cells. Further studies will be required to address this hypothesis.

Loss of SPATA2 also affected the levels of ubiquitination of TNFR complex I subunits, showing an increase in the deposition of ubiquitin chains on RIPK1

but reduced ubiquitination of TNFR complex I subunits and total M1 and K63 chains. Overall NF-κB signalling did not appear to be affected; however, other TNF signalling process have been reported to be affected by loss of SPATA2, including the formation of cell death inducing complexes, as has also been described previously for loss of CYLD [79, 81, 82, 216, 225].

This data collectively highlights how PUB:PIM interactions underpin the functions of LUBAC, with DUB activity being essential for controlling its activity. Thus, this adds SPATA2 to an increasing list of LUBAC regulatory components as well as secondary factors controlling DUB function through facilitating their recruitment to complexes [165].

5

The activity of CYLD is dependent on phosphorylation

Contents

5.1 Introduction 92
5.2 CYLD is phosphorylated in response to TNF and L18-MDP stimulation 92
5.2.1 Confirmation that CYLD within the TNFR complex I is phosphorylated. 92
5.2.2 CYLD in phosphorylated in an IKK/TAK1-dependent manner 94
5.3 Identifying novel TNF-induced CYLD phosphorylation sites 96
5.3.1 LC-MS/MS analysis to identify novel TNF-induced phosphorylation sites 96
5.4 S568 and S418 regulate the DUB activity of CYLD . . 99
5.4.1 CYLD^{S568A} and CYLD$^{S418A/S568A}$ stable lines display enhanced phospho-mediated signalling 100
5.4.2 CYLD$^{S418A/S568A}$ shows enhanced pro-inflammatory transcript production in TNF and NOD2 signalling 101
5.4.3 CYLD$^{S418A/S568A}$ shows enhanced CXCL-8 production with NOD2 signalling 103
5.4.4 CYLD$^{S418A/S568A}$ impairs CYLDs ability to regulate the ubiquitin landscape of the NOD2 receptor complex . . . 103
5.4.5 CYLD$^{S418A/S568A}$ shows deregulation of TNFR complex I ubiquitin landscape 106
5.5 Discussion 108

5.1 Introduction

Having characterised the CYLD:SPATA2 interaction as being crucial for the recruitment of CYLD to signalling complexes, I next aimed to investigate the specific cues responsible for its activation, as these have thus far remained elusive.

Phosphorylation of CYLD by IKK family members has been reported as a regulatory mechanism, inhibiting its function [214, 215, 230]. Whilst these studies document the PTM-mediated control of CYLD, the validity of the effects has been questioned in recent years. From figure 4.13, it can be observed that CYLD is modified to a higher MW upon TNF stimulation. As this may represent phosphorylation, I aimed to characterise if this was the case and, if so, what effect this is imparting on CYLD function.

5.2 CYLD is phosphorylated in response to TNF and L18-MDP stimulation

5.2.1 Confirmation that CYLD within the TNFR complex I is phosphorylated.

As shown in figure 4.13, CYLD was rapidly recruited to the TNFR complex I where it underwent a form of post-translational modification, resulting in a shift to a higher MW state, particularly at the 15min time point. In fact, numerous previous reports have also observed this shift following stimulation [80–82, 132, 133, 135].

As previous reports indicate that CYLD phosphorylation is important for regulating its function, I tested if the higher MW state I observed represents phosphorylated CYLD [214, 215, 230]. To investigate this, U2OS/NOD2 cells were stimulated for 15 min with biotin-TNF and the TNFR complex I was pulled down by streptavidin. Following this, one condition was treated with lambda phosphatase, which is a Mn_2-dependent protein phosphatase with high activity towards phosphorylated Thr, Ser , and Tyr residues (figure 5.1). As previously described, purified material that was not dephosphorylated showed a double band

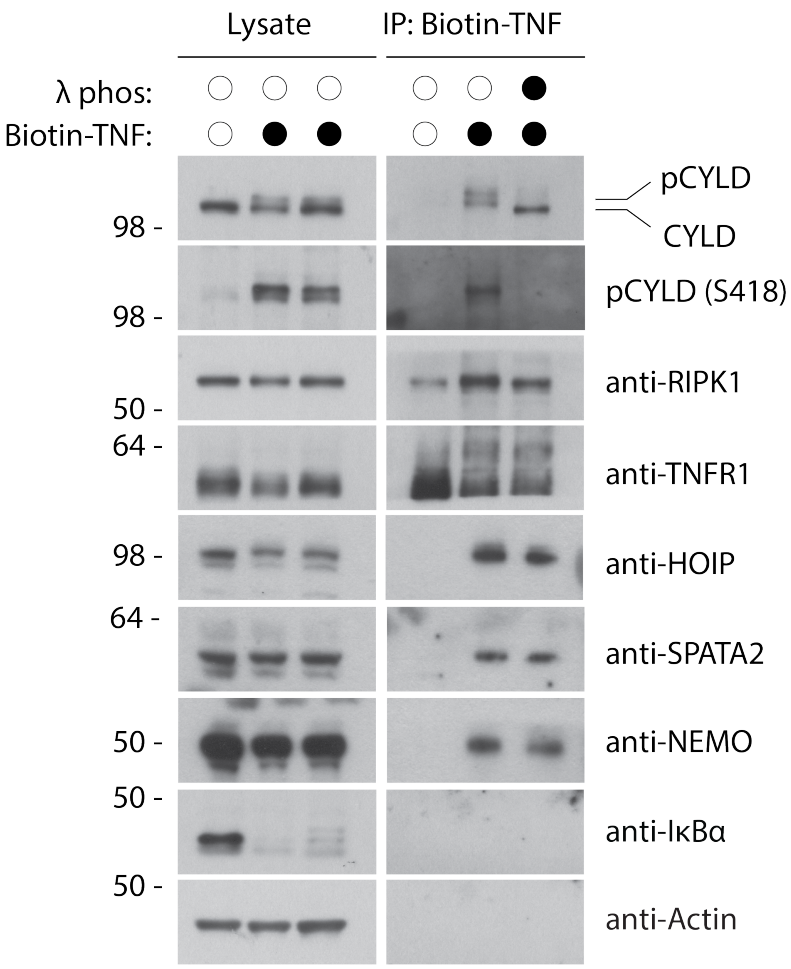


Figure 5.1: CYLD exists in a phosphorylated state within the TNFR complex I. Immunoblot showing biotin-TNF pulldown of the TNFR complex I using 1 μg of TNF per pulldown. Following pulldown, one 15 min time point was subjected to lambda phosphatase treatment for 1 h at 30 ^{o}C.

for CYLD; however, material treated with lambda phosphatase showed no double band and, in fact, was reduced to a MW lower than the lower band observed in the untreated sample. Thus, it may be concluded that CYLD within the active TNFR complex I exists only in a phosphorylated state.

Further to this, it was also observed that the previously annotated phosphorylation site for regulation of CYLD function (S418 - see pCYLD panel), displayed a double band following stimulation (though this was removed following lambda phosphatase treatment). This suggested that CYLD phosphorylated at S418 is present within the TNFR complex I but is not the main modification resulting in a shift to a higher MW state.

5.2.2 CYLD in phosphorylated in an IKK/TAK1-dependent manner

Ongoing work I performed within the lab showed that, following RNAi-mediated gene silencing of OTULIN, CYLD is constitutively modified in a manner similar to that observed following TNF stimulation. As I confirmed that this modification is phosphorylation, I investigated whether this was also the case for OTULIN knockdown as well as NOD2 receptor stimulation. Furthermore, as IKK family members have been implicated in the phosphorylation of CYLD, I investigated whether their inhibition would affect the phosphorylation of CYLD.

U2OS/NOD2 cells transiently transfected with siRNA targeting OTULIN or a MM control were stimulated with L18-MDP or TNF in the presence or absence of two commercially available IKK inhibitors (inhibitor VII and inhibitor XII)(figure 5.2). CYLD was phosphorylated following TNF and L18-MDP stimulation and this was effectively blocked by pre-treatment with IKK inhibitors. Furthermore, CYLD was also phosphorylated following the transient knockdown of OTULIN and, similar to receptor stimulation, this was blocked by IKK inhibition.

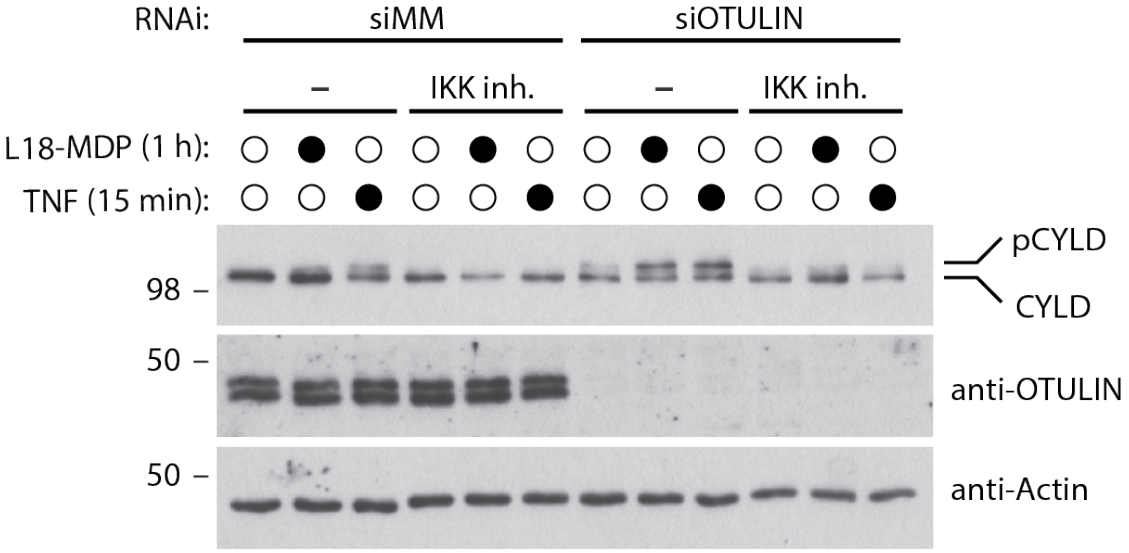


Figure 5.2: IKK inhibition prevents CYLD phosphorylation. Immunoblot showing IKK inhibitor treatment (inhibitor VII and XII both at 1 μM conc.) 30 min prior to stimulation with 20 ng/ml TNF for 15 min or 200 ng/ml L18-MDP for 1 h. Parental (WT) U2OS/NOD2 cells with or without RNAi knockdown (KD) of OTULIN shown.

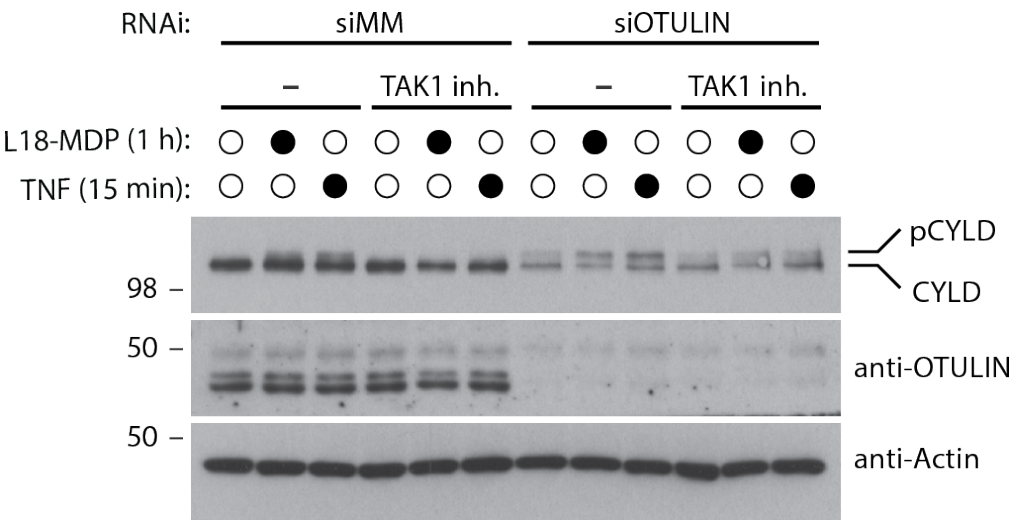


Figure 5.3: TAK1 inhibition prevents CYLD phosphorylation. Immunoblot showing 1 μM Oxozeaonol, a TAK1 inhibitor, treatment 30 min prior to stimulation with 20 ng/ml TNF for 15 min or 200 ng/ml L18-MDP for 1 h. Parental (WT) U2OS/NOD2 cells with or without RNAi knockdown (KD) of OTULIN shown.

This demonstrated that CYLD is phosphorylated in response to TNF and L18-MDP treatment and that the absence of OTULIN leads to the constitutive phosphorylation, and potentially activation, of CYLD.

To validate the specificity of the IKK inhibitors in preventing CYLD phosphorylation, I stimulated U2OS/NOD2 cells transfected with siRNA targeting OTULIN or a MM control with TNF or L18-MDP in the presence or absence of the TAK1 inhibitor, oxozeaeonol (figure 5.3). As previously discussed, TAK1 is an upstream activator of the IKK complex and therefore its inhibition should also abrogate CYLD phosphorylation. Indeed, in the presence of TAK1 inhibition, CYLD phosphorylation following TNF and L18-MDP stimulation was prevented. However, TAK1 inhibition did not completely prevent the phosphorylation of CYLD following siRNA-mediated knockdown of OTULIN, though it was markedly reduced compared to non-treated samples.

Taken together, this demonstrated that CYLD is phosphorylated in a TAK1 and IKK-dependent manner following stimulation with TNF and L18-MDP. Furthermore, siRNA-mediated knockdown of OTULIN results in the constitutive phosphorylation

of CYLD, which can be effectively blocked by IKK inhibitors and partially blocked by TAK1 inhibition.

5.3 Identifying novel TNF-induced CYLD phosphorylation sites

Multiple studies have identified numerous phosphorylation sites on CYLD; however, the reported function of the previously characterised S418 site was unclear and other sites had not been confirmed in a stimulus-dependent manner [214, 215]. Thus, I aimed to determine the stimulus-dependent phosphorylation sites of CYLD, which may be important for its activity.

LC-MS/MS analysis was chosen to identify phosphorylated sites of CYLD as it provides comprehensive identification of numerous modifications following stimulation which can be specifically mapped on the protein [231].

5.3.1 LC-MS/MS analysis to identify novel TNF-induced phosphorylation sites

To identify phosphorylated sites of CYLD following TNF stimulation, CYLD KO U2OS/NOD2 cells stably reconstituted with FLAG-tagged WT CYLD were stimulated with TNF for 15 min (figure 5.4a). Immunoprecipitation of the FLAG-CYLD was performed and the sample was digested with elastase prior to phospho-enrichment with TiO_2 columns (figure 5.4b). The purified material was subjected to LC-MS/MS and analysed using PEAKS Server V.7/v8.5 to map identified phosphorylation sites - see section 3.2.6.

Identified phosphorylation events are shown in figure 5.5, with previously annotated sites marked by asterisk and those identified only in the TNF stimulated sample highlighted in red. As expected, the previously mapped S418 site, which is located within the phosphorylation-rich region of CYLD, was identified as being induced by TNF stimulation.

Whilst several TNF-dependent sites were identified, of particular interest was S568 as Paul Elliot also confirmed this as a potentially important site for regulating

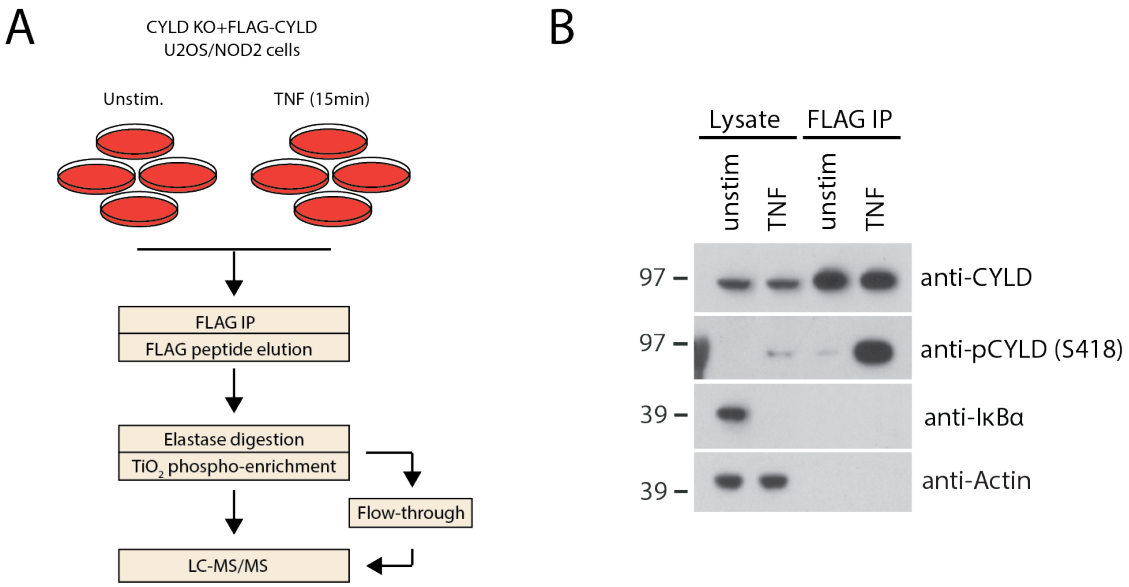


Figure 5.4: LC-MS/MS analysis of CYLD phosphorylation. (A) Graphical representation of the experimental procedures for analysis of CYLD phosphorylation sites following TNF stimulation at 20 ng/ml. (B) Immunoblot of the purified material sent for MS analysis. Pull down by FLAG-TNF as described in section 3.2.6

the DUB activity of CYLD *in vitro*. The resulting spectra from the analysed CYLD peptide 563-586 are shown in figure 5.6, confirming the presence of phosphorylation at S568. Interpretation of this data was through the analysis of the resulting b and y ions. In low energy collisions, the most common fragmentation ions generated are a, b, and y ions (with a ions being lower abundance than b ions). These ions are detected based on the presence of the charge left from the fragmentation of the peptide [232, 233]. As shown, b ions (blue) extend from the N-terminus whereas y ions (red) extend from the C-terminus (vertical lines indicate where the break occurred). Phosphorylation events typically result in a mass change of +80 Da compared to unmodified peptides; However, for increased confidence, the detection of the facile loss of phosphoric acid (-98Da) was used to map phosphorylated sites [234]. As shown for S568, a -98 Da mass change first occurs with the b7 ion (representing the N-terminus until E569) and the y17 ion (representing the C-terminus until S568), providing evidence from both peptide terminals that the phosphorylation site is located at S568 (as b fragments obtained upstream of b7, and y fragments upstream of y17, do not display a mass change).

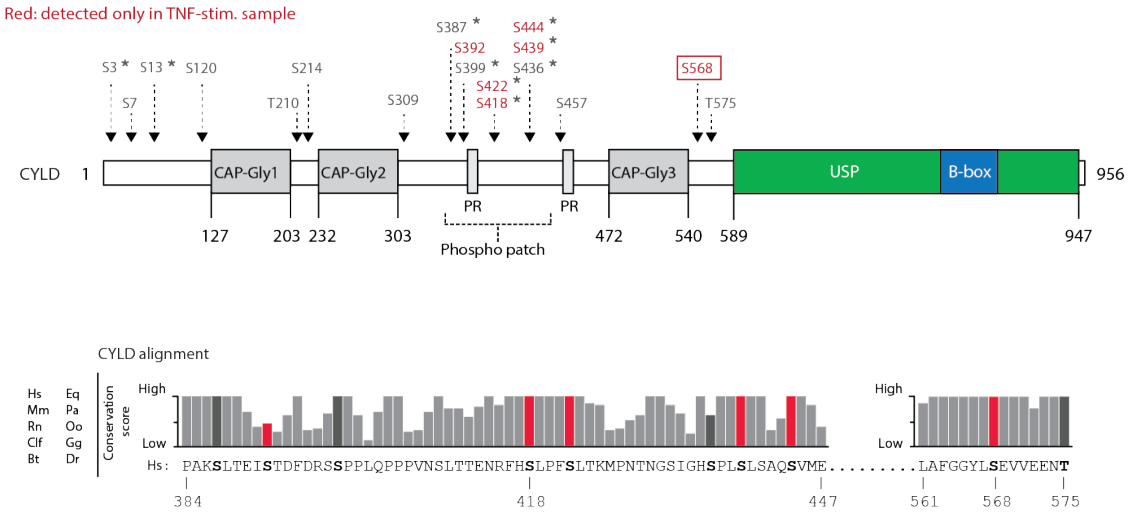


Figure 5.5: The identified phosphorylation sites of CYLD. Graphical representation showing the identified phosphorylation sites of CYLD. Showing in red are sites only identified following TNF stimulation. Sites with an asterisk represent previously annotated sites. Of note is the identified phosphorylation of S568.

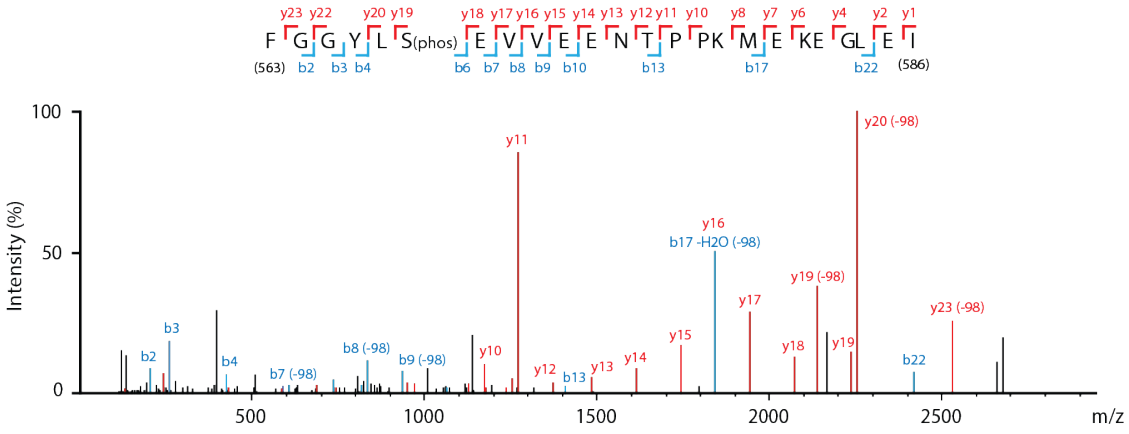


Figure 5.6: Spectra of S568 phosphorylation. Spectra from the LC-MS/MS analysis of CYLD showing peptide 563-586. Fragmentation coverage showing b and y ions is shown in blue and red respectively. The ion table for this spectra can be found in supplementary figure 7.2.

To investigate the evolutionary importance of identified sites, conservation analysis of CYLD was performed and showed that, of the identified TNF-induced phosphorylation events, all but S392 are highly conserved amongst species, suggesting an importance of these residues for the function of CYLD (figure 5.5).

5.4 S568 and S418 regulate the DUB activity of CYLD

As S568 was identified within the MS screen, and also by Paul Elliott as an important site for CYLD function, I investigate it further alongside the previously published S418 site. To do so, I created virally induced stable cell lines expressing FLAG-tagged CYLD^{S418A}, CYLD^{S568A}, and CYLD$^{S418A/S568A}$ in a CYLD KO U2OS/NOD2 background. For controls, cells expressing CYLD^{WT} and CYLD^{C601A} were also created.

Each cell line was examined to ensure similar expression levels of CYLD (figure 5.7). In addition to verification by western blot, densitometry analysis was performed in ImageJ to more accurately assess reintroduced levels as shown in supplementary figure 7.1.

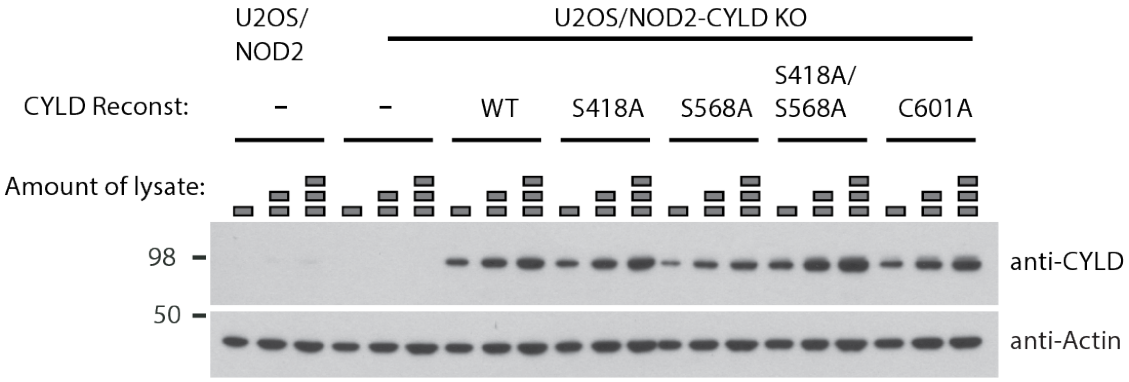


Figure 5.7: Reintroduced levels of CYLD phosphorylation mutants. Immunoblot showing the reintroduced levels of the generated CYLD phosphorylation mutants. Densitometry of three blots was performed to ensure levels were matched across mutants, as shown in supplementary figure 7.1.

5.4.1 CYLD^{S568A} and CYLD$^{S418A/S568A}$ stable lines display enhanced phospho-mediated signalling

As phosphorylation has been reported to affect CYLD function, I investigated whether the mutation of these sites has any effect on the phosphorylation-mediated signalling events following TNF or NOD2 receptor stimulation. Cells were stimulated with TNF or L18-MDP and whole cell lysate was analysed by western blot analysis to probe for key signalling mediators (figure 5.8).

CYLD^{S418A} cells showed no differences in MAPK signalling or degradation of IκB/phosphorylation of p65 in response to TNF or L18-MDP stimulation when compared to CYLD^{WT} cells. This is contrary to previous reports suggesting that S418 is an inhibitory site of CYLD dampening its function in TNF-induced MAPK signalling [215]. CYLD KO U2OS/NOD2 cells showed less p-IκB and an increase in p-p38 when compared to CYLD^{WT} cells (as we have previously shown [132]), but otherwise show no differences in signalling. This is in contrast to *Draber et al* who show that CYLD KO in BMDMs results in an increase in p-IκB in response to L18-MDP [133].

CYLD^{C601A} cells show low levels of baseline signalling observed by p-p65 and p-p38 activation in unstimulated conditions. This low level activation is constitutively present in CYLD^{C601A} cells and may represent a feature of this mutation of CYLD whereby it binds to ubiquitin chains but, unable to cleave them, inadvertently protects them from cleavage by other DUBS (this chain protection by DUBs has been previously reported in the TNFR complex I [133]).

CYLD^{S568A} and CYLD$^{S418A/S568A}$ cells showed enhanced signalling through greater levels of p-p38 in response to both TNF and NOD2 signalling. These cell lines also displayed a reduction in the levels of p-IκB following L18-MDP stimulation, as was seen for CYLD KO and CYLD^{C601A} cells.

As the CYLD^{C601A} cells have no catalytic activity and the CYLD^{S568A} and CYLD$^{S418A/S568A}$ cells phenocopy this, it can be concluded that these mutations result in loss-of-function phenotypes for CYLD activity.

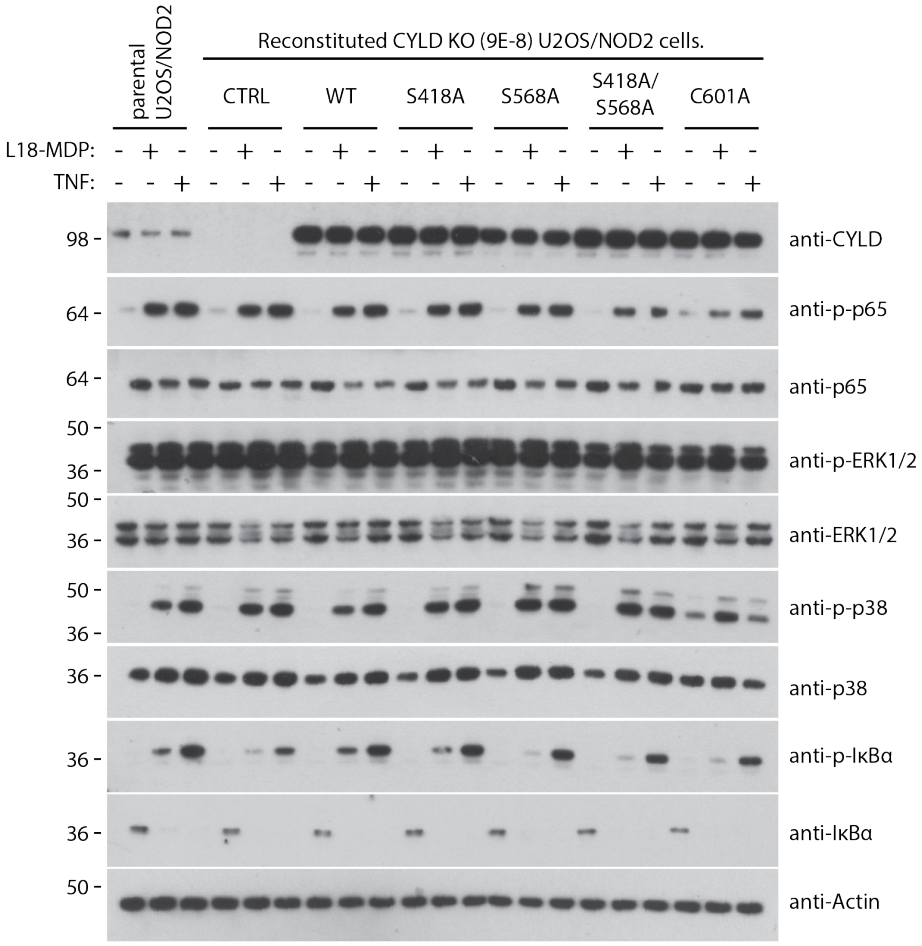


Figure 5.8: CYLD^{S568A} and CYLD$^{S418A/S568A}$ show enhanced signalling. Immunoblot showing the effect of the phosphorylated CYLD mutants on signalling events in response to 20 ng/ml TNF for 15 min or 200 ng/ml L18-MDP for 1 h.

5.4.2 CYLD$^{S418A/S568A}$ shows enhanced pro-inflammatory transcript production in TNF and NOD2 signalling

As we and others have shown, cellular ablation of CYLD by genetic KO or RNAi-mediated gene silencing results in the increased production of pro-inflammatory mediators in response to NOD2 receptor signalling [80, 132]. As the CYLD^{S568A} and CYLD$^{S418A/S568A}$ cells displayed a loss-of-function phenotype in phosphorylation-mediated signalling events, phenocopying the CYLD^{C601A} or CYLD KO cells, I investigated whether these cell lines would also induce the increased production of inflammatory mediators in response to NOD2 signalling.

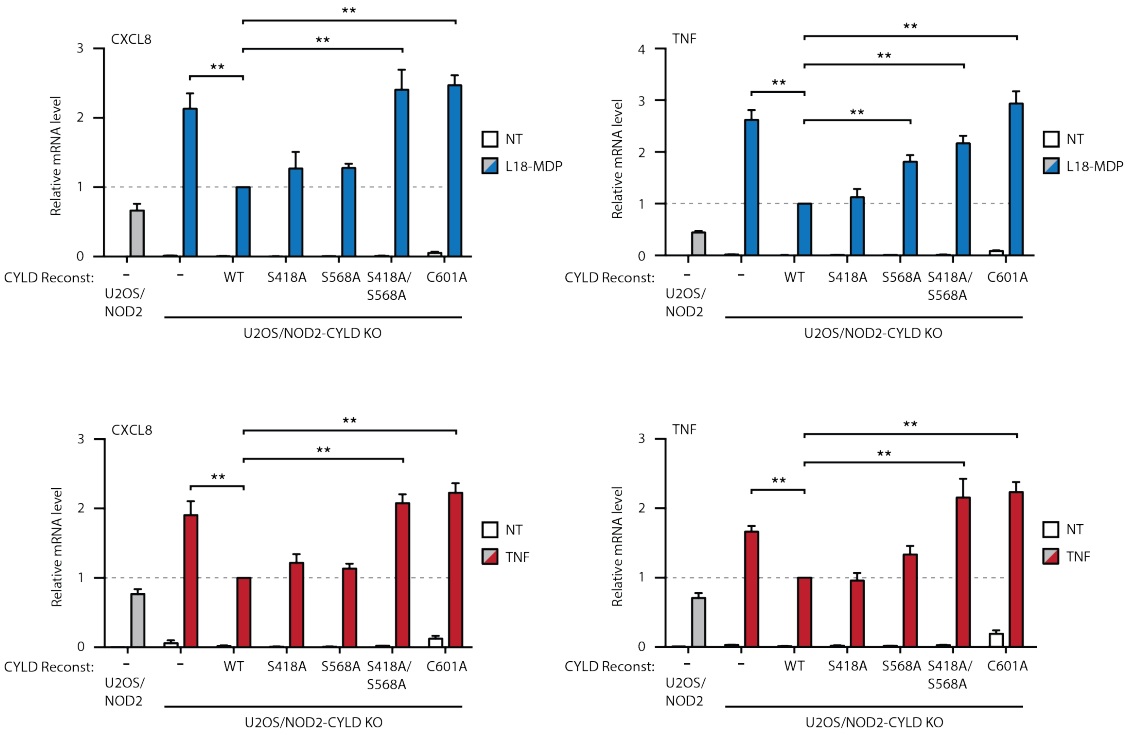


Figure 5.9: CYLD$^{S418A/S568A}$ shows enhanced pro-inflammatory transcripts. qRT-PCR analysis of the production of pro-inflammatory transcripts following stimulation with 20 ng/ml TNF or 200 ng/ml L18-MDP for 3 h. Data normalised to HPRT control and subsequently the CYLD^{WT} stimulated condition. Data was collated from three experiments and analysed in Graphpad Prism 6 with statistical tests by two-way ANOVA.

I performed qRT-PCR analysis following TNF or L18-MDP stimulation for 3 h and checked for production of proinflammatory transcripts for CXCL-8 and TNF (figure 5.9 - NFKBIA and A20 qRT-PCR are also shown in supplementary figure 7.4).

CYLD^{S418A} and CYLD^{S568A} cells did not display differences in L18-MDP- or TNF-mediated signalling compared to the reconstituted CYLD^{WT} cells following stimulation, with the exception of the production of TNF transcripts in response to L18-MDP stimulation in the CYLD^{S568A} cell line.

In contrast, the CYLD$^{S418A/S568A}$ cell line displayed a loss-of-function phenotype, mirroring the response of CYLD^{C601A} or CYLD KO cells for both CXCL-8 and TNF transcripts following L18-MDP and TNF stimulation.

CYLD^{S418A} and CYLD^{S568A} cells displayed minor differences in the production of the NF-κB-response genes, A20 and NFKBIA (supplementary figure 7.4). However, the CYLD$^{S418A/S568A}$ cell line displayed a significant increase in A20 transcript

production in response to L18-MDP stimulation and IκB transcript production in response to TNF stimulation (alongside the CYLD^{C601A} mutant) when compared to the CYLD^{WT} cell line.

Taken together, this data showed a role for the double mutant, CYLD$^{S418A/S568A}$, in the positive regulation of CYLD function as its mutation leads to a loss-of-function phenotype for CYLD, similar to CYLD KO or CYLD^{C601A} cells.

5.4.3 CYLD$^{S418A/S568A}$ shows enhanced CXCL-8 production with NOD2 signalling

As the CYLD$^{S418A/S568A}$ cells displayed similar properties to the catalytic-dead CYLD^{C601A} mutant or CYLD KO cells, I investigated whether they would also induce an increase in the production of the pro-inflammatory chemokine, CXCL-8, in response to NOD2 receptor signalling as I have previously shown with the CYLD KO cells [80, 132].

To investigate this, cells were stimulated with L18-MDP in the presence of brefeldin A and monensin for 5 h and subjected to flow cytometry analysis to detect the presence of CXCL-8, as previously described.

CYLD^{S418A} and CYLD^{S568A} cell lines showed no difference when measuring the percentage of CXCL-8 - positive cells compared to CYLD^{WT} cells; however, CYLD$^{S418A/S568A}$ cells showed a significant increase in the percentage of CXCL-8 positive cells, which was similar to that seen with the CYLD^{C601A} and CYLD KO cell lines.

This data highlights an important role for both S418 and S568 of CYLD in the regulation of proinflammatory transcript and protein production in response to NOD2 and/or TNF receptor signalling.

5.4.4 CYLD$^{S418A/S568A}$ impairs CYLDs ability to regulate the ubiquitin landscape of the NOD2 receptor complex

CYLD KO cells have an inability to control the ubiquitin landscape of the NOD2 adaptor protein, RIPK2. Thus, as the CYLD$^{S418A/S568A}$ mutant cell line showed

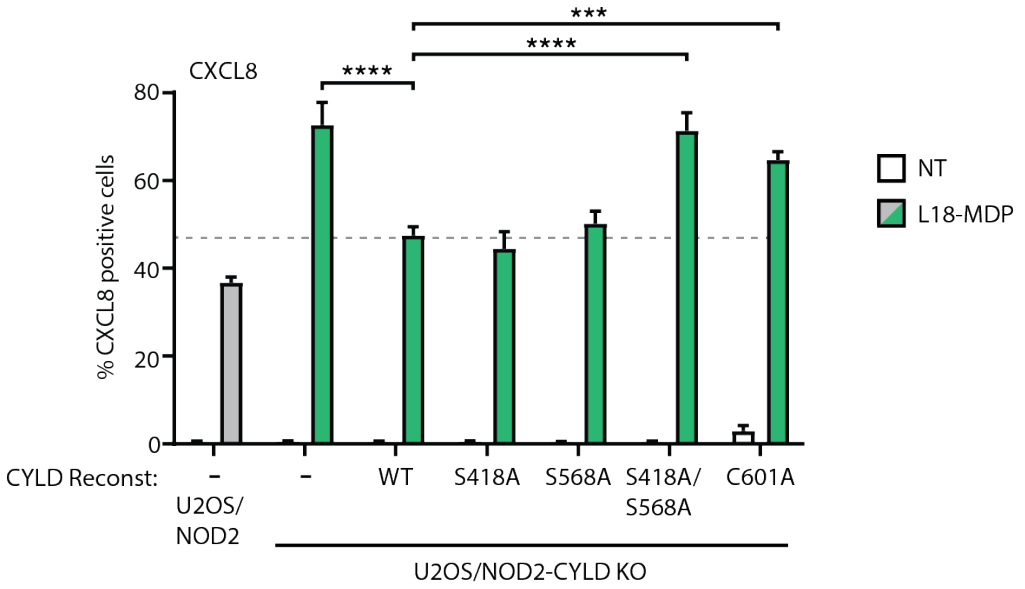


Figure 5.10: CYLD$^{S418A/S568A}$ shows enhanced CXCL8 production. Flow cytometry analysis of CXCL-8 production in phosphorylation mutants of CYLD following 200 ng/ml L18-MDP for 5 h in the presence of 5 μg/ml brefeldin A and 2 μM monensin. n=3. Data was collated from three experiments and analysed in Graphpad Prism 6 with statistical tests by two-way ANOVA. Representative histograms are shown in supplementary figure 7.3.

a loss-of-function phenotype, I investigated whether it would also lose the ability to control ubiquitin deposition following stimulation.

To investigate this, cells were stimulated with L18-MDP with or without pre-stimulation with the SMAC mimetic, CpA, to remove the IAPs from the NOD2 signalling complex, as previously described. Following this, a TUBE pulldown was performed to enrich for ubiquitinated substrates and the purified material was analysed by western blot to detect ubiquitin deposition on the adaptor, RIPK2 (figure 5.11).

Parental U2OS/NOD2 cells, from which the CYLD KO cells were generated, and CYLD^{WT} cells displayed a ubiquitin smear following L18-MDP stimulation, which was abolished when the cells were pretreated with CpA (lanes 2, 3, 8, and 9). In contrast, the CYLD KO cells retained the ubiquitin smear when pretreated with CpA, indicating that the loss of CYLD affected the removal of chains such that the remaining minimal rate of the deposition of ubiquitin was preserved to give a signal (lane 6). The single mutant CYLD^{S418A} and CYLD^{S568A} cells were comparable to

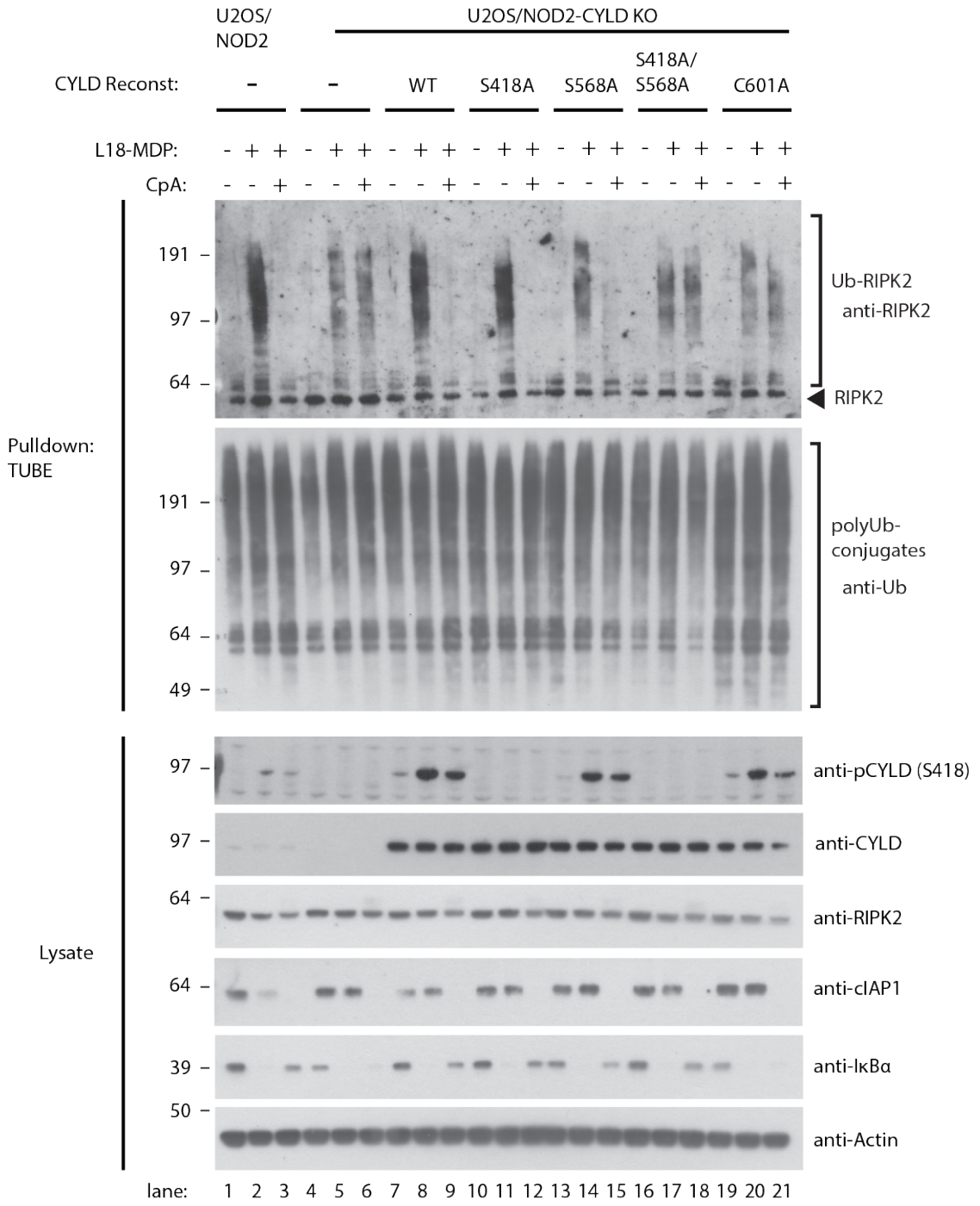


Figure 5.11: CYLD$^{S418A/S568A}$ shows enhanced RIPK2 ubiquitination. Immunoblot showing TUBE pulldown of ubiquitination substrates, and subsequent blotting for RIPK2, after 200 ng/ml L18-MDP stimulation with or without prestimulation for 30 min with 1 μM CpA.

CYLD^{WT} and parental cells as they did not retain the ability to preserve RIPK2 ubiquitination following CpA, indicating functional activity of CYLD (lanes 3, 12, and 15); however, CYLD$^{S418A/S568A}$ cells, and the catalytic dead CYLD^{C601A} cells, were comparable to the CYLD KO where the ubiquitination of RIPK2 was preserved when cells were prestimulated with CpA prior to L18-MDP stimulation.

This data showed that the double mutation of S418 and S568 sites within CYLD leads to a loss-of-function phenotype, affecting pro-inflammatory mediator production, via interfering with CYLDs ability to hydrolyse ubiquitin chains in the NOD2 receptor system.

5.4.5 CYLD$^{S418A/S568A}$ shows deregulation of TNFR complex I ubiquitin landscape

As CYLD KO, and SPATA2 KO, affected the ubiquitin landscape of TNFR complex I, I investigated whether the loss-of-function double mutation of CYLD would have similar effects. Cells were stimulated with biotin-TNF for 15 min before being washed and lysed for streptavidin pulldown of the TNFR complex I. Purified material was taken for analysis by western blot to detect TNFR1 and RIPK1 ubiquitination as well as total levels of K63 and M1 ubiquitin within the complex (figure 5.12).

CYLD^{S418A} and CYLD^{S568A} cells were comparable to CYLD^{WT} or the parental U2OS/NOD2 cells, displaying similar levels of ubiquitination of TNFR1 and RIPK1. CYLD^{S418A} cells were also comparable to CYLD^{WT} with similar total levels of M1 and K63 polyubiquitin within the complex, whereas CYLD^{S568A} cells displayed slightly higher levels of total M1 ubiquitin chains compared to CYLD^{WT} cells (though similar to parental cells) and reduced levels of total K63 ubiquitin.

CYLD$^{S418A/S568A}$ cells showed a loss-of-function phenotype, mirroring the CYLD KO and CYLD^{C601A} cells, with reduced levels of polyubiquitin chains on RIPK1 and TNFR1. Furthermore, these cell lines also showed reduced levels of total M1 and K63 chains in the TNFR complex I, consistent with previous data within this study (figure 4.17).

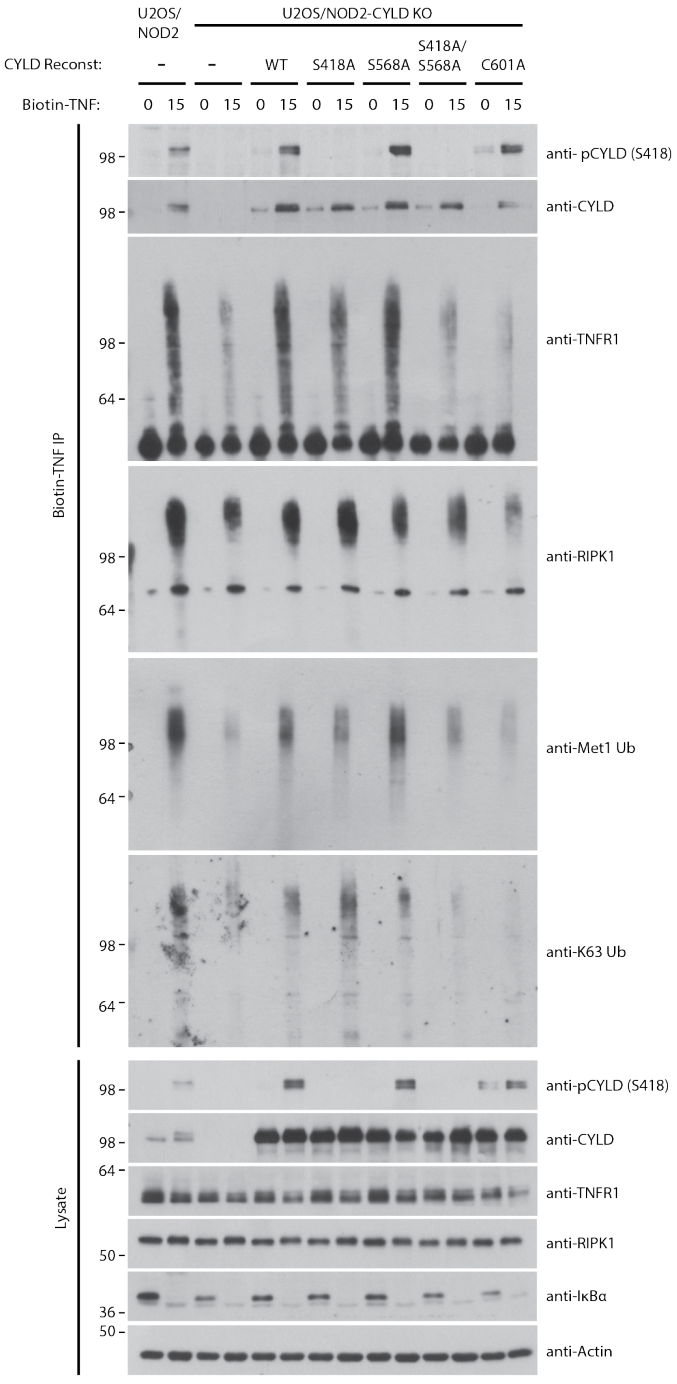


Figure 5.12: CYLD$^{S418A/S568A}$ dysregulates TNFR complex I. Immunoblot showing a Biotin-TNF pulldown (1 μg per pulldown for indicated time points) in parental, CYLD KO, and CYLD KO with reintroduced mutants U2OS/NOD2 cells.

As shown previously, CYLD^{C601A} cells displayed low levels of basal signalling through the increase of pCYLD (S418) and reduced IκBα in unstimulated conditions, when compared to other cells.

Notably, CYLD was phosphorylated following stimulation in all cell lines, including those containing a mutation of S418 and/or S568. This was contrary to *Reiley et al* who show that a mutation of CYLD^{S418A} transfected into HEK293 cells alongside IKKγ/IKKβ resulted in inhibition of the double band observed for activated CYLD [206]. Whilst this may be a cell line-specific effect, it is apparent that additional phosphorylation sites are present on activated CYLD, which shift it to a higher MW state as a result of TNF stimulation.

This data strengthens the role for the dual phosphorylation of CYLD at S418 and S568 in mediating CYLD function as mutation of these sites impaired the ability of CYLD to regulate the ubiquitin landscape of the TNFR complex I, akin to CYLD KO.

5.5 Discussion

CYLD was initially observed to be modified in response to both TNF and L18-MDP treatment. Through lambda phosphatase treatment, this was confirmed to be phosphorylation and, furthermore, pre-treatment with TAK1 or IKK inhibitors prior to stimulation also prevented this modification (figure 5.1, 5.2, 5.3). IKK has previously been reported as a kinase for CYLD and, being activated by the TAK1 complex, it follows that upstream TAK1 inhibition would block its phosphorylation. *Reiley et al*, who initially reported IKK phosphorylation of CYLD, also report that CYLD may deubiquitinate TAK1 to prevent its autoactivation, perhaps suggesting a negative feedback loop whereby CYLD deactivates TAK1 through its catalytic activity [206].

Phosphoproteomics approaches were employed to identify TNF-induced phosphorylation sites (as this gave the strongest phospho signal (figure 5.5)). In addition to confirming the published S418 site, several other residues were identified including S568, which was also confirmed to potentially affect the function of CYLD by Paul

Elliott. Single point mutation of this site (S418A) did not have any effect on the production of proinflammatory mediators (transcripts or protein), nor did it affect CYLDs ability to control the ubiquitin landscape of the TNF or NOD2 adaptor proteins, RIPK1 or RIPK2 respectively. Single mutation of the newly identified S568 (S568A) site showed some dysregulation of the enzymatic function of CYLD. In contrast, mutation of S568A in combination with S418 ($CYLD^{S418A/S568A}$), shows a near complete loss-of-function phenotype.

The double band of CYLD is also still present regardless of the mutation of both the S418 and S568 residues following TNF stimulation (figure 5.12). Mutation of these residues is sufficient to inactivate CYLD, however, they are clearly not the only phosphorylated residues of CYLD when it is within the TNFR complex I. Thus, other combinations of phosphorylation mutants may also lead to an impaired ability of CYLD to regulate receptor complexes.

The phosphorylation-rich Ser patch of CYLD represents a domain that may be highly dynamic in the regulation of the CYLD function and interactions. From the LC-MS/MS analysis shown in figure 5.5, it can be seen that, with the exception of S568, all identified TNF-dependent phosphorylation sites are within this region. Though numerous sites were TNF-dependent, this only represents a fraction of the modified sites within this patch. Thus, this region represents a large area that, when multi-phosphorylated, will display a significant change in charge and potentially conformation to alter CYLD function or protein interactions. This may explain why, in the systems tested within this study, a single mutation of S418 of CYLD to inhibit its phosphorylation did not exhibit any effects on signalling outcome, as it may only contribute to the overall negative charge conferred by multi-phosphorylation of the Ser-rich patch.

Mutation of the S568 of CYLD results in a partial loss-of-function of CYLD, which leads to a dysregulation in NF-κB signalling (inflammatory transcript production) in response to L18-MDP stimulation (figure 5.9). In contrast, double mutation of S568 and S418 leads to a near complete loss-of-mutation phenotype for

TNF and L18-MDP treatment resulting in increased production of pro-inflammatory mediators and inability to regulate the ubiquitin landscape of RIPK2 and the TNFR complex I (figures 5.9, 5.10, 5.11, 5.12). The S568 of CYLD is somewhat isolated with regards to surrounding sites that may be modified by phosphorylation and may therefore play a major role in the regulation of the function of CYLD; however, the S418 sits within the Ser-rich patch of CYLD and is surrounded by multiple phosphorylation sites. It may be that the S568 mutation, in combination with one or more mutations within the Ser-rich patch of CYLD affecting the overall charge, would result in a similar loss-of-function phenotype as observed for $\text{CYLD}^{S418A/S568A}$. Additional studies will be required to address this question. Furthermore, the phosphorylation landscape of CYLD in response to different stimuli has not been fully addressed. Such studies may therefore identify phosphorylation sites on CYLD that are crucial for its function and context-dependent.

6 Discussion

Contents

6.1 CYLD, OTULIN, and A20 in immune signalling . . . 111
6.2 The recruitment of DUBs to LUBAC 113
6.3 Summary and future perspectives 116

6.1 CYLD, OTULIN, and A20 in immune signalling

CYLD and OTULIN are constitutively expressed in most cell types, whereas A20 expression is low or absent in most cell types at basal conditions [235]. OTULIN and CYLD are primarily acting on early signalling complexes and A20 is upregulated by NF-κB signalling in a negative feedback loop to shut down signalling [235]. Whilst this expression-mediated control of signalling may provide a mechanism through which the overlapping functions of these DUBs are coordinated, it does not take into account cell types with higher levels of A20, or the possibility that other active signalling events may affect the levels of these DUBs. An additional layer of direct regulation via phosphorylation may therefore provide additional controls for these DUBs to exert their effects on active complexes.

OTULIN constitutively prevents the spontaneous auto-ubiquitination of LUBAC, indicating that its DUB function is constitutively active at steady state levels. In contrast, this study demonstrates the reliance of CYLD on phosphorylation for its function. This phosphorylation mediated control of CYLD is similar to that of A20, which displays enhanced activity towards K63 chains following modification [140].

Previous reports on the phosphorylation of CYLD proposed that it inhibited its function [214, 215]. Whilst phosphorylation-mediated activation has been described for numerous DUBs, these reports were the only indications of a negative regulation of DUB function [55]. This study therefore brings the phosphorylation of CYLD in line with other DUBs by providing evidence that the S418 site of CYLD is not responsible for its negative regulation but, in combination with mutation of the novel S568 site, activates its function. Whether phosphorylation is solely an activation signal for DUBs remains unanswered but may be addressed in further studies. Additionally, it is unclear how the phosphorylation-mediated activation of CYLD occurs. It may be that the function is increased as a result of structural rearrangements, increasing the affinity for ubiquitin chains, or that these modifications directly act to increase the catalytic activity.

CYLD may also be attributed to pathology of TAK1- and IKK family member-associated diseases, as these mediate CYLD phosphorylation and therefore activation in inflammatory signalling. Modulation of the cellular levels of these kinases may have drastic effects on CYLD phosphorylation and subsequently inflammatory signalling.

Ongoing work by our collaboration with Paul Elliott has identified a now common feature of these DUBs that is their ability to directly interact with ubiquitin chains as well as be recruited to signalling complexes by other mediators (LUBAC recruiting OTULIN and CYLD; and TAX1BP1 and ABIN1 recruiting A20 to K63 and M1 chains, respectively) [236, 237].

Paul performed NMR studies suggesting that L475 in the CAPGly domain would be important for Ub binding. I therefore generated stably expressing CYLD cells harbouring an L475P mutation ($CYLD^{L475P}$)(supplementary figure 7.5). Though

I have yet to obtain mechanistic data for any interaction, these cells showed a complete loss-of-function phenotype (akin to CYLD KO cells) when measuring pro-inflammatory transcript and chemokine production (supplementary figures 7.6 and 7.7). Additionally, these cells completely lose the ability to control ubiquitination of the NOD2 receptor adaptor, RIPK2 (supplementary figure 7.8). Taken together, this introduces a ubiquitin-binding function for the third CAPGly of CYLD that has been shown *in vitro*, with effects in cellular models requiring validation.

A20 exerts protective effects on M1 chains via its ZF7 domain. The ubiquitin binding activity of CYLD bears no specificity for any polyubiquitin linkage, however, context dependent signalling events may result in its binding to a chain type which it cannot hydrolyse (or will not based on the cellular context). Further to this, CYLD may exert a regulatory effect on preventing aberrant NF-κB signalling as expression of catalytically inactive CYLD results in low levels of basal signalling. This effect may be the result of the basal activity of CYLD being sufficient for controlling the activation of an inflammatory signalling pathway. Alternatively, expression of this mutant may trigger the low level activation of NF-κB signalling events through alternative cellular functions of CYLD reliant on this DUB activity.

6.2 The recruitment of DUBs to LUBAC

CYLD is recruited to LUBAC via the PIM of SPATA2, whereas OTULIN interacts directly with LUBAC via its own PIM. The molecular mechanism governing which DUB is associated with LUBAC is not clear though it has been proposed to involve the phosphorylation of the key Tyr residue (Y56) in the PIM of OTULIN [137, 176]. In addition to low throughput studies (LTS) by *Elliott et al* and *Schaeffer et al*, a further 23 high throughput study (HTS) datasets have identified phosphorylation on Y56 of OTULIN by MS analyses, as reported on 'phosphositeplus.org' [137, 176]. These datasets provide a comprehensive list of phosphorylation events but often as steady-state 'snapshots' of <1% of the cellular pool of proteins, with no information on the relative abundance of modifications or dynamic information, which makes assessing the importance or context of particular modifications difficult.

As phosphorylation of the PIM of OTULIN has been repeatedly found in these conditions, one may hypothesise that a significant portion is phosphorylated at steady-state conditions. Cellular levels of OTULIN have been described to be in excess of HOIP [137]; as such, it may be that free cellular OTULIN, possibly previously associated with LUBAC, is the main cellular pool of OTULIN with phosphorylated Y56.

Draber et al previously reported that treatment of cells with pervanadate, a compound irreversibly inhibiting Tyr phosphatases, did not inhibit the association between OTULIN and HOIP at steady-state levels [133]. This demonstrates that OTULIN cannot be removed from the LUBAC complex as a result of phosphorylation events occurring at steady-state. However, this study also shows that stimulation of cells with TNF does not affect OTULIN association with LUBAC, as identified by HOIP immunoprecipitation, and as such they suggested that this process is not stimulus dependent. However, this does not take into account that likely only a fraction of the cellular LUBAC is recruited to the TNFR complex I upon stimulation and that, in this context, it may be TNF-dependent.

The other previously identified PIM-containing protein, p97, is well documented to be controlled by phosphorylation as more than 250 HTS datasets exist on 'phosphositeplus.org' showing phosphorylation of the key Tyr residue within its PIM. Furthermore, LTS have documented roles for phosphorylation of p97 in a variety of cellular contexts including sperm capacitation, DNA repair, transitional endoplasmic reticulum assembly, and T cell receptor activation [238]. Phosphorylation of the p97 PIM is also reported to directly mediate its interaction with PUB domains as, like OTULIN, the phosphorylation of the key Tyr residue completely abolishes interactions [238].

SPATA2 represents a newly discovered PIM-containing protein; however, thus far, no HTS datasets exist that show phosphorylation of the key Tyr residue within its PIM. As HTS datasets are often analyses of steadystate conditions, it may be that the phosphorylation of the SPATA2 PIM, if it occurs, is stimulus or

context-dependent. *Schlicher et al* proposed that SPATA2, when overexpressed, can outcompete OTULIN for binding to LUBAC and that it is the competition between these that underpins binding to LUBAC [82]. Though this could be an effect from overexpression (and may not translate to endogenous protein levels), it may suggest that an absence of one component could free up LUBAC for the binding of the second. This strengthens the hypothesis that OTULIN is actively excluded from the TNFR complex I as in SPATA2 KO cells OTULIN does not form part of the active complex [80–82].

One possible explanation for this exclusion of OTULIN may be that a kinase would phosphorylate the PIM of OTULIN but not that of SPATA2. It may be that it would act transiently on the complex or would be membrane associated, ensuring that LUBAC complexes recruited to the TNFR complex I are not associated with OTULIN. It is also unknown whether SPATA2:CYLD and OTULIN are actively recruited and removed individually, or whether the entire LUBAC complex with its associated DUB is recruited and removed from active complexes. OTULIN and SPATA2:CYLD both immunoprecipitate with LUBAC, but not each other, therefore it may be that separate complexes exist that are recruited in a context dependent manner. If this were indeed the case, it could also be that the association of OTULIN with LUBAC results in some form of steric hindrance, preventing recruitment to the TNFR complex I.

PUB:PIM interactions are crucial for LUBAC interactions with its associated DUBs. Therefore, one may question if OTULIN and SPATA2 are the only proteins interacting in this manner. Due to the nature of PIMs (small, four amino acid sequence), it is difficult to ascertain the number of PIM-containing proteins existing in cells. Further studies may look into identifying such proteins through the use of known PUB domains, including HOIP, as mutation of the PIM-binding pocket within each respective PUB domain, followed by MS analysis, may identify novel PIM-containing proteins.

Interestingly, the second most enriched CYLD-interacting protein in our MS analysis was SPATA2LIKE (SPATA2L), a 420 amino acid protein which, by domain structure, is similar to SPATA2, containing a PUB domain, putative PIM, and C-terminal ZnF domain (though shares only 29% protein sequence similarity). As a B-box-dependent interaction partner of CYLD, one may expect that it would function in a similar manner to SPATA2; however, as all cell lines used in this study retain endogenous SPATA2L, it is apparent that it cannot compensate for the loss of SPATA2 in recruiting CYLD to the NOD2 or TNFR complexes. Furthermore, initial attempts to silence or genetically ablate SPATA2L from a variety of cell types lead to excessive cell death and no viable clones (data not shown). I performed a rescue experiment whereby siRNA-resistant SPATA2L expressing cell lines were created (U2OS/NOD2 cells). siRNA-resistant protein was induced by doxycycline and endogenous protein was knocked down by the corresponding siRNA (supplementary figure 7.9). Induction of siRNA-resistant SPATA2L prevented the cell death phenotype, indicating potential roles in cell death for SPATA2L. Interestingly, ongoing work within our lab lead to the acquisition of SPATA2L$^{-/-}$ mice which, in contrast to the cell death phenotype observed in cells, develop with no apparent abnormalities at normal Mendelian ratios (data not shown).

Further studies are required to investigate the CYLD:SPATA2L interaction; however, given the links between CYLD and cell death, it may be that SPATA2L represents a separate mechanism regulating this function [133, 210]. This could seem counter-intuitive as CYLD is cell death-promoting in complexes, yet SPATA2L does not appear to recruit CYLD to the TNF signalling complex I. Thus, SPATA2L may only mediate CYLD function in other complexes or sequester CYLD to prevent its recruitment to complexes. This may serve as a means to remove CYLD from active complexes without affecting its cellular levels.

6.3 Summary and future perspectives

Contrary to the classical view that DUBs are constitutively active, it is emerging that they can often require interacting partners or PTMs to perform a variety

of cellular functions [55].

The direct recruitment of OTULIN to LUBAC serves to prevent its autoubiquitination, whereas this study demonstrates that the indirect association with CYLD via SPATA2 allows LUBAC to recruit the function of a DUB that has activity beyond its own specificity [132]. E3s have the potential to recruit DUBs specifically as a regulatory mechanism and also to extend their function within signalling complexes with various DUBs displaying activities towards different polyubiquitin linkages. *Sowa et al* previously showed that 26 DUBs can interact with E3 ligases. However, interestingly they did not see LUBAC components in their MS screen when using CYLD as bait [239]. It may therefore be that their estimate of 26 E3-interacting DUBs is under-representative of the level to which DUBs associate with E3s, particularly via secondary proteins linking them to complexes. Thus, these potential mechanisms warrant further investigation. Further to this, such interactions may also be important when considering disease associations of DUBs e.g. Brooke-Spiegler syndrome, familial cylindromatosis or multiple familial trichoepitheliomas associations with CYLD mutation. The mutational landscape of DUB-interacting proteins has not been addressed but may represent a mechanism whereby inactivating mutations of DUB adaptor proteins may result in disease, though no mutations of the apparently causative DUB are present.

Phosphorylation-mediated activation of DUBs is also emerging as a regulatory mechanism within the ubiquitin field and represents an additional layer of control of signalling events above their recruitment. Numerous DUBs, and ubiquitin itself, have been reported to be phosphorylated for the control of their function, including activation or switching of DUB activity. Future research within this area should therefore consider the PTMs of DUBs in the control of their function and work towards the identification of regulatory factors affecting their ability to mediate signalling events.

7 Appendices

Contents

7.1 Supplementary figures 118
7.2 Publications 125

7.1 Supplementary figures

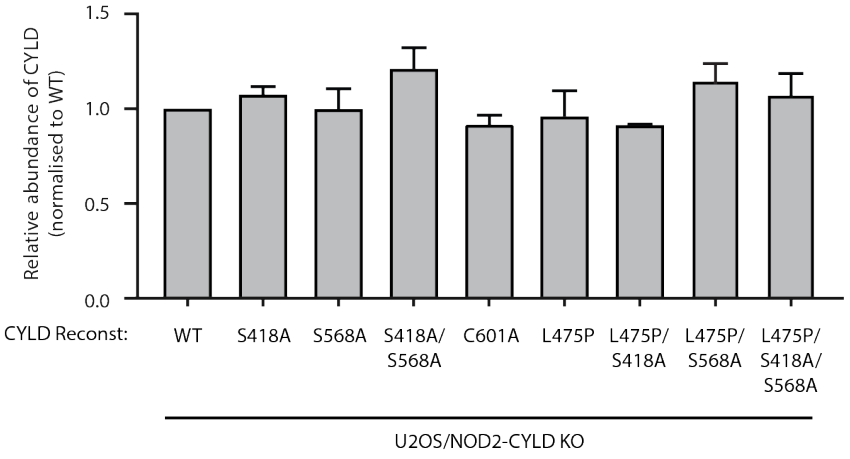


Figure 7.1: Levels of all CYLD mutants by densitometry. Immunoblot showing the reintroduced levels of all CYLD mutants. Densitometry of three blots was performed to ensure levels were matched across mutants.

#	b	b-H2O	b-NH3	b (2+)	Seq	y	y-H2O	y-NH3	y (2+)	#
1	148.08	130.07	131.05	74.54	F					24
2	205.10	187.09	188.07	103.05	G	2628.21	2610.20	2611.19	1314.61	23
3	262.12	244.09	245.09	131.56	G	2571.19	2553.18	2554.17	1286.10	22
4	425.18	407.17	408.16	213.09	Y	2514.17	2496.16	2497.15	1257.59	21
5	538.27	520.26	521.24	269.63	L	2351.11	2333.10	2334.08	1176.05	20
6	705.26	687.25	688.24	353.13	S(+79.97)	2238.02	2220.01	2221.00	1119.51	19
7	834.31	816.30	817.28	417.65	E	2071.03	2053.02	2054.00	1036.02	18
8	933.38	915.37	916.35	467.19	V	1941.99	1923.97	1924.96	971.50	17
9	1032.44	1014.43	1015.42	516.72	V	1842.91	1824.90	1825.89	921.96	16
10	1161.49	1143.48	1144.46	581.24	E	1743.85	1725.84	1726.82	872.42	15
11	1290.53	1272.52	1273.50	645.76	E	1614.80	1596.79	1597.78	807.90	14
12	1404.57	1386.56	1387.55	702.79	N	1485.77	1467.75	1468.73	743.39	13
13	1505.62	1487.61	1488.59	753.31	T	1371.72	1353.71	1354.69	686.36	12
14	1602.67	1584.66	1585.65	801.84	P	1270.67	1252.66	1253.66	635.84	11
15	1699.73	1681.72	1682.70	850.36	P	1173.62	1155.61	1156.59	587.31	10
16	1827.82	1809.81	1810.79	914.41	K	1076.57	1058.56	1059.54	538.78	9
17	1958.86	1940.85	1941.83	979.93	M	948.47	930.46	931.44	474.74	8
18	2087.90	2069.89	2070.88	1044.45	E	817.43	799.42	800.40	409.22	7
19	2216.00	2197.99	2198.97	1108.50	K	688.38	670.38	671.36	344.69	6
20	2345.04	2327.03	2328.01	1173.02	E	560.29	542.28	543.27	280.65	5
21	2402.06	2384.05	2385.04	1201.53	G	431.25	413.24	414.22	216.12	4
22	2515.15	2497.14	2498.12	1258.07	L	374.23	356.22	357.20	187.61	3
23	2644.19	2626.18	2627.16	1322.59	E	261.14	243.13	244.09	131.07	2
24					I	132.10	114.09	115.07	66.55	1

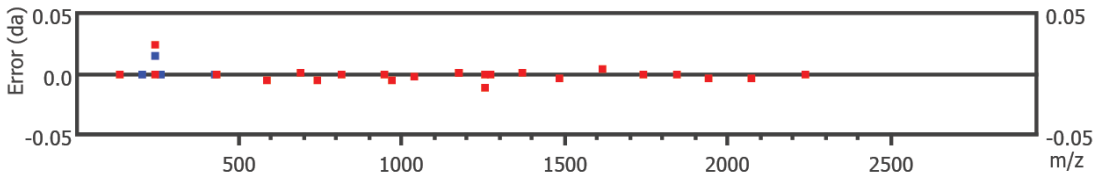


Figure 7.2: Ion table of the S568 spectra. Ion table showing the mass recorded for each b and y ion as per figure 5.6.

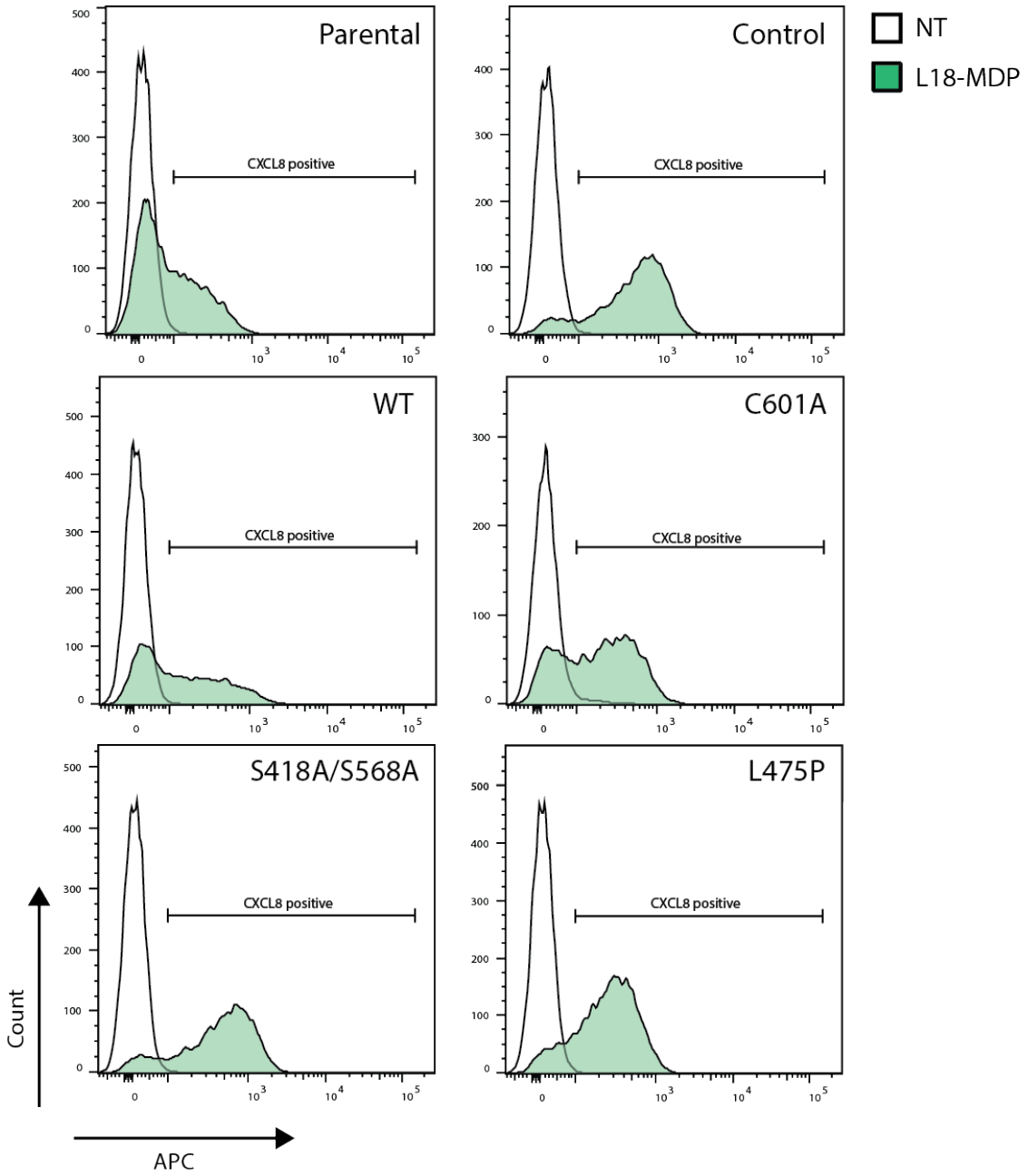


Figure 7.3: Histograms of CXCL8 production in CYLD mutants. Flow cytometry analysis of CXCL-8 production in CYLD mutants following 200 ng/ml L18-MDP for 5 h in the presence of 5 μg/ml brefeldin A and 2 μM monensin.

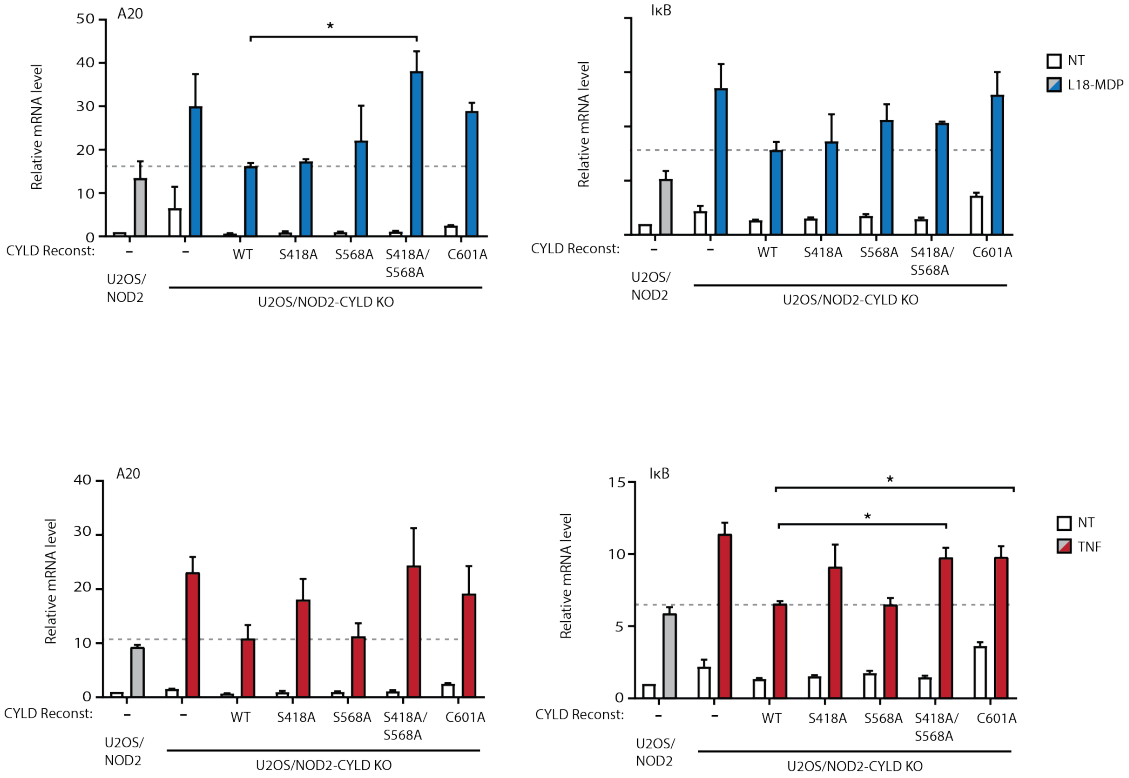


Figure 7.4: IkB/A20 transcript production in phosphomutant CYLD lines.. qRT-PCR analysis of the production of pro-inflammatory transcripts following stimulation with 20 ng/ml TNF or 200 ng/ml L18-MDP for 3 h. Data normalised to HPRT control and subsequently the CYLD^{WT} stimulated condition. Data was collated and analysed in Graphpad Prism 6 with statistic tests by two-way ANOVA.

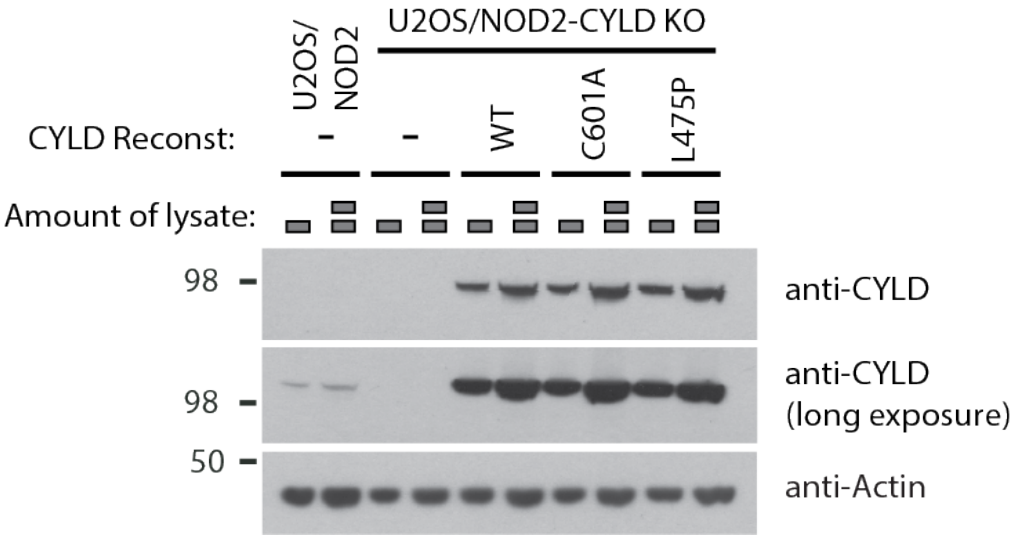


Figure 7.5: Reintroduced levels of CYLD capgly mutants Immunoblot showing reintroduced levels of the stably expressing CYLD CAPGly mutants in the CYLD KO U2OS/NOD2 background. Densitometry of of three blots was performed to ensure levels were matched between all generated mutants as shown in supplementary figure 7.1.

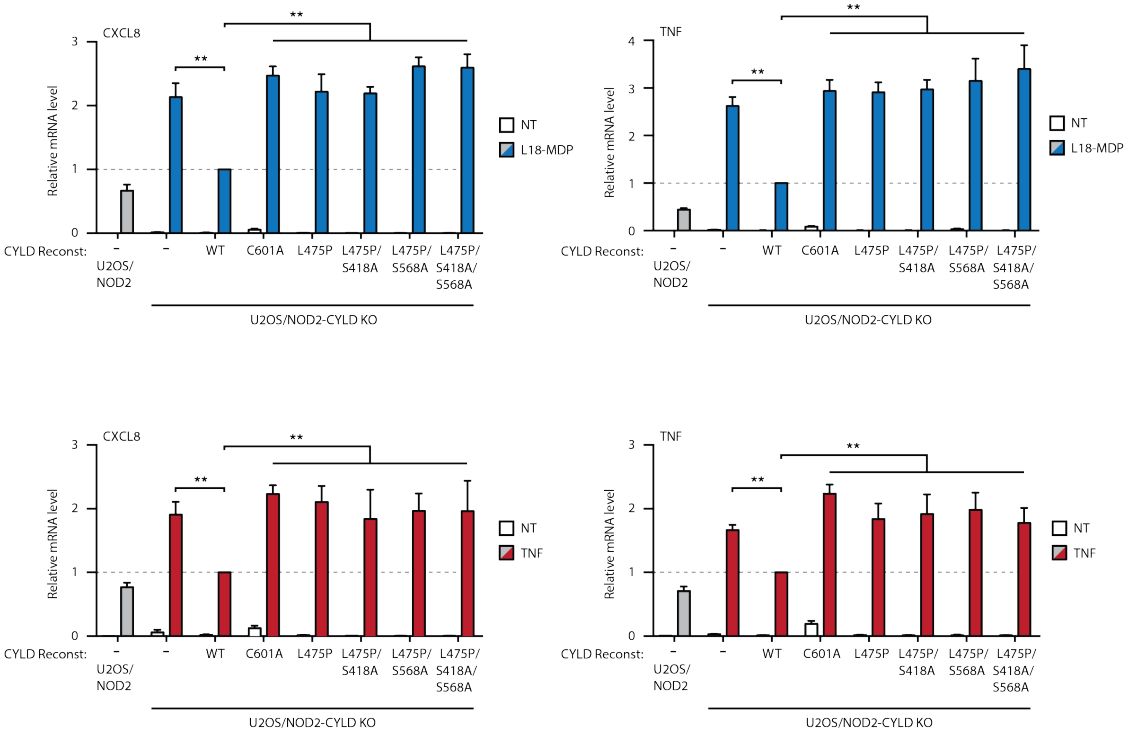


Figure 7.6: Pro-inflammatory trascript production in all CYLD^{L475P} mutants. qRT-PCR analysis of the production of pro-inflammatory transcripts following stimulation with 20 ng/ml TNF or 200 ng/ml L18-MDP for 3 h. Data normalised to HPRT control and subsequently the CYLD^{WT} stimulated condition. Data was collated and analysed in Graphpad Prism 6 with statistic tests by two-way ANOVA.

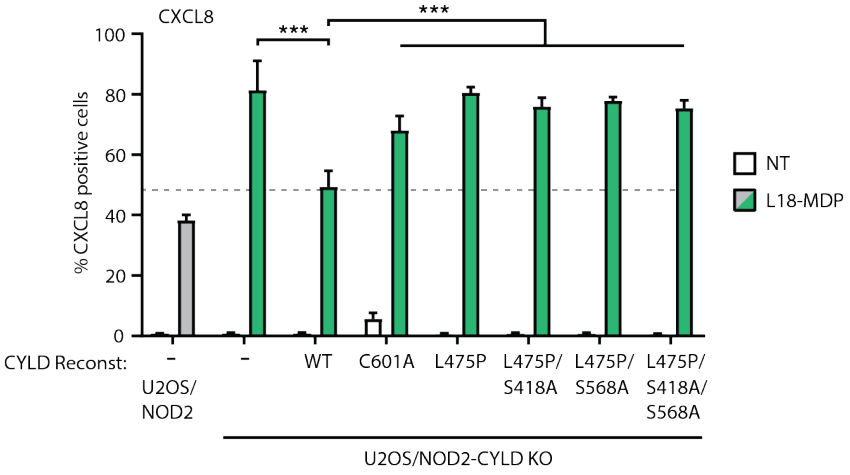


Figure 7.7: CXCL8 production in all CYLD^{L475P} mutants. Flow cytometry analysis of CXCL-8 production in phosphorylation mutants of CYLD following 200 ng/ml L18-MDP for 5 h in the presence of 5 μg/ml brefeldin A and 2 μM monensin. Data was collated and analysed in Graphpad prism 6 with statistical tests by two-way ANOVA. Representative histograms are also shown in supplementary figure 7.3.

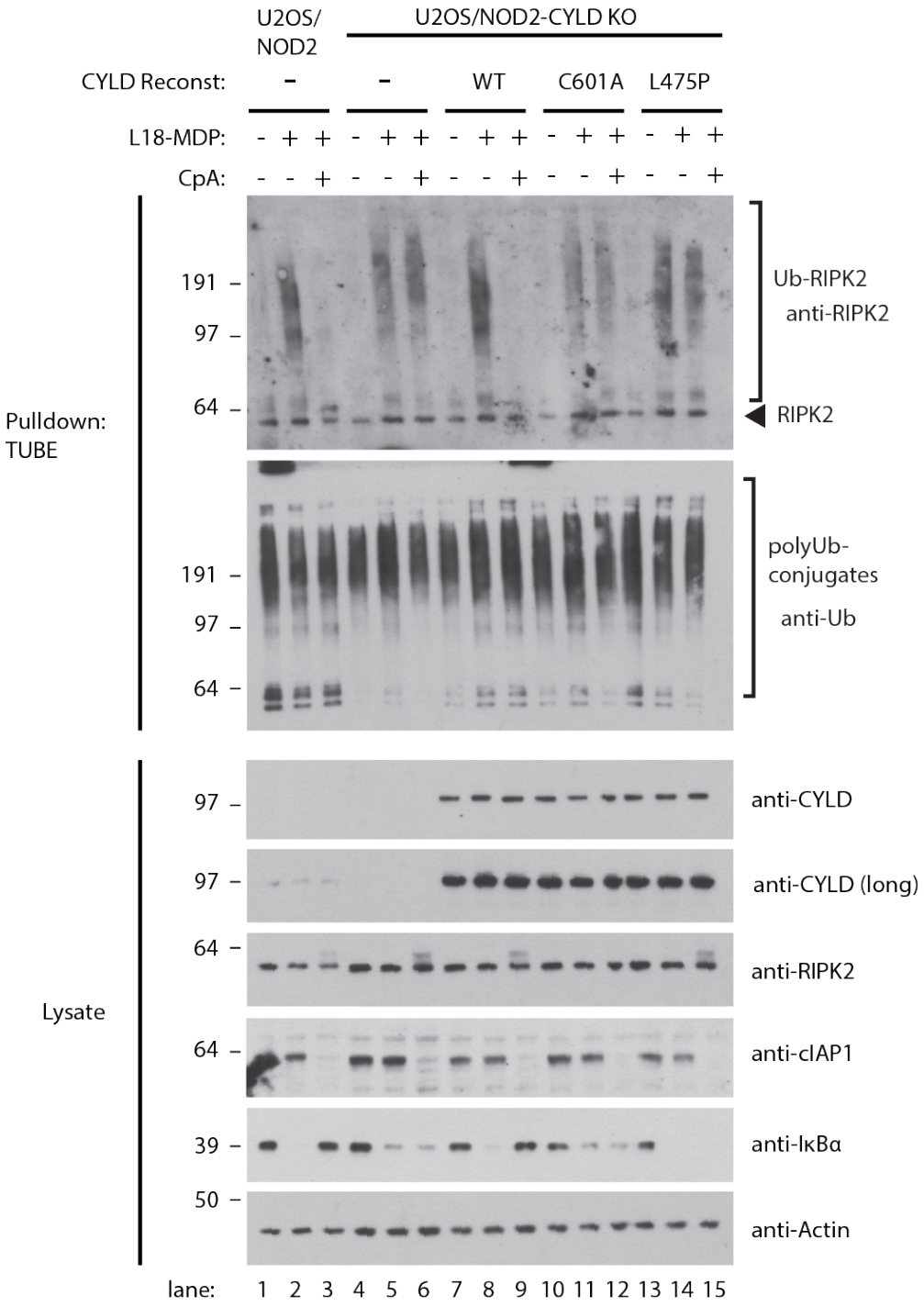


Figure 7.8: CYLD^{L475P} results in enhanced RIPK2 ubiquitination. Immunoblot showing TUBE pulldown of ubiquitination substrates, and subsequent blotting for RIPK2, after 200 ng/ml L18-MDP stimulation with or without prestimulation for 30 min with 1 μM CpA.

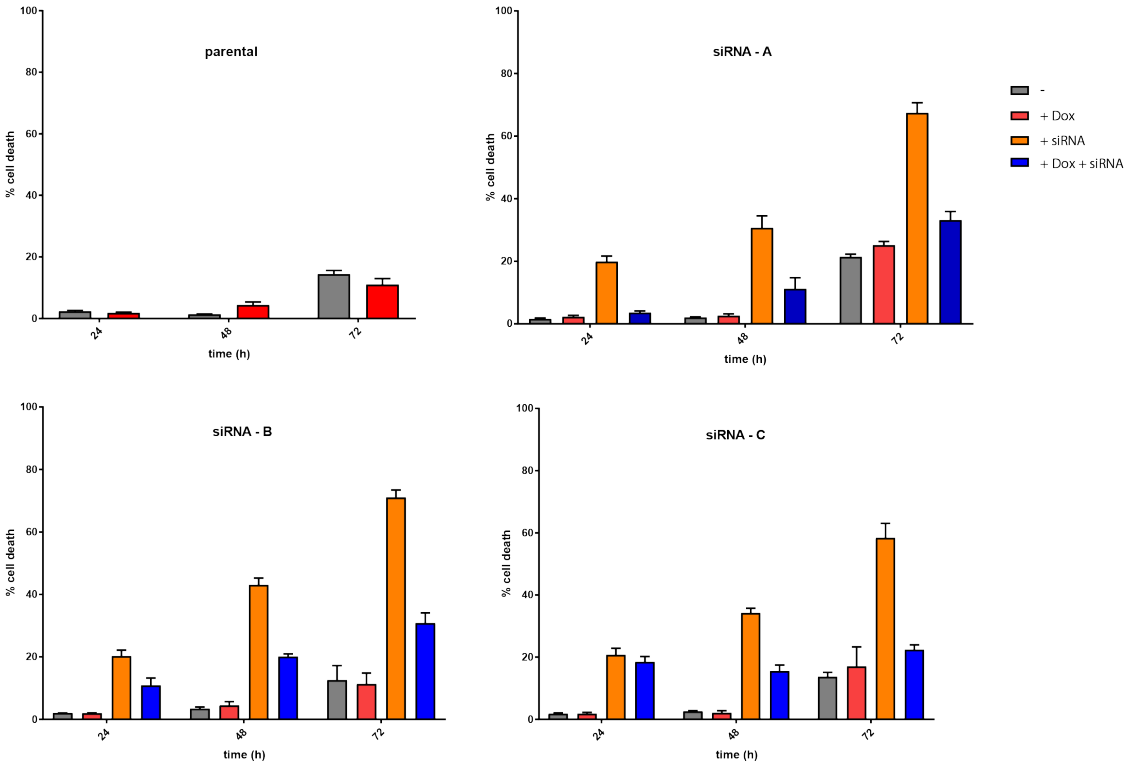


Figure 7.9: SPATA2L-induced cell death is rescued by re-introduction. U2OS/NOD2 cells were created from the Trex FlpIn system. cell lines A, B, and C represent siRNA-resistant versions of SPATA2L. siRNA was introduced to cells for given time points and Hoecsht and Sytox green stain was used to determine the percentage of cell death. As shown, each SPATA2L siRNA results in cell death, which is rescued through the Dox-induced expression of siRNA-resistant SPATA2L.

7.2 Publications

Selected data from this thesis was published and cited in the following articles:

CYLD limits Lys63- and Met1-linked ubiquitin at receptor complexes to regulate innate immune signaling.
Matous Hrdinka, Berthe Katrine Fiil, Mattia Zucca, ***Derek Leske****, Katrin Bagola, Monica Yabal, Paul R. Elliott, Rune Busk Damgaard, David Komander, Philipp J. Jost, Mads Gyrd-Hansen.* Cell reports, 2016

SPATA2 links CYLD to LUBAC, activates CYLD, and controls LUBAC signaling
Paul R Elliott,* ****Derek Leske**, Matous Hrdinka, Katrin Bagola, Berthe Katrine Fiil, Stephen H McLaughlin, Jane L Wagstaff, Norbert Volkmar, John C Christianson, Benedikt M Kessler, Stefan M V Freund, David Komander, Mads Gyrd-Hansen.* Molecular Cell, 2016
* Co-first authors

References

1. Gooley, A. A. & Packer, N. H. in *Proteome Research: New Frontiers in Functional Genomics* (eds Wilkins, M. R., Williams, K. L., Appel, R. D. & Hochstrasser, D. F.) 65–91 (Springer Berlin Heidelberg, Berlin, Heidelberg, 1997).
2. Komander, D. & Rape, M. The Ubiquitin Code. *Annual Review of Biochemistry* **81,** 203–229 (Apr. 2012).
3. Sharp, P. M. & Li, W.-H. Molecular evolution of ubiquitin genes. *TREE* **2,** 1–5 (Nov. 1987).
4. Shigi, N. Posttranslational Modification of Cellular Proteins by a Ubiquitin-like Protein in Bacteria. *Journal of Biological Chemistry* **287,** 17568–17577 (May 2012).
5. Humbard, M. A. *et al.* Ubiquitin-like small archaeal modifier proteins (SAMPs) in Haloferax volcanii. *Nature* **463,** 54–60 (Jan. 2010).
6. Ciechanover, A., Heller, H., Elias, S., Haas, A. L. & Hershko, A. ATP-dependent conjugation of reticulocyte proteins with the polypeptide required for protein degradation. *Proceedings of the National Academy of Sciences of the United States of America* **77,** 1365–1368 (Mar. 1980).
7. Wilkinson, K. D., Urban, M. K. & Haas, A. L. **Ubiquitin Is the ATP-dependent Proteolysis FactorI of Rabbit Reticulocytes**. *Journal of Biological Chemistry* **255,** 7529–7532 (Aug. 1980).
8. Hershko, A., Ciechanover, A., Heller, H., Haas, A. L. & Rose, I. A. Proposed role of ATP in protein breakdown: conjugation of protein with multiple chains of the polypeptide of ATP-dependent proteolysis. *Proceedings of the National Academy of Sciences of the United States of America* **77,** 1783–1786 (Apr. 1980).
9. Chen, Z. J. & Sun, L. J. Nonproteolytic Functions of Ubiquitin in Cell Signaling. *MOLCEL* **33,** 275–286 (Feb. 2009).
10. Kerscher, O., Felberbaum, R. & Hochstrasser, M. Modification of Proteins by Ubiquitin and Ubiquitin-Like Proteins. *Annu. Rev. Cell Dev. Biol.* **22,** 159–180 (Nov. 2006).
11. Pickart, C. M. Mechanisms Underlying Ubiquitination. *Annual Review of Biochemistry* **70,** 503–533 (June 2001).
12. Vijay-Kumar, S., Bugg, C. E. & Cook, W. J. Structure of ubiquitin refined at 1.8Åresolution. *Journal of Molecular Biology* **194,** 531–544 (1987).
13. Hochstrasser, M. Origin and Function of Ubiquitin-like Protein Conjugation. *Nature* **458,** 422 (Mar. 2009).
14. Van der Veen, A. G. & Ploegh, H. L. Ubiquitin-Like Proteins. *Annual Review of Biochemistry* **81,** 323–357 (July 2012).

15. Jentsch, S. & Pyrowolakis, G. Ubiquitin and its kin: how close are the family ties? *Trends in Cell Biology* **10,** 335–342 (2000).

16. Kirisako, T. *et al.* A ubiquitin ligase complex assembles linear polyubiquitin chains. *The EMBO Journal* **25,** 4877–4887 (Oct. 2006).

17. Mulder, M. P. C. *et al.* A cascading activity-based probe sequentially targets E1–E2–E3 ubiquitin enzymes. *Nature Chemical Biology* **12,** 523–530 (May 2016).

18. Jin, J., Li, X., Gygi, S. P. & Harper, J. W. Dual E1 activation systems for ubiquitin differentially regulate E2 enzyme charging. *Nature* **447,** 1135–1138 (June 2007).

19. Zhu, Y. *et al.* Structure of a Shigella effector reveals a new class of ubiquitin ligases. *Nature Structural &Amp; Molecular Biology* **15,** 1302–1308.

20. Markson, G. *et al.* Analysis of the human E2 ubiquitin conjugating enzyme protein interaction network. *Genes & Development* **19,** 1905–1911 (Oct. 2009).

21. Michelle, C., Vourc'h, P., Mignon, L. & Andres, C. R. What Was the Set of Ubiquitin and Ubiquitin-Like Conjugating Enzymes in the Eukaryote Common Ancestor? *Journal of Molecular Evolution* **68,** 616–628 (May 2009).

22. Pelzer, C. *et al.* UBE1L2, a Novel E1 Enzyme Specific for Ubiquitin. *Journal of Biological Chemistry* **282,** 23010–23014 (Aug. 2007).

23. Van Wijk, S. J. L. *et al.* A comprehensive framework of E2 - RING E3 interactions of the human ubiquitin - proteasome system. **5,** 1–16 (Aug. 2009).

24. Lake, M. W., Wuebbens, M. M., Rajagopalan, K. V. & Schindelin, H. Mechanism of ubiquitin activation revealed by the structure of a bacterial MoeB–MoaD complex. *Nature* **414,** 325–329 (Nov. 2001).

25. Huang, D. T. *et al.* Basis for a ubiquitin-like protein thioester switch toggling E1–E2 affinity. *Nature* **445,** 394–398 (Jan. 2007).

26. Ye, Y. & Rape, M. Building ubiquitin chains: E2 enzymes at work. *Nature Reviews Molecular Cell Biology* **10,** 755–764 (Nov. 2009).

27. Jin, L., Williamson, A., Banerjee, S., Philipp, I. & Rape, M. Mechanism of Ubiquitin-Chain Formation by the Human Anaphase-Promoting Complex. *Cell* **133,** 653–665 (May 2008).

28. VanDemark, A. P., Hofmann, R. M., Tsui, C., Pickart, C. M. & Wolberger, C. Molecular Insights into Polyubiquitin Chain Assembly: Crystal Structure of the Mms2/Ubc13 Heterodimer. *Cell* **105,** 711–720 (June 2001).

29. Komander, D., Clague, M. J. & Urbé, S. Breaking the chains: structure and function of the deubiquitinases. **10,** 550–563 (Aug. 2009).

30. Pickart, C. M. & Eddins, M. J. Ubiquitin: structures, functions, mechanisms. *Biochimica et Biophysica Acta (BBA) - Molecular Cell Research* **1695,** 55–72 (Nov. 2004).

31. Jaakkola, P. *et al.* Targeting of HIF-α to the von Hippel-Lindau Ubiquitylation Complex by O2-Regulated Prolyl Hydroxylation. *Science* **292,** 468–472 (2001).

32. Deshaies, R. J. & James E Ferrell, J. Multisite Phosphorylation Minireview and the Countdown to S Phase. *Cell* **107,** 819–822 (Dec. 2001).

33. Rotin, D. & Kumar, S. Physiological functions of the HECT family of ubiquitin ligases. *Nature Reviews Molecular Cell Biology* **10,** 398–409 (May 2009).

34. Kim, H. C. & Huibregtse, J. M. Polyubiquitination by HECT E3s and the Determinants of Chain Type Specificity. *Molecular and Cellular Biology* **29,** 3307–3318 (May 2009).

35. Deshaies, R. J. & Joazeiro, C. A. P. RING Domain E3 Ubiquitin Ligases. *Annual Review of Biochemistry* **78,** 399–434 (June 2009).

36. Hicke, L. PROTEIN REGULATION BY MONOUBIQUITIN. *Nature Reviews Molecular Cell Biology* **2,** 195–201 (Feb. 2001).

37. Ulrich, H. D. & Walden, H. Ubiquitin signalling in DNA replication and repair. *Nature Reviews Molecular Cell Biology* **11,** 479–489 (June 2010).

38. Mueller, T. D., Kamionka, M. & Feigon, J. Specificity of the Interaction between Ubiquitin-associated Domains and Ubiquitin. *Journal of Biological Chemistry* **279,** 11926–11936 (Mar. 2004).

39. Kang, R. S. *et al.* Solution Structure of a CUE-Ubiquitin Complex Reveals a Conserved Mode of Ubiquitin Binding. *Cell* **113,** 621–630 (May 2003).

40. Varadan, R. *et al.* Solution Conformation of Lys 63-linked Di-ubiquitin Chain Provides Clues to Functional Diversity of Polyubiquitin Signaling. *Journal of Biological Chemistry* **279,** 7055–7063 (Feb. 2004).

41. Hicke, L., Schubert, H. L. & Hill, C. P. Ubiquitin-binding domains. *Nature Reviews Molecular Cell Biology* **6,** 610–621 (Aug. 2005).

42. Dikic, I., Wakatsuki, S. & Walters, K. J. Ubiquitin-binding domains — from structures to functions. *Nature Reviews Molecular Cell Biology* **10,** 659–671 (Oct. 2009).

43. Hofmann, K. Ubiquitin-binding domains and their role in the DNA damage response. *Ubiquitin, SUMO and the Maintenance of Genome Stability* **8,** 544–556 (2009).

44. Husnjak, K. & Dikic, I. Ubiquitin-Binding Proteins: Decoders of Ubiquitin-Mediated Cellular Functions. *Annual Review of Biochemistry* **81,** 291–322 (July 2012).

45. Garner, T. P. *et al.* Independent Interactions of Ubiquitin-Binding Domains in a Ubiquitin-Mediated Ternary Complex. *Biochemistry* **50,** 9076–9087 (Oct. 2011).

46. Trempe, J.-F. Reading the ubiquitin postal code. *Current Opinion in Structural Biology* **21,** 792–801 (2011).

47. Kaiser, S. E. *et al.* Protein standard absolute quantification (PSAQ) method for the measurement of cellular ubiquitin pools. *Nature Methods* **8,** 691–699 (July 2011).

48. Sato, Y. *et al.* Structural basis for specific recognition of Lys 63-linked polyubiquitin chains by tandem UIMs of RAP80. **28,** 2461–2468 (June 2009).

49. Kulathu, Y., Akutsu, M., Bremm, A., Hofmann, K. & Komander, D. Two-sided ubiquitin binding explains specificity of the TAB2 NZF domain. *Nature Structural &Amp; Molecular Biology* **16,** 1328–1330 (Nov. 2009).

50. Trempe, J.-F. *et al.* Mechanism of Lys48-linked polyubiquitin chain recognition by the Mud1 UBA domain. *The EMBO Journal* **24,** 3178–3189 (Sept. 2005).

51. Hoeller, D. *et al.* Regulation of ubiquitin-binding proteins by monoubiquitination. *Nature Cell Biology* **8,** 163–169 (Jan. 2006).

52. Matsumoto, G., Wada, K., Okuno, M., Kurosawa, M. & Nukina, N. Serine 403 Phosphorylation of p62/SQSTM1 Regulates Selective Autophagic Clearance of Ubiquitinated Proteins. *MOLCEL* **44,** 279–289 (Oct. 2011).

53. Komander, D., Clague, M. J. & Urbé, S. Breaking the chains: structure and function of the deubiquitinases. **10,** 550–563 (Aug. 2009).

54. Rehman, S. A. A. *et al.* MINDY-1 Is a Member of an Evolutionarily Conserved and Structurally Distinct New Family of Deubiquitinating Enzymes. *MOLCEL* **63,** 146–155 (July 2016).

55. Leznicki, P. & Kulathu, Y. Mechanisms of regulation and diversification of deubiquitylating enzyme function. *Journal of Cell Science* **130,** 1997–2006 (2017).

56. Sowa, M. E., Bennett, E. J., Gygi, S. P. & Harper, J. W. Defining the Human Deubiquitinating Enzyme Interaction Landscape. *Cell* **138,** 389–403 (July 2009).

57. Mevissen, T. E. T. *et al.* OTU Deubiquitinases Reveal Mechanisms of Linkage Specificity and Enable Ubiquitin Chain Restriction Analysis. *Cell* **154,** 169–184 (July 2013).

58. Keusekotten, K. *et al.* OTULIN Antagonizes LUBAC Signaling by Specifically Hydrolyzing Met1-Linked Polyubiquitin. *Cell* **153,** 1312–1326 (June 2013).

59. Kwasna, D. *et al.* Discovery and Characterization of ZUFSP/ZUP1, a Distinct Deubiquitinase Class Important for Genome Stability. *Molecular Cell* **70,** 150–164.e6 (Apr. 2018).

60. Todi, S. V. *et al.* Ubiquitination directly enhances activity of the deubiquitinating enzyme ataxin-3. *Embo Journal* **28,** 372–382 (Jan. 2009).

61. Mohideen, F. & Lima, C. D. SUMO Takes Control of a Ubiquitin-Specific Protease. *Molecular Cell* **30,** 539–540 (June 2008).

62. Huang, X. *et al.* Deubiquitinase USP37 Is Activated by CDK2 to Antagonize APCCDH1 and Promote S Phase Entry. *MOLCEL* **42,** 511–523 (May 2011).

63. Li, J. *et al.* USP33 regulates centrosome biogenesis via deubiquitination of the centriolar protein CP110. *Nature* **495,** 255–259 (Mar. 2013).

64. Pahl, H. L. Activators and target genes of Rel/NF-κB transcription factors. *Oncogene* **18,** 6853–6866 (Nov. 1999).

65. Sun, S.-C. CYLD: a tumor suppressor deubiquitinase regulating NF-κB activation and diverse biological processes. *Cell Death and Differentiation* **17,** 25–34 (Jan. 2010).

66. Zhang, L. *et al.* USP4 is regulated by AKT phosphorylation and directly deubiquitylates TGF-β type I receptor. *Nature Cell Biology* **14,** 717–726 (June 2012).

67. Collins, G. A. & Goldberg, A. L. The Logic of the 26S Proteasome. *Cell* **169,** 792–806 (May 2017).

68. Yao, T. *et al.* Distinct Modes of Regulation of the Uch37 Deubiquitinating Enzyme in the Proteasome and in the Ino80 Chromatin-Remodeling Complex. *Molecular Cell* **31,** 909–917 (Sept. 2008).

69. Sahtoe, D. D. *et al.* Mechanism of UCH-L5 Activation and Inhibition by DEUBAD Domains in RPN13 and INO80G. *MOLCEL* **57,** 887–900 (Mar. 2015).

70. Zeqiraj, E. *et al.* Higher-Order Assembly of BRCC36–KIAA0157 Is Required for DUB Activity and Biological Function. *Molecular Cell* **59,** 970–983 (Sept. 2015).

71. Feng, L., Wang, J. & Chen, J. The Lys 63-specific Deubiquitinating Enzyme BRCC36 Is Regulated by Two Scaffold Proteins Localizing in Different Subcellular Compartments. *Journal of Biological Chemistry* **285,** 30982–30988 (Sept. 2010).

72. Zheng, H. *et al.* A BRISC-SHMT Complex Deubiquitinates IFNAR1 and Regulates Interferon Responses. *Cell Reports* **5,** 180–193 (Oct. 2013).

73. Shao, G. *et al.* The Rap80-BRCC36 de-ubiquitinating enzyme complex antagonizes RNF8-Ubc13-dependent ubiquitination events at DNA double strand breaks. *Proceedings of the National Academy of Sciences of the United States of America* **106,** 3166–3171 (Mar. 2009).

74. Koutelou, E., Hirsch, C. L. & Dent, S. Y. Multiple faces of the SAGA complex. *Current Opinion in Cell Biology* **22,** 374–382 (June 2010).

75. Cohn, M. A., Kee, Y., Haas, W., Gygi, S. P. & D'Andrea, A. D. UAF1 Is a Subunit of Multiple Deubiquitinating Enzyme Complexes. *Journal of Biological Chemistry* **284,** 5343–5351 (Feb. 2009).

76. Kee, Y. *et al.* WDR20 Regulates Activity of the USP12 · UAF1 Deubiquitinating Enzyme Complex. *Journal of Biological Chemistry* **285,** 11252–11257 (Apr. 2010).

77. Kedersha, N. *et al.* G3BP–Caprin1–USP10 complexes mediate stress granule condensation and associate with 40S subunits. *The Journal of Cell Biology* **212,** 845–860 (Mar. 2016).

78. Clague, M. J. & Urbé, S. Integration of cellular ubiquitin and membrane traffic systems: focus on deubiquitylases. *FEBS Journal* **284,** 1753–1766 (Jan. 2017).

79. Kupka, S. *et al.* SPATA2-Mediated Binding of CYLD to HOIP Enables CYLD Recruitment to Signaling Complexes. *CellReports* **16,** 2271–2280 (Aug. 2016).

80. Elliott, P. R. *et al.* SPATA2 Links CYLD to LUBAC, Activates CYLD, and Controls LUBAC Signaling. *MOLCEL* **63,** 990–1005 (Aug. 2016).

81. Wagner, S. A., Satpathy, S., Beli, P. & Choudhary, C. SPATA2 links CYLD to the TNF-α receptor signaling complex and modulates the receptor signaling outcomes. *Embo Journal* **35,** 1868–1884 (Sept. 2016).

82. Schlicher, L. *et al.* SPATA2 promotes CYLD activity and regulates TNF-induced NF-κB signaling and cell death. *EMBO reports* **17,** 1485–1497 (Oct. 2016).

83. Wei, R. *et al.* SPATA2 regulates the activation of RIPK1 by modulating linear ubiquitination. *Genes & Development* **31,** 1162–1176 (June 2017).

84. Thrower, J. S., Hoffman, L., Rechsteiner, M. & Pickart, C. M. Recognition of the polyubiquitin proteolytic signal. *The EMBO Journal* **19,** 94–102 (Jan. 2000).

85. Lander, G. C. *et al.* Complete subunit architecture of the proteasome regulatory particle. *Nature* **482,** 186–191 (Jan. 2012).

86. Matyskiela, M. E., Lander, G. C. & Martin, A. Conformational switching of the 26S proteasome enables substrate degradation. *Nature Structural & Molecular Biology* **20,** 781–788 (June 2013).

87. Kirkpatrick, D. S. *et al.* Quantitative analysis of in vitro ubiquitinated cyclin B1 reveals complex chain topology. *Nature Cell Biology* **8,** 700–710 (June 2006).

88. Flick, K., Raasi, S., Zhang, H., Yen, J. L. & Kaiser, P. A ubiquitin-interacting motif protects polyubiquitinated Met4 from degradation by the 26S proteasome. *Nature Cell Biology* **8,** 509–515 (Apr. 2006).

89. Flick, K. *et al.* Proteolysis-independent regulation of the transcription factor Met4 by a single Lys 48-linked ubiquitin chain. *Nature Cell Biology* **6,** 634–641 (June 2004).

90. Rahighi, S. *et al.* Specific Recognition of Linear Ubiquitin Chains by NEMO Is Important for NF-κB Activation. *Cell* **136,** 1098–1109 (Mar. 2009).

91. Haas, T. L. *et al.* Recruitment of the Linear Ubiquitin Chain Assembly Complex Stabilizes the TNF-R1 Signaling Complex and Is Required for TNF-Mediated Gene Induction. *MOLCEL* **36,** 831–844 (Dec. 2009).

92. Tokunaga, F. & Iwai, K. LUBAC, a novel ubiquitin ligase for linear ubiquitination, is crucial for inflammation and immune responses. *Microbes and Infection* **14,** 563–572 (July 2012).

93. Wickliffe, K. E., Williamson, A., Meyer, H.-J., Kelly, A. & Rape, M. K11-linked ubiquitin chains as novel regulators of cell division. *Trends in Cell Biology* **21,** 656–663 (Nov. 2011).

94. Bremm, A. & Komander, D. Emerging roles for Lys11-linked polyubiquitin in cellular regulation. *Trends in Biochemical Sciences* **36,** 355–363 (June 2011).

95. Hu, H. *et al.* OTUD7B controls non-canonical NF-κB activation through deubiquitination of TRAF3. *Nature* **494,** 371–374 (Feb. 2013).

96. Hu, H. *et al.* Otud7b facilitates T cell activation and inflammatory responses by regulating Zap70 ubiquitination. *Journal of Experimental Medicine* **213,** 399–414 (Mar. 2016).

97. Pareja, F. *et al.* Deubiquitination of EGFR by Cezanne-1 contributes to cancer progression. *Oncogene* **31,** 4599–4608 (Dec. 2011).

98. Wu-Baer, F., Lagrazon, K., Yuan, W. & Baer, R. The BRCA1/BARD1 Heterodimer Assembles Polyubiquitin Chains through an Unconventional Linkage Involving Lysine Residue K6 of Ubiquitin. *Journal of Biological Chemistry* **278,** 34743–34746 (Sept. 2003).

99. Geisler, S. *et al.* PINK1/Parkin-mediated mitophagy is dependent on VDAC1 and p62/SQSTM1. *Nature Cell Biology* **12,** 119–131 (Jan. 2010).

100. Tran, H., Hamada, F., Schwarz-Romond, T. & Bienz, M. Trabid, a new positive regulator of Wnt-induced transcription with preference for binding and cleaving K63-linked ubiquitin chains. *Genes & Development* **22,** 528–542 (Feb. 2008).

101. Jin, J. *et al.* Epigenetic regulation of the expression of Il12 and Il23 and autoimmune inflammation by the deubiquitinase Trabid. *Nature Immunology* **17,** 259–268 (Jan. 2016).

102. Yuan, W.-C. *et al.* K33-Linked Polyubiquitination of Coronin 7 by Cul3-KLHL20 Ubiquitin E3 Ligase Regulates Protein Trafficking. *MOLCEL* **54,** 586–600 (2014).

103. Emmerich, C. H. *et al.* Activation of the canonical IKK complex by K63/M1-linked hybrid ubiquitin chains. *Proceedings of the National Academy of Sciences of the United States of America* **110,** 15247–15252 (Sept. 2013).

104. Hadian, K. *et al.* NF-κB Essential Modulator (NEMO) Interaction with Linear and Lys-63 Ubiquitin Chains Contributes to NF-κB Activation. *Journal of Biological Chemistry* **286,** 26107–26117 (July 2011).

105. Grice, G. L. *et al.* The Proteasome Distinguishes between Heterotypic and Homotypic Lysine-11-Linked Polyubiquitin Chains. *CellReports* **12,** 545–553 (July 2015).

106. Meyer, H.-J. & Rape, M. Enhanced Protein Degradation by Branched Ubiquitin Chains. *Cell* **157,** 910–921 (May 2014).

107. Boname, J. M. *et al.* Efficient Internalization of MHC I Requires Lysine-11 and Lysine-63 Mixed Linkage Polyubiquitin Chains. *Traffic* **11,** 210–220 (Feb. 2010).

108. Kim, H. T. *et al.* Certain Pairs of Ubiquitin-conjugating Enzymes (E2s) and Ubiquitin-Protein Ligases (E3s) Synthesize Nondegradable Forked Ubiquitin Chains Containing All Possible Isopeptide Linkages. *Journal of Biological Chemistry* **282,** 17375–17386 (May 2007).

109. Ohtake, F. *et al.* Ubiquitin acetylation inhibits polyubiquitin chain elongation. *EMBO reports* **16,** 192–201 (Feb. 2015).

110. Liu, Z. *et al.* Ubiquitylation of Autophagy Receptor Optineurin by HACE1 Activates Selective Autophagy for Tumor Suppression. *Cancer Cell* **26,** 106–120 (July 2014).

111. Michel, M. A. *et al.* Assembly and Specific Recognition of K29- and K33- Linked Polyubiquitin. *MOLCEL* **58,** 95–109 (Apr. 2015).

112. Kristariyanto, Y. A. *et al.* K29-Selective Ubiquitin Binding Domain Reveals Structural Basis of Specificity and Heterotypic Nature of K29 Polyubiquitin. *MOLCEL* **58,** 83–94 (Apr. 2015).

113. Parkin, J. & Cohen, B. An overview of the immune system. *The Lancet* **357,** 1777–1789 (June 2001).

114. Takeuchi, O. & Akira, S. Pattern Recognition Receptors and Inflammation. *Cell* **140,** 805–820 (Mar. 2010).

115. Schattgen, S. A. & Fitzgerald, K. A. The PYHIN protein family as mediators of host defenses. *Immunological reviews* **243,** 109–118 (Aug. 2011).

116. Hu, H. & Sun, S.-C. Ubiquitin signaling in immune responses. *Cell Research* **26,** 457–483 (Apr. 2016).

117. Wang, C. *et al.* TAK1 is a ubiquitin-dependent kinase of MKK and IKK. *Nature* **412,** 346–351 (July 2001).

118. Chen, Z. J. Ubiquitination in Signaling to and Activation of IKK. *Immunological reviews* **246,** 95–106 (Mar. 2012).

119. Hubeau, M. *et al.* New mechanism of X-linked anhidrotic ectodermal dysplasia with immunodeficiency: impairment of ubiquitin binding despite normal folding of NEMO protein. *Blood* **118,** 926–935 (July 2011).

120. Sun, S.-C. & Ley, S. C. New insights into NF-κB regulation and function. *Trends in Immunology* **29,** 469–478 (Oct. 2008).

121. Caruso, R., Warner, N., Inohara, N. & Nuñez, G. NOD1 and NOD2: Signaling, Host Defense, and Inflammatory Disease. *Immunity* **41,** 898–908 (Dec. 2014).

122. Kobayashi, K. *et al.* RICK/Rip2/CARDIAK mediates signalling for receptors of the innate and adaptive immune systems. *Nature* **416,** 194–199 (Mar. 2002).

123. Hasegawa, M. *et al.* A critical role of RICK/RIP2 polyubiquitination in Nod-induced NF-κB activation. *The EMBO Journal* **27,** 373–383 (Jan. 2008).

124. Damgaard, R. B. *et al.* Disease-causing mutations in the XIAPBIR2 domain impair NOD2-dependent immune signalling. *EMBO Molecular Medicine* **5,** 1278–1295 (July 2013).

125. Hrdinka, Matous *et al.* Small molecule inhibitors reveal an indispensable scaffolding role of RIPK2 in NOD2 signaling. *Embo Journal,* e99372 (July 2018).

126. Damgaard, R. B. *et al.* The Ubiquitin Ligase XIAP Recruits LUBAC for NOD2 Signaling in Inflammation and Innate Immunity. *MOLCEL* **46,** 746–758 (June 2012).

127. Marinis, J. M., Homer, C. R., McDonald, C. & Abbott, D. W. A Novel Motif in the Crohn's Disease Susceptibility Protein, NOD2, Allows TRAF4 to Down-regulate Innate Immune Responses. *Journal of Biological Chemistry* **286,** 1938–1950 (Jan. 2011).

128. Zhang, R. *et al.* The E3 Ligase RNF34 is a Novel Negative Regulator of the NOD1 Pathway. *Cellular Physiology and Biochemistry* **33,** 1954–1962 (2014).

129. Bertrand, M. J. M. *et al.* Cellular Inhibitors of Apoptosis cIAP1 and cIAP2 Are Required for Innate Immunity Signaling by the Pattern Recognition Receptors NOD1 and NOD2. *Immunity* **30,** 789–801 (June 2009).

130. Tao, M. *et al.* ITCH K63-Ubiquitinates the NOD2 Binding Protein, RIP2, to Influence Inflammatory Signaling Pathways. *Current Biology* **19,** 1255–1263 (Aug. 2009).

131. Feltham, R. *et al.* Smac Mimetics Activate the E3 Ligase Activity of cIAP1 Protein by Promoting RING Domain Dimerization. *Journal of Biological Chemistry* **286,** 17015–17028 (May 2011).

132. Hrdinka, Matous *et al.* CYLD Limits Lys63- and Met1-Linked Ubiquitin at Receptor Complexes to Regulate Innate Immune Signaling. *CellReports* **14,** 2846–2858 (Mar. 2016).

133. Draber, P. *et al.* LUBAC-Recruited CYLD and A20 Regulate Gene Activation and Cell Death by Exerting Opposing Effects on Linear Ubiquitin in Signaling Complexes. *CellReports* **13,** 2258–2272 (Dec. 2015).

134. Fiil, B. K. *et al.* OTULIN Restricts Met1-Linked Ubiquitination to Control Innate Immune Signaling. *Molecular Cell* **50,** 818–830 (June 2013).

135. Wei, R. *et al.* SPATA2 regulates the activation of RIPK1 by modulating linear ubiquitination. *Genes & Development* **31,** 1162–1176 (July 2017).

136. Rivkin, E. *et al.* The linear ubiquitin-specific deubiquitinase Gumby/Fam105b regulates angiogenesis. *Nature* **498,** 318–324 (June 2013).

137. Elliott, P. R. *et al.* Molecular Basis and Regulation of OTULIN-LUBAC Interaction. *MOLCEL* **54,** 335–348 (May 2014).

138. Tokunaga, F. *et al.* Specific recognition of linear polyubiquitin by A20 zinc finger 7 is involved in NF-κB regulation. *The EMBO Journal* **31,** 3856–3870 (Oct. 2012).

139. Verhelst, K. *et al.* A20 inhibits LUBAC-mediated NF-κB activation by binding linear polyubiquitin chains via its zinc finger 7. *The EMBO Journal* **31,** 3845–3855 (Oct. 2012).

140. Wertz, I. E. *et al.* De-ubiquitination and ubiquitin ligase domains of A20 downregulate NF-κB signalling. *Nature* **430,** 694–699 (Aug. 2004).

141. Shembade, N. *et al.* The E3 ligase Itch negatively regulates inflammatory signaling pathways by controlling the function of the ubiquitin-editing enzyme A20. *Nature Immunology* **9,** 254–262 (Feb. 2008).

142. Shembade, N., Parvatiyar, K., Harhaj, N. S. & Harhaj, E. W. The ubiquitin-editing enzyme A20 requires RNF11 to downregulate NF-κB signalling. *The EMBO Journal* **28,** 513–522 (Mar. 2009).

143. Black, R. A. *et al.* A metalloproteinase disintegrin that releases tumour-necrosis factor-α from cells. *Nature* **385,** 729–733 (Feb. 1997).

144. Sabio, G. & Davis, R. J. TNF and MAP kinase signalling pathways. *Seminars in Immunology* **26,** 237–245 (June 2014).

145. Grell, M., Wajant, H., Zimmermann, G. & Scheurich, P. The type 1 receptor (CD120a) is the high-affinity receptor for soluble tumornecrosisfactor. *Proceedings of the National Academy of Sciences of the United States of America* **95,** 570–575 (Jan. 1998).

146. Hsu, H., Xiong, J. & Goeddel, D. V. The TNF Receptor I-Associated Protein TRADD Signals Cell Death and NF-KB Activation. *Cell* **81,** 495–504 (May 1995).

147. Vince, J. E. *et al.* TRAF2 Must Bind to Cellular Inhibitors of Apoptosis for Tumor Necrosis Factor (TNF) to Efficiently Activate NF-κB and to Prevent TNF-induced Apoptosis. *The Journal of biological chemistry* **284,** 35906–35915 (Dec. 2009).

148. Pobezinskaya, Y. L. *et al.* The function of TRADD in signaling through tumor necrosis factor receptor 1 and TRIF-dependent Toll-like receptors. *Nature Immunology* **9,** 1047–1054 (July 2008).

149. Dynek, J. N. *et al.* c-IAP1 and UbcH5 promote K11-linked polyubiquitination of RIP1 in TNF signalling. *The EMBO Journal* **29,** 4198–4209 (Dec. 2010).

150. Varfolomeev, E. *et al.* c-IAP1 and c-IAP2 Are Critical Mediators of Tumor Necrosis Factor α (TNFα)-induced NF-κB Activation. *The Journal of biological chemistry* **283,** 24295–24299 (Sept. 2008).

151. Gerlach, B. *et al.* Linear ubiquitination prevents inflammation and regulates immune signalling. *Nature* **471,** 591–596 (Mar. 2011).

152. Xu, G. *et al.* Ubiquitin-specific Peptidase 21 Inhibits Tumor Necrosis Factor α-induced Nuclear Factor κB Activation via Binding to and Deubiquitinating Receptor-interacting Protein 1. *The Journal of biological chemistry* **285,** 969–978 (Jan. 2010).

153. Kovalenko, A. *et al.* The tumour suppressor CYLD negatively regulates NF-κB signalling by deubiquitination. *Nature* **424,** 801–805 (Aug. 2003).

154. Brummelkamp, T. R., Nijman, S. M. B., Dirac, A. M. G. & Bernards, R. Loss of the cylindromatosis tumour suppressor inhibits apoptosis by activating NF-κB. *Nature* **424,** 797–801 (2003).

155. Trompouki, E. *et al.* CYLD is a deubiquitinating enzyme that negatively regulates NF-κB activation by TNFR family members. *Nature* **424,** 793–796 (Aug. 2003).

156. Enesa, K. *et al.* NF-κB Suppression by the Deubiquitinating Enzyme Cezanne: A NOVEL NEGATIVE FEEDBACK LOOP IN PRO-INFLAMMATORY SIGNALING. *Journal of Biological Chemistry* **283,** 7036–7045 (2008).

157. Pasparakis, M. & Vandenabeele, P. Necroptosis and its role in inflammation. *Nature* **517,** 311–320 (Jan. 2015).

158. Wang, L., Du, F. & Wang, X. TNF-α Induces Two Distinct Caspase-8 Activation Pathways. *Cell* **133,** 693–703 (May 2008).

159. Micheau, O. & Tschopp, J. Induction of TNF Receptor I-Mediated Apoptosis via Two Sequential Signaling Complexes. *Cell* **114,** 181–190 (July 2003).

160. Nagata, S. Apoptosis and Clearance of Apoptotic Cells. *Annual Review of Immunology* **36,** 489–517 (Apr. 2018).

161. Li, J. *et al.* The RIP1/RIP3 Necrosome Forms a Functional Amyloid Signaling Complex Required for Programmed Necrosis. *Cell* **150,** 339–350 (July 2012).

162. Weinlich, R. & Green, D. R. The Two Faces of Receptor Interacting Protein Kinase-1. *Molecular Cell* **56,** 469–480 (Nov. 2014).

163. Wang, H. *et al.* Mixed Lineage Kinase Domain-like Protein MLKL Causes Necrotic Membrane Disruption upon Phosphorylation by RIP3. *MOLCEL* **54,** 133–146 (2014).

164. Tokunaga, F. *et al.* SHARPIN is a component of the NF-κB-activating linear ubiquitin chain assembly complex. *Nature* **471,** 633–636 (Mar. 2011).

165. Hrdinka, Matous & Gyrd-Hansen, M. The Met1-Linked Ubiquitin Machinery: Emerging Themes of (De)regulation. *Molecular Cell* **68,** 265–280 (Oct. 2017).

166. Stieglitz, B. *et al.* Structural basis for ligase-specific conjugation of linear ubiquitin chains by HOIP. *Nature* **503,** 422–426 (Oct. 2013).

167. Stieglitz, B., Morris-Davies, A. C., Koliopoulos, M. G., Christodoulou, E. & Rittinger, K. LUBAC synthesizes linear ubiquitin chains via a thioester intermediate. *EMBO reports* **13,** 840–846 (Sept. 2012).

168. Yagi, H. *et al.* A non-canonical UBA–UBL interaction forms the linear-ubiquitin-chain assembly complex. *EMBO reports* **13,** 462–468 (May 2012).

169. Ikeda, F. *et al.* SHARPIN forms a linear ubiquitin ligase complex regulating NF-κB activity and apoptosis. *Nature* **471,** 637–641 (Mar. 2011).

170. Smit, J. J. *et al.* The E3 ligase HOIP specifies linear ubiquitin chain assembly through its RING-IBR-RING domain and the unique LDD extension. *The EMBO Journal* **31,** 3833–3844 (Oct. 2012).

171. Boisson, B. *et al.* Human HOIP and LUBAC deficiency underlies autoinflammation, immunodeficiency, amylopectinosis, and lymphangiectasia. *The Journal of experimental medicine* **212,** 939–951 (June 2015).

172. Peltzer, N. *et al.* HOIP Deficiency Causes Embryonic Lethality by Aberrant TNFR1-Mediated Endothelial Cell Death. *Cell Reports* **9,** 153–165 (Oct. 2014).

173. Tokunaga, F. *et al.* Involvement of linear polyubiquitylation of NEMO in NF-κB activation. *Nature Cell Biology* **11,** 123–132 (Jan. 2009).

174. Schaab, C., Geiger, T., Stoehr, G., Cox, J. & Mann, M. Analysis of High Accuracy, Quantitative Proteomics Data in the MaxQB Database. *Molecular & cellular proteomics : MCP* **11,** M111.014068 (Mar. 2012).

175. Fujita, H. *et al.* Cooperative Domain Formation by Homologous Motifs in HOIL-1L and SHARPIN Plays A Crucial Role in LUBAC Stabilization. *Cell Reports* **23,** 1192–1204 (Apr. 2018).

176. Schaeffer, V. *et al.* Binding of OTULIN to the PUB Domain of HOIP Controls NF-κB Signaling. *MOLCEL* **54,** 349–361 (May 2014).

177. Takiuchi, T. *et al.* Suppression of LUBAC-mediated linear ubiquitination by a specific interaction between LUBAC and the deubiquitinases CYLD and OTULIN. *Genes to Cells* **19,** 254–272 (Jan. 2014).

178. Emmerich, C. H. *et al.* Lys63/Met1-hybrid ubiquitin chains are commonly formed during the activation of innate immune signalling. *BIOCHEMICAL AND BIOPHYSICAL RESEARCH COMMUNICATIONS* **474,** 452–461 (June 2016).

179. Inn, K.-S. *et al.* Linear ubiquitin assembly complex negatively regulates RIG-I and TRIM25 mediated type-I interferon induction. *Molecular Cell* **41,** 354–365 (Feb. 2011).

180. Sasaki, Y. *et al.* Defective immune responses in mice lacking LUBAC-mediated linear ubiquitination in B cells. *The EMBO Journal* **32,** 2463–2476 (Sept. 2013).

181. Shimizu, Y. *et al.* The Linear ubiquitin chain assembly complex acts as a liver tumor suppressor and inhibits hepatocyte apoptosis and hepatitis. *Hepatology (Baltimore, Md.)* **65,** 1963–1978 (June 2017).

182. Peltzer, N. *et al.* LUBAC is essential for embryogenesis by preventing cell death and enabling haematopoiesis. *Nature* **557,** 112–117 (2018).

183. HogenEsch, H. *et al.* A spontaneous mutation characterized by chronic proliferative dermatitis in C57BL mice. *The American Journal of Pathology* **143,** 972–982 (Sept. 1993).

184. Kumari, S. *et al.* Sharpin prevents skin inflammation by inhibiting TNFR1-induced keratinocyte apoptosis. *eLife* **3,** e03422 (2014).

185. Rickard, J. A. *et al.* TNFR1-dependent cell death drives inflammation in Sharpin-deficient mice. *eLife* **3,** e03464 (2014).

186. Berger, S. B. *et al.* RIP1 kinase activity is dispensable for normal development but is a key regulator of inflammation in SHARPIN-deficient mice. *Journal of immunology (Baltimore, Md. : 1950)* **192,** 5476–5480 (June 2014).

187. Damgaard, R. B. *et al.* The Deubiquitinase OTULIN Is an Essential Negative Regulator of Inflammation and Autoimmunity. *Cell* **166,** 1215–1230 (Aug. 2016).

188. Zhou, Q. *et al.* Biallelic hypomorphic mutations in a linear deubiquitinase define otulipenia, an early-onset autoinflammatory disease. *Proceedings of the National Academy of Sciences of the United States of America* **113,** 10127–10132 (Sept. 2016).

189. Yang, Y. *et al.* Essential Role of the Linear Ubiquitin Chain Assembly Complex in Lymphoma Revealed by Rare Germline Polymorphisms. *Cancer Discovery* **4,** 480–493 (Apr. 2014).

190. Yang, Y.-K. *et al.* Molecular Determinants of Scaffold-induced Linear Ubiquitinylation of B Cell Lymphoma/Leukemia 10 (Bcl10) during T Cell Receptor and Oncogenic Caspase Recruitment Domain-containing Protein 11 (CARD11) Signaling. *Journal of Biological Chemistry* **291,** 25921–25936 (Dec. 2016).

191. Ashida, H., Kim, M. & Sasakawa, C. Exploitation of the host ubiquitin system by human bacterial pathogens. *Nature Reviews Microbiology* **12,** 399–413 (May 2014).

192. De Jong, M. F., Liu, Z., Chen, D. & Alto, N. M. Shigella flexneri suppresses NF-kB activation by inhibiting linear ubiquitin chain ligation. *Nature microbiology* **1,** 16084–16084 (2016).

193. Pruneda, J. N. *et al.* E2Ub conjugates regulate the kinase activity of Shigella effector OspG during pathogenesis. *The EMBO Journal* **33,** 437–449 (Mar. 2014).

194. Jing, H. *et al.* Porcine Reproductive and Respiratory Syndrome Virus nsp1α Inhibits NF-κB Activation by Targeting the Linear Ubiquitin Chain Assembly Complex. *Journal of Virology* **91,** 783 (Jan. 2017).

195. Wang, L. *et al.* The Linear Ubiquitin Assembly Complex Modulates Latent Membrane Protein 1 Activation of NF-κB and Interferon Regulatory Factor 7. *Journal of Virology* **91,** 144 (Jan. 2017).

196. Greenfeld, H. *et al.* TRAF1 Coordinates Polyubiquitin Signaling to Enhance Epstein-Barr Virus LMP1-Mediated Growth and Survival Pathway Activation. *PLoS Pathogens* **11,** e1004890 (May 2015).

197. Khan, M., Syed, G. H., Kim, S.-J. & Siddiqui, A. Hepatitis B Virus-Induced Parkin-Dependent Recruitment of Linear Ubiquitin Assembly Complex (LUBAC) to Mitochondria and Attenuation of Innate Immunity. *PLoS Pathogens* **12,** e1005693 (June 2016).

198. Biggs, P. J. *et al.* Familial cylindromatosis (turban tumour syndrome) gene localised to chromosome 16q12–q13: evidence for its role as a tumour suppressor gene. *Nature Genetics* **11,** 441–443 (Dec. 1995).

199. Bignell, G. R. *et al.* Identification of the familial cylindromatosis tumour-suppressor gene. *Nature Genetics* **25,** 160–165 (June 2000).

200. Trompouki, E. *et al.* Truncation of the Catalytic Domain of the Cylindromatosis Tumor Suppressor Impairs Lung Maturation. *Neoplasia (New York, N.Y.)* **11,** 469–476 (May 2009).

201. Massoumi, R., Chmielarska, K., Hennecke, K., Pfeifer, A. & Fässler, R. Cyld Inhibits Tumor Cell Proliferation by Blocking Bcl-3-Dependent NF-κB Signaling. *Cell* **125,** 665–677 (May 2006).

202. Zhang, J. *et al.* Impaired regulation of NF-κB and increased susceptibility to colitis-associated tumorigenesis in CYLD-deficient mice. *Journal of Clinical Investigation* **116,** 3042–3049 (Nov. 2006).

203. Nikolaou, K. *et al.* Inactivation of the Deubiquitinase CYLD in Hepatocytes Causes Apoptosis, Inflammation, Fibrosis, and Cancer. *Cancer Cell* **21,** 738–750 (2012).

204. Komander, D. *et al.* The Structure of the CYLD USP Domain Explains Its Specificity for Lys63-Linked Polyubiquitin and Reveals a B Box Module. *MOLCEL* **29,** 451–464 (2008).

205. Saito, K. *et al.* The CAP-Gly Domain of CYLD Associates with the Proline-Rich Sequence in NEMO/IKKγ. *Structure/Folding and Design* **12,** 1719–1728 (2004).

206. Reiley, W. W. *et al.* Deubiquitinating enzyme CYLD negatively regulates the ubiquitin-dependent kinase Tak1 and prevents abnormal T cell responses. *Journal of Experimental Medicine* **204,** 1475–1485 (June 2007).

207. Koga, T. *et al.* Tumor Suppressor Cylindromatosis Acts as a Negative Regulator for Streptococcus pneumoniae-induced NFAT Signaling. *The Journal of biological chemistry* **283,** 12546–12554 (May 2008).

208. Lim, J. H., Ha, U. H., Woo, C.-H., Xu, H. & Li, J.-D. CYLD is a crucial negative regulator of innate immune response in Escherichia colipneumonia. *Cellular Microbiology* **10,** 2247–2256 (Nov. 2008).

209. Friedman, C. S. *et al.* The tumour suppressor CYLD is a negative regulator of RIG-I-mediated antiviral response. *EMBO reports* **9,** 930–936 (Sept. 2008).

210. Wright, A. *et al.* Regulation of Early Wave of Germ Cell Apoptosis and Spermatogenesis by Deubiquitinating Enzyme CYLD. *Developmental Cell* **13,** 705–716 (Nov. 2007).

211. Jin, W. *et al.* Deubiquitinating enzyme CYLD negatively regulates RANK signaling and osteoclastogenesis in mice. *Journal of Clinical Investigation* **118,** 1858–1866 (May 2008).

212. An, J. *et al.* Inactivation of the CYLD Deubiquitinase by HPV E6 Mediates Hypoxia-Induced NF-κB Activation. *Cancer Cell* **14,** 394–407 (Nov. 2008).

213. Kobayashi, T., Masoumi, K. C. & Massoumi, R. Deubiquitinating activity of CYLD is impaired by SUMOylation in neuroblastoma cells. *Oncogene* **34,** 2251–2260 (Apr. 2015).

214. Hutti, J. E. *et al.* Phosphorylation of the Tumor Suppressor CYLD by the Breast Cancer Oncogene IKKe Promotes Cell Transformation. *Molecular Cell* **34,** 461–472 (May 2009).

215. Reiley, W., Zhang, M., Wu, X., Granger, E. & Sun, S.-C. Regulation of the Deubiquitinating Enzyme CYLD by I B Kinase Gamma-Dependent Phosphorylation. *Molecular and Cellular Biology* **25,** 3886–3895 (Apr. 2005).

216. O'Donnell, M. A. *et al.* Caspase 8 inhibits programmed necrosis by processing CYLD. *Nature Cell Biology* **13,** 1437–1442 (Oct. 2011).

217. Costello, C. M. *et al.* Dissection of the Inflammatory Bowel Disease Transcriptome Using Genome-Wide cDNA Microarrays. *PLOS Medicine* **2,** e199 (Aug. 2005).

218. Graziotto, R. *et al.* cDNA Cloning and Characterization of PD1: A Novel Human Testicular Protein with Different Expressions in Various Testiculopathies. *Experimental Cell Research* **248,** 620–626 (1999).

219. Griswold, M. D. The central role of Sertoli cells in spermatogenesis. *Seminars in Cell and Developmental Biology* **9,** 411–416 (1998).

220. Onisto, M. *et al.* A novel gene (PD1) with a potential role on rat spermatogenesis. *Journal of Endocrinology* **23,** 605–608 (Jan. 2000).

221. Onisto, M. *et al.* Evidence for FSH-Dependent Upregulation of SPATA2 (Spermatogenesis-Associated Protein 2). *BIOCHEMICAL AND BIOPHYSICAL RESEARCH COMMUNICATIONS* **283,** 86–92 (2001).

222. Maran, C., Tassone, E., Masola, V. & Onisto, M. The Story of SPATA2 (Spermatogenesis-Associated Protein 2): From Sertoli Cells to Pancreatic Beta-Cells. *Current Genomics* **10,** 361–363 (Aug. 2009).

223. Moro, E. *et al.* Zebrafish spata2 is expressed at early developmental stages. *The International Journal of Developmental Biology* **51,** 241–246 (2007).

224. Capon, F. *et al.* Identification of ZNF313/RNF114 as a novel psoriasis susceptibility gene. *Human molecular genetics* **17,** 1938–1945 (July 2008).

225. Hitomi, J. *et al.* Identification of a Molecular Signaling Network that Regulates a Cellular Necrotic Cell Death Pathway. *Cell* **135,** 1311–1323 (Dec. 2008).

226. Montoya, A., Beltran, L., Casado, P., Rodrıguez-Prados, J.-C. & Cutillas, P. R. Characterization of a TiO(2) enrichment method for label-free quantitative phosphoproteomics. *Methods (San Diego, Calif.)* **54,** 370–378 (Aug. 2011).

227. Zhao, G. *et al.* Studies on peptide:N-glycanase–p97 interaction suggest that p97 phosphorylation modulates endoplasmic reticulum-associated degradation. *Proceedings of the National Academy of Sciences* **104,** 8785–8790 (May 2007).

228. Sato, Y. *et al.* Structures of CYLD USP with Met1- or Lys63-linked diubiquitin reveal mechanisms for dual specificity. *Nature Structural & Molecular Biology* **22,** 222–229 (Feb. 2015).

229. Stieglitz, B., Haire, L. F., Dikic, I. & Rittinger, K. Structural Analysis of SHARPIN, a Subunit of a Large Multi-protein E3 Ubiquitin Ligase, Reveals a Novel Dimerization Function for the Pleckstrin Homology Superfold. *Journal of Biological Chemistry* **287,** 20823–20829 (June 2012).

230. Wu, X., Zhang, M. & Sun, S.-C. Mutual regulation between deubiquitinase CYLD and retroviral oncoprotein Tax. *Cell & Bioscience* **1,** 27–27 (2011).

231. Breitkopf, S. B. & Asara, J. M. Determining In Vivo Phosphorylation Sites Using Mass Spectrometry. *Current Protocols in Molecular Biology* **98,** 1–27 (Apr. 2012).

232. Biemann, K. Contributions of mass spectrometry to peptide and protein structure. *Biological Mass Spectrometry* **16,** 99–111 (Oct. 1988).

233. Roepstorff, P. & Fohlman, J. Proposal for a common nomenclature for sequence-specific ions in mass spectra of peptides. *Biological Mass Spectrometry* **11,** 601–601 (Nov. 1984).

234. Hunter, A. P. & Games, D. E. Chromatographic and Mass Spectrometric Methods for the Identification of Phosphorylation Sites in Phosphoproteins. *rapid communications in mass spectrometry* **8,** 559–570 (Jan. 1994).

235. Verstrepen, L. *et al.* Expression, biological activities and mechanisms of action of A20 (TNFAIP3). *Biochemical Pharmacology* **80,** 2009–2020 (2010).

236. Shembade, N., Harhaj, N. S., Liebl, D. J. & Harhaj, E. W. Essential role for TAX1BP1 in the termination of TNF-α-, IL-1- and LPS-mediated NF-κB and JNK signaling. *Embo Journal* **26,** 3910–3922 (Aug. 2007).

237. Wagner, S. *et al.* Ubiquitin binding mediates the NF-κB inhibitory potential of ABIN proteins. *Oncogene* **27,** 3739–3745 (June 2008).

238. Zhao, G. *et al.* Studies on peptide:N-glycanase–p97 interaction suggest that p97 phosphorylation modulates endoplasmic reticulum-associated degradation. *Proceedings of the National Academy of Sciences of the United States of America* **104,** 8785–8790 (May 2007).

239. Sowa, M. E., Bennett, E. J., Gygi, S. P. & Harper, J. W. Defining the Human Deubiquitinating Enzyme Interaction Landscape. *Cell* **138,** 389–403 (July 2009).

List of Figures

1.1 **Crystal structure of ubiquitin.** (A) Ribbon structure of ubiquitin highlighting key lysine residues (yellow) and the N-terminal methionine (pink). Structure from PDB code: 1UBQ [12]. (B) Structure of ubiquitin (rotated relative to ribbon structure) showing each of the hydrophobic patches implicated in typical ubiquitin interactions with ubiquitin-binding domains (UBDs). 3

1.2 **The enzymatic cascade of ubiquitination.** Diagrammatic representation of the enzymatic cascade for: 1. Activation of the ubiquitin by an E1; 2. The E1 facilitates the transfer of the ubiquitin to the activate site cysteine of an E2; 3. an E3 facilitates the transfer of ubiquitin to a lysine residue on a target protein; 4. ubiquitinated substrates me be modified in various ways include the addition of a single (mono) ubiquitin on one or more (multi-mono) sites. Alternatively, ubiquitin may be conjugated to an existing ubiquitin molecule to facilitate the production of polyubiquitin chains; 5. a group of enzymes collectively known as deubiquitinating enzymes (DUBs) facilitates the removal of these ubiquitins; 6. free ubiquitin is often recycled for conjugation to another substrate in a separate reaction. 5

1.3 **Cartoon representation of the E3 ligase classes.** Diagrammatic representation of the mode of action of each class of E3. 7

1.4 **Structural representation of closed and extended chains.** Shown are examples of the extended (M1 (2W9N) and K63 (2JF5)) and closed (K11 (2MBO) and K48 (5GOI)) structure, which polyubiquitin chains adopt. 9

1.5 **Pattern recognition signalling.** Diagrammatic representation of each of the major types of pattern recognition receptors (PRRs), their respective ligands, and the main groups of transcription factors activated upon receptor stimulation. Importantly, all of these signalling events are reliant on ubiquitin-mediated signalling events. 19

1.6 **Signalling events mediated by PRR signalling modules.** Diagrammatic representation of each of the PRR signalling modules, the IKK, TAK1, and IKK/TBK1 complexes, and their mode of activation. 21

1.7 **Diagrammatic representation of the NOD1/2 structure.** The domain structure of NOD1 and NO2 highlights their similarity with NOD2 containing an extra CARD domain. NOD1/2 conformation resulting in an autoinhibited state is also shown. 23

1.8 **The NOD1/2 signalling cascade.** Upon stimulation with muramyl dipeptide (MDP) constituents of peptidoglycan (a component of bacteria cell walls), RIPK2 is recruited to NOD2 along with numerous E3s to facilitate its polyubiquitination. The TAK1 and IKK signalling modules are recruited by these chains to facilitate the activation of the NF-κB and MAPK pathways for production of pro-inflammatory mediators. Various DUBs act throughout this process to hydrolyse the polyubiquitin chains and therefore negatively regulate signalling. 24
1.9 **The TNF receptor complex I signalling cascade.** Following TNFR1 activat5ion, the adaptors TRADD and RIPK1 are recruited and ubiquitinated by numerous E3s resulting in activation of the TAK1 and IKK signalling modules. E3 act on this complex to negatively regulate it and promote its instability, which may lead to the formation of cell death-inducing complexes as shown in figure **??**. 27
1.10 **Diagrammatic representation of the structure of LUBAC.** The domain structure of the constituent components of LUBAC (HOIP, HOIL-1, and SHARPIN) are shown with arrows indicating the known domains required to allow them to form the LUBAC complex. Domains shown in colour are discussed further within this chapter and are important for the function of LUBAC. Adapted from [165]. 29
1.11 **Cartoon representation of the domain structure of CYLD.** The domain structure of CYLD showing each CAPGly domain and the USP domain (with the embedded B-box domain). Also annotated is the binding areas for microtubule association, TRAF2, and NEMO. 35

4.1 **WT/ΔB-box CYLD structure and LC-MS/MS analysis.** (A) A cartoon of the structure of Flag-tagged CYLD, showing the B-box region deleted for LC-MS/MS analysis. (B) A $\log_2$ plot of WT CYLD against ΔB-box CYLD showing identified interacting proteins. ***This LC-MS/MS experiment was performed by Matous Hrdinka of the Gyrd-Hansen lab, including analysis of the resulting data.*** Figure from [80]. 66
4.2 **CYLD B-box is required for SPATA2:HOIP interactions.** (A) Shown is a western blot from an IP of WT/ΔB-box CYLD highlighting the B-box dependent interaction with SPATA2. (B) Confirmation of the specificity of the SPATA2 (Bethyl, A302-494A) antibody using two siRNA targeting SPATA2. Figure from [80]. 67
4.3 **The domain structure of SPATA2.** (A) The domain structure of SPATA2 showing the corresponding amino acid residues for the PUB domain and PIM (B) Constructs of SPATA2 generated for this study. Figure from [80]. 68
4.4 **Confirmation of SPATA2 KO U2OS/NOD2 cells.** Shown is an IP of endogenous CYLD, blotting for SPATA2, on several SPATA2 KO clones. Figure from [80]. 68
4.5 **The SPATA2 PUB domain interacts with CYLD.** IP of Myc-tagged WT and R212X SPATA2 constructs in SPATA2 KO U2OS / NOD2 cells. Figure from [80]. 69
4.6 **Fold structure of the SPATA2 PUB domain** (A) A comparison of the fold structure of the SPATA2 PUB domain with that of HOIP and PNGase. (B) Sequence overlay of the amino acid sequences of the SPATA2 and HOIP PUB domains. ***The crystal structures of the SPATA2 PUB domain and alignment were performed by Paul Elliott of the Komander lab, LMB, Cambridge.*** Figure from [80]. 70

4.7 **SPATA2 contains a conserved PIM.** Conservation analysis of the SPATA2 PIM with the OTULIN and p97 PIMs. Figure from [80]. 71
4.8 **The SPATA2 PIM is required for binding to HOIP.** IP of full length (WT), R212X truncation (PUB only), and V357X truncation (PUB and PIM) SPATA2 to assess binding to HOIP. Figure from [80]. 72
4.9 **Mutating the SPATA2 PIM abrogates HOIP interactions.** IP of Myc-tagged WT, or PIM-mutated (Y338A/F) SPATA2 to assess HOIP binding. Figure from [80]. 72
4.10 **The SPATA2 PIM binds HOIP PUB domain.** Crystal structure of the HOIP PUB domain binding the SPATA2 PIM (2.7 Å resolution). ***The crystal structure of the SPATA2 PIM bound to the HOIP PUB domain was performed by Paul Elliott of the Komander lab, LMB, Cambridge.*** Figure from [80]. 73
4.11 **SPATA2 KO inhibits CYLD:HOIP interactions.** IP of reintroduced V5-tagged HOIP into WT, CYLD KO, and SPATA2 KO U2OS/NOD2 cells to assess the requirement of SPATA2 for CYLD recruitment to LUBAC. Figure from [80]. 74
4.12 **WT SPATA2 restores CYLD:HOIP interactions.** IP of V5 - HOIP in SPATA2 KO background with the transient reintroduction of WT or PIM-mutated (Y338A/F) SPATA2. Figure from [80]. . . 74
4.13 **SPATA2 is required for CYLD recruitment to TNFR complex I.** FLAG-TNF IP of the TNFR complex I, with 1 μg of FLAG-TNF per IP, to assess binding of CYLD in the absence of SPATA2. Figure from [80]. 76
4.14 **SPATA2 links CYLD to high MW complexes.** Sucrose gradient sedimentation of CYLD in WT, CYLD KO, and SPATA2 KO U2OS/NOD2 cells. ***The sucrose gradient sedimentation step was performed by Norbert Volkmar of the Christianson lab, Oxford. All other steps were performed by myself.*** Figure from [80]. 77
4.15 **SPATA2 regulates CYLDs ability to control ubiquitination.** TUBE pulldown from parental (WT), CYLD KO, and SPATA2 KO U2OS/NOD2 cells following stimulation with 5 ng/ml TNF for 15 min and 200 ng/ml L18-MDP for 1 h to assess ubiquitination of their key adaptor proteins, RIPK1 and RIPK2. Figure from [80]. 79
4.16 **SPATA2 regulates RIPK2 ubiquitination following CpA/MDP.** TUBE pulldown from parental (WT), CYLD KO, and SPATA2 KO U2OS/NOD2 cells following stimulation with 1 μM CpA for 30 min prior to 200 ng/ml L18-MDP for 1h to assess ubiquitination of RIPK2. Figure from [80]. 81
4.17 **SPATA2 KO affects ubiquitination of TNFR complex I substrates.** FLAG - TNF pulldown of the TNFR complex I, with 1 μg of FLAG-TNF per IP, in parental (WT) and SPATA2 KO U2OS/NOD2 cells to assess how SPATA2 affects ubiquitination of the complex. Figure from [80]. 82
4.18 **SPATA2 and CYLD do not regulate TNF signalling.** qRT- PCR performed on parental (WT), CYLD KO, and SPATA2 KO U2OS/NOD2 cells following stimulation with 5 ng/ml TNF for 3 h. Data normalised to HPRT control and subsequently the $CYLD^{WT}$ stimulated condition. Data was collated from three experiments and analysed in Graphpad prism 6 with statistic tests by two-way ANOVA. Figure from [80]. . 83

4.19 **SPATA2 is important for the regulation of NOD2 signalling.** qRT-PCR performed on parental (WT), CYLD KO, and SPATA2 KO U2OS/NOD2 cells following stimulation with 200 ng/ml L18-MDP for 3 h. Data normalised to HPRT control and subsequently the $CYLD^{WT}$ stimulated condition. Data was collated from three experiments and analysed in Graphpad prism 6 with statistical tests by two-way ANOVA. Figure from [80]. 85

4.20 **SPATA2 regulates CXCL8 production from NOD2 signalling.** Flow cytometry analysis to assess CXCL-8 production performed on parental (WT), CYLD KO, and SPATA2 KO U2OS/NOD2 cells following stimulation with 200 ng/ml L18-MDP for 5 h the presence of 5 μg/ml brefeldin A and 2 μM monensin. Data was collated from 15 biological replicates and analysed in Graphpad prism 6 with statistical tests by two-way ANOVA. Figure from [80]. 85

4.21 **OTULIN controls steady-state LUBAC activation.** Immunoblot of an M1-specific TUBE pulldown from U2OS/NOD2 cells with a stable virally-expressed shRNA targeting a NS control, OTULIN, or CYLD. Blotting with anti-HOIP (sigma antibody) shows ubiquitination of HOIP at steady state levels. Figure from [132]. 87

4.22 **Schematic representation of the structure of LUBAC.** Cartoon representation of the dynamic structure of LUBAC with OTULIN or SPATA2:CYLD bound via the HOIP PUB domain. Figure from [80]. 89

5.1 **CYLD exists in a phosphorylated state within the TNFR complex I.** Immunoblot showing biotin-TNF pulldown of the TNFR complex I using 1 μg of TNF per pulldown. Following pulldown, one 15 min time point was subjected to lambda phosphatase treatment for 1 h at 30 ^{o}C. 93

5.2 **IKK inhibition prevents CYLD phosphorylation.** Immunoblot showing IKK inhibitor treatment (inhibitor VII and XII both at 1 μM conc.) 30 min prior to stimulation with 20 ng/ml TNF for 15 min or 200 ng/ml L18-MDP for 1 h. Parental (WT) U2OS/NOD2 cells with or without RNAi knockdown (KD) of OTULIN shown. . . 94

5.3 **TAK1 inhibition prevents CYLD phosphorylation.** Immunoblot showing 1 μM Oxozeaonol, a TAK1 inhibitor, treatment 30 min prior to stimulation with 20 ng/ml TNF for 15 min or 200 ng/ml L18-MDP for 1 h. Parental (WT) U2OS/NOD2 cells with or without RNAi knockdown (KD) of OTULIN shown. 95

5.4 **LC-MS/MS analysis of CYLD phosphorylation.** (A) Graphical representation of the experimental procedures for analysis of CYLD phosphorylation sites following TNF stimulation at 20 ng/ml. (B) Immunoblot of the purified material sent for MS analysis. Pull down by FLAG-TNF as described in section 3.2.6 97

5.5 **The identified phosphorylation sites of CYLD.** Graphical representation showing the identified phosphorylation sites of CYLD. Showing in red are sites only identified following TNF stimulation. Sites with an asterisk represent previously annotated sites. Of note is the identified phosphorylation of S568. 98

5.6 **Spectra of S568 phosphorylation.** Spectra from the LC-MS/MS analysis of CYLD showing peptide 563-586. Fragmentation coverage showing b and y ions is shown in blue and red respectively. The ion table for this spectra can be found in supplementary figure 7.2. . . . 98

5.7 **Reintroduced levels of CYLD phosphorylation mutants.** Immunoblot showing the reintroduced levels of the generated CYLD phosphorylation mutants. Densitometry of three blots was performed to ensure levels were matched across mutants, as shown in supplementary figure 7.1. 99

5.8 **CYLD^{S568A} and CYLD$^{S418A/S568A}$ show enhanced signalling.** Immunoblot showing the effect of the phosphorylated CYLD mutants on signalling events in response to 20 ng/ml TNF for 15 min or 200 ng/ml L18-MDP for 1 h. 101

5.9 **CYLD$^{S418A/S568A}$ shows enhanced pro-inflammatory transcripts.** qRT-PCR analysis of the production of pro-inflammatory transcripts following stimulation with 20 ng/ml TNF or 200 ng/ml L18-MDP for 3 h. Data normalised to HPRT control and subsequently the CYLD^{WT} stimulated condition. Data was collated from three experiments and analysed in Graphpad Prism 6 with statistical tests by two-way ANOVA. 102

5.10 **CYLD$^{S418A/S568A}$ shows enhanced CXCL8 production.** Flow cytometry analysis of CXCL-8 production in phosphorylation mutants of CYLD following 200 ng/ml L18-MDP for 5 h in the presence of 5 μg/ml brefeldin A and 2 μM monensin. n=3. Data was collated from three experiments and analysed in Graphpad Prism 6 with statistical tests by two-way ANOVA. Representative histograms are shown in supplementary figure 7.3. 104

5.11 **CYLD$^{S418A/S568A}$ shows enhanced RIPK2 ubiquitination.** Immunoblot showing TUBE pulldown of ubiquitination substrates, and subsequent blotting for RIPK2, after 200 ng/ml L18-MDP stimulation with or without prestimulation for 30 min with 1 μM CpA. 105

5.12 **CYLD$^{S418A/S568A}$ dysregulates TNFR complex I.** Immunoblot showing a Biotin-TNF pulldown (1 μg per pulldown for indicated time points) in parental, CYLD KO, and CYLD KO with reintroduced mutants U2OS/NOD2 cells. 107

7.1 **Levels of all CYLD mutants by densitometry.** Immunoblot showing the reintroduced levels of all CYLD mutants. Densitometry of three blots was performed to ensure levels were matched across mutants. 118

7.2 **Ion table of the S568 spectra**. Ion table showing the mass recorded for each b and y ion as per figure 5.6. 119

7.3 **Histograms of CXCL8 production in CYLD mutants.** Flow cytometry analysis of CXCL-8 production in CYLD mutants following 200 ng/ml L18-MDP for 5 h in the presence of 5 μg/ml brefeldin A and 2 μM monensin. 120

7.4 **IkB/A20 transcript production in phosphomutant CYLD lines.**. qRT-PCR analysis of the production of pro-inflammatory transcripts following stimulation with 20 ng/ml TNF or 200 ng/ml L18-MDP for 3 h. Data normalised to HPRT control and subsequently the CYLD^{WT} stimulated condition. Data was collated and analysed in Graphpad Prism 6 with statistic tests by two-way ANOVA. 121

7.5 **Reintroduced levels of CYLD capgly mutants** Immunoblot showing reintroduced levels of the stably expressing CYLD CAPGly mutants in the CYLD KO U2OS/NOD2 background. Densitometry of of three blots was performed to ensure levels were matched between all generated mutants as shown in supplementary figure 7.1. 121

7.6 **Pro-inflammatory trascript production in all CYLD^{L475P} mutants**. qRT-PCR analysis of the production of pro-inflammatory transcripts following stimulation with 20 ng/ml TNF or 200 ng/ml L18-MDP for 3 h. Data normalised to HPRT control and subsequently the CYLD^{WT} stimulated condition. Data was collated and analysed in Graphpad Prism 6 with statistic tests by two-way ANOVA. 122

7.7 **CXCL8 production in all CYLD^{L475P} mutants**. Flow cytometry analysis of CXCL-8 production in phosphorylation mutants of CYLD following 200 ng/ml L18-MDP for 5 h in the presence of 5 μg/ml brefeldin A and 2 μM monensin. Data was collated and analysed in Graphpad prism 6 with statistical tests by two-way ANOVA. Representative histograms are also shown in supplementary figure 7.3. 122

7.8 **CYLD^{L475P} results in enhanced RIPK2 ubiquitination.** Immunoblot showing TUBE pulldown of ubiquitination substrates, and subsequent blotting for RIPK2, after 200 ng/ml L18-MDP stimulation with or without prestimulation for 30 min with 1 μM CpA. 123

7.9 **SPATA2L-induced cell death is rescued by re-introduction**. U2OS/NOD2 cells were created from the Trex FlpIn system. cell lines A, B, and C represent siRNA-resistant versions of SPATA2L. siRNA was introduced to cells for given time points and Hoecsht and Sytox green stain was used to determine the percentage of cell death. As shown, each SPATA2L siRNA results in cell death, which is rescued through the Dox-induced expression of siRNA-resistant SPATA2L. 124

List of Tables

1.1 The total members of each DUB family with details of the number of catalytically active members. Table adapted from [55]. 11

2.1 Reagents used in this study 39
2.2 Buffers used in this study 42
2.3 Commercial kits used in this study 43
2.4 Antibodies used in this study 43
2.5 Plasmids used in this study 44
2.6 Oligos used in this study for template amplification 45
2.7 Oligos used in this study for site-directed mutagenesis 45
2.8 qRT-PCR oligos used in this study 46
2.9 Parental cell lines used in this study 46
2.10 Self-generated genetically modified cell lines 47

3.1 Volumes/concentrations of FuGENE 6/HD transfection mix 49
3.2 Volumes/concentrations of Lipofectamine RNAiMAX transfection mix 50
3.3 Volumes/quantities of reagents used for cDNA synthesis and qPCR 52
3.4 Details of the qPCR programme used on the Lightcycler 480 52
3.5 Reaction mix for SPATA2 template PCR 60
3.6 Details of the PCR cycles for SPATA2 template amplification . . . 61
3.7 Ligation mix for SPATA2 into pcDNA3.1/CYLD into pBABE . . . 61
3.8 Reaction mix for SPATA2/CYLD mutagenesis PCR 62
3.9 Details of the PCR cycles for SPATA2 mutagenesis 62
3.10 Reaction mix for FLAG-CYLD PCR 62
3.11 Details of the PCR cycles for FLAG-CYLD amplification 63